Title
Mechanistic Origins of Activity and Selectivity in Transition Metal Catalyzed Organic Reactions

Permalink
https://escholarship.org/uc/item/2sj60690

Author
Xiang, Shuhuai

Publication Date
2016

Peer reviewed|Thesis/dissertation

UNIVERSITY OF CALIFORNIA, MERCED

Mechanistic Origins of Activity and Selectivity in
Transition Metal Catalyzed Organic Reactions

A dissertation submitted in partial satisfaction of the
requirements for the degree Doctor of Philosophy

in

Organic Chemistry

by

Shuhuai Xiang

Committee in charge:

      Professor Andy LiWang, Chair
      Professor Patricia LiWang
      Professor Matthew P. Meyer, Advisor
      Professor Benjamin J. Stokes

The Dissertation of Shuhuai Xiang is approved, and it is acceptable in quality and form for publication on microfilm and electronically:

Professor Patricia LiWang

Professor Matthew P. Meyer

Professor Benjamin J. Stokes

Professor Andy LiWang   Chair

University of California, Merced

2016

DEDICATION

I dedicate this dissertation to my parents, who valued my education and devoted their life to it.

TABLE OF CONTENTS

LIST OF ABBREVIATIONS

ACN	acetonitrile
AIBN	azobisisobutyronitrile
CHCR	combined C-H activation/Cope rearrangement
DBU	1,8-Diazabicyclo[5.4.0]undec-7-ene
DMB	2,2-dimethyl-butane
DMF	*N,N*-dimethyl formaldehyde
EIE	equilibrium isotope effect
EXC	vibrational excitation
HMBC	heteronuclear multiple bond correlation
HSQC	heteronuclear single quantum coherence
INADEQATE	Incredible Natural Abundance DoublE QUAntum Transfer Experiment
IRMS	isotope-ratio mass spectrometry
KIE	kinetic isotope effect
LFER	linear free energy relationship
MMI	mass and moment of inertia
MS	mass spectroscopy
NBS	n-bromosuccinimide
NMR	nuclear magnetic resonance
NOESY	nuclear overhauser effect spectroscopy
PDS	product determining step
PES	potential energy surface
RBF	round bottom flask
RDS	rate determining step
RPKA	reaction progress kinetic analysis
THF	tetrahydrofuran
TS	transition state
TST	transition state theory
WMS	whole mass spectroscopy
ZPE	zero-point energy

ACKNOWLEDGEMENT

I would like to express my deepest appreciation to my advisor, Professor Matthew P. Meyer, whose patience, supervision, knowledge, scrutiny, dedication and spirit for life guided me through my Ph.D. journey.

I am sincerely thankful to all the members of my committee, Professor Andy LiWang, Professor Patricia LiWang and Benjamin J. Stokes for their support and guidance on my research and dissertation.

I am deeply grateful for Professor Andy LiWang, who guided me on theories and practices in NMR with his expertise and enthusiasm.

I would like to acknowledge Professor Meng-lin Tsao, Dr. Dennis Mckean and Carrie King for their guidance and support during the entirety of my graduate education.

I am heartily thankful to Dusty Ventura for editing my manuscript and support all the way through my dissertation preparation.

I would like to acknowledge the American Chemical Society for their permission to use copyrighted materials "Xiang, S.; Meyer, M. P. *J. Am. Chem. Soc.* **2014**, *136*, 5832–5835, Copyright 2014, American Chemical Society" in Chapter 3.

2008	Bachelor of Science, Sichuan University, China, 2008
2008-2015	Teaching Assistant and Teaching Fellow, Department of Chemistry and Chemical Biology, University of California, Merced
2016	Doctor of Philosophy, University of California, Merced

PUBLICATIONS

5. **Shuhuai Xiang**; Matthew P. Meyer* A General Approach to Mechanism in Multi-product Reactions: Product-specific Intermolecular KIEs *J. Am. Chem. Soc.* **2014**, *136*, 5832–5835.

4. Gökçe Uğˇur; Jiyoung Chang; **Shuhuai Xiang**; Liwei Lin; Jennifer Lu* A Near-Infrared Mechano Responsive Polymer System *Adv. Mater.* **2012**, *24*, 2685–2690.

3. Tzu-I Chao[1]; **Shuhuai Xiang**[1]; Changchun Wang; Weichun Chin; Jennifer Lu* Polymer Grafted Carbon Nanotube Scaffolds Enhance Differentiation of hESC into Neuronal Cells *Adv. Mater.* **2010**, *22*, 3542–3547. (1: Both authors contributed equally to this work).

2. Tzu-I Chao; **Shuhuai Xiang**; Chi-Shuo Chen; Wei-Chun Chin; A.J. Nelson; Changchun Wang; Jennifer Lu* Carbon Nanotubes Promote Neuron Differentiation from Human Embryonic Stem Cells *Biochem. Biophys. Res. Commun.* **2009**, *384*, 426–430.

1. Jennifer Lu; **Shuhuai Xiang** Novel Responsive Polymer System and Nanohybrid Thin Films US 20120038249 A1, Feb 16, 2012.

ABSTRACT OF THE DISSERTATION

Mechanistic Origins of Activity and Selectivity in
Transition Metal Catalyzed Organic Reactions
by

Shuhuai Xiang

Doctor of Philosophy in Organic Chemistry

University of California, Merced, 2016

Professor Andy LiWang, Chair
Professor Matthew P. Meyer, Advisor

Transition states are the gate keepers of chemical reactions. The free energies associated with transition states determine everything of interest in a chemical reaction, namely the rate and product distribution. Attempts to categorize the repulsive and attractive forces that dictate structural and energetic features of transition states dominate mechanistic organic chemistry. Kinetic isotope effects (KIEs) provide a direct quantitative probe into transition structure because they report directly upon changes in bond strength. Furthermore, KIEs provide a satisfying means of comparison with computational efforts. However, KIE methods are almost exclusively applied to spot to spot reactions with only a single product. The information provided by studying these somewhat rare, well-behaved reactions, can be helpful, but more versatile methods are needed to investigate reactions that yield more than one product.

In this dissertation, product-specific KIE, a new method developed in the lab which can simultaneously measure the KIE of all pathways in a multi-product reaction, will be introduced. In principle, the product-specific KIE methodology is able to reveal the energetic landscape of all pathways by analysis of the isotopic fractionation which records the bonding changes that occur along a reaction pathway. The information provided can be illuminating to discover the branching events in chemo-, regio- and stereo-selective reactions. Secondly, the mechanisms of two transition-metal catalyzed multi-product reactions have been discussed as examples for the application of this method with both natural abundance ^{13}C and deuterium KIE experiments. One of them is cobalt catalyzed [2+2] and Alder-ene reaction, where a common intermediate was found before it branches to two different products. In another case, a dirhodium tetraacetate catalyzed C-H insertion was found to proceed via an initial hydride transfer transition state, followed by formation of two interconverting zwitterion intermediates before the

formation of two diastereomers. Product-specific KIEs have the potential to address mechanistic questions in reactions under development and provide a basic understanding of the key transition state features necessary to develop more selective catalysis.

Chapter 1: Introduction to Kinetic Isotope Effects

1.1 General Goal of This Research

Organic chemistry has been applied to almost every aspect of human society and plays an essential role in modern civilization. It drives a number of critical industries, including manufacturing, energy, pharmaceuticals, and agriculture. In all of these industries, there is a clear need and great potential for more efficient and environmentally-conscious organic reactions. Chemically speaking, shorter synthesis routes, greater atom economy, and milder reaction conditions are required. Critical to achieving the above-mentioned goal is the development of more efficient and selective catalysts. Most of the current successful non-enzymatic catalysts have a heavy precious metal such as palladium, platinum, rhodium, at their core, although organocatalysts are being increasingly explored as viable alternatives. To reduce the cost and lower the environmental impact of chemical transformations, more efficient and cost-effective catalysts are desired. While a sort of trial and error approach has been successful in catalyst development, paradigm changes in catalysis are often spurred by increased mechanistic understanding. Thus it is crucial to understand how catalysts work in a chemical reaction. This is the practical motivation for studying organic reaction mechanism besides pure scientific interests.

The general methods for mechanistic study of organic reactions include kinetic isotope effect (KIE),[1–5] free energy relationships (e.g. Hammett plots[6]), kinetic analysis (e.g. reaction progress kinetic analysis[7]), intermediate trapping, isotope scrambling, crossover experiments, and other more specialized techniques. Each category has its strengths and weaknesses, and it is important to point out that a complete understanding of a reaction mechanism may require more than one of these methods mentioned above. For example, isotope scrambling can track the origin of specific atoms thus allow us to distinguish between intramolecular and intermolecular transformation; intermediate trapping provides a possible pathway from starting material to the product; kinetic analysis reveals reaction orders, induction period, and indications of product inhibition and catalyst resting state(s). Free energy relationships can deliver meaningful trends relating substituent effects to reactivity and selectivity. However, KIE experiment is the only method that provides a quantitative connection to the transition structure which offers the basis for causality analysis between structures, reactivity and selectivity, except in very simple systems whose transition state characters can be directly observed.[8,9] Besides affording direct information about the bond strength and vibrational frequency change from reactant to transition state, the results from a KIE experiment can also be coupled with fast emerging powerful computation chemistry to gain direct structural insight into the transition state and the reaction mechanism.

1.2 Physical Origins of Isotope Effects

Isotopes are defined by their different number of neutrons in for a particular element. For instance, ^{1}H (hydrogen), ^{2}H (deuterium), ^{3}H (tritium) all have only one proton but zero, one and two neutrons in their nuclei, respectively. Due to their identical electronic structures under the Born-Oppenheimer approximation, they react in a chemically (electronically) identical fashion but exhibit differential mass effects via zero-point energy differences. The KIE is defined as the rate ratio for reactants that differ only in isotopic substitution. It is a convention to report the KIE as the rate for conversion of the light isotopologue divided by that for the conversion of the heavy isotopologue (e.g. k_H/k_D). The existence of KIE is because the fundamental difference in how different isotopologues behave regarding the mass difference. The origin of isotope effects[2,3] has been discussed thoroughly for reactions that obey conventional transition state theory (TST).[10] This introduction is intended to demonstrate the origins of KIEs starting from the assumption of TST, yielding the widely used Bigeleisen-Mayer equation for KIE calculation. An intuitive explanation of KIEs and the information they confer will also be developed to aid the reader in the discussion of results presented in this thesis.

To obtain the energy of a molecule composed of nuclei and electrons, with very good accuracy, Born-Oppenheimer approximation treats the nucleus as if it were stationary, with the electrons responding only to the position of the nucleus and other electrons. This treatment can be justified by the observation that electrons are less than one thousandth the mass of nucleons. This treatment allows the separation of molecular wave function into electronic and nuclear components, thus greatly simplifying the calculation of the total energy. Since the electronic wave function only parametrically depends on the coordinates and charge of the nucleus, so does the electronic energy. This electronic energy, plus the constant nuclear repulsion provide a potential for nuclear motion. In this way, the relationship between structure and energy can be obtained. This multidimensional map is called the potential energy surface (PES).[11] In practice, a cross section of the PES along the reaction coordinate is usually showed for ease of discussion. For example, the curved line in Figure 1a shows the potential well for the reactant on the left, the transition state at the middle and the potential well for the product. This potential energy surface reflects only the electronic energy of the molecule(s). To get the total energy, the energies associated with vibrational, rotational, and translational motions need to be calculated. The vibration at the bottom of the PES can be well approximated by a quantum harmonic oscillator whose energy is $(n + 1/2)h\nu$, with n as the quantum number, $\nu=\sqrt{k/\mu}$ as the frequency defined by a force constant k and the reduced mass. In a diatomic harmonic oscillator, $\mu=m_1m_2/(m_1+m_2)$. The substitution of an isotope at a given position in a molecule does not change the electronic or potential energy at any point thus the force constant k, which is the second derivative of this potential respect to the normal coordinates, does not change. However, according to Heisenberg's

uncertainty principle, the position and momentum for a system cannot be simultaneously determined with arbitrary great precision. It means the atomic positions are not confined at the absolute bottom of the potential well because the lowest vibrational state (n = 0) has a zero-point energy (ZPE) of $1/2\mathbf{h}\nu$. Since the force constant does change upon substitution of an isotope, because the reduced mass does, it makes two isotopologues have different amount of ZPE. If a chemical bond is completely broken at the transition state, the ZPE is lost, resulting in free energies of activation ($\Delta G^{\ddagger}$) for the two isotopologues differ by the difference in ZPE in the reactants. This is a simplified picture, but it motivates a basic understanding of primary KIEs discussed below.

1.3 Theoretical Calculation of KIE

To find the difference between the rates of reaction of isotopologues, we can start with an arbitrary single step reaction with only one pair of isotopic molecules, R_1 and R_2,

$$R_1 + X + \cdots \xrightarrow{\ k_1\ } P_1$$

$$R_2 + X + \cdots \xrightarrow{\ k_2\ } P_2$$
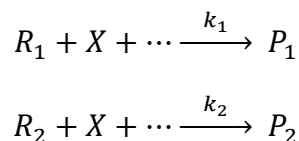
reacting with other nonisotopic molecules X, with rate constants k_1 and k_2, respectively. Transition state theory assumes an ensemble of activated complexes that are close in energy and geometry which reside near the top of the barrier between reactants and products. This ensemble is called the transition state in TST. These complexes are in quasi equilibrium [12] with the reactant molecules.

$$R_1 + X + \cdots \longleftrightarrow M_1^{\ddagger} + N + \cdots$$

$$R_2 + X + \cdots \longleftrightarrow M_2^{\ddagger} + N + \cdots$$
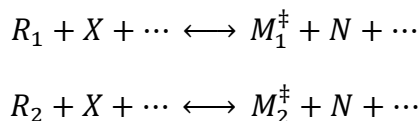
According to TST, how fast a reaction happens depends on the concentration of the activated complex $[M^{\ddagger}]$ and its decomposition frequency, providing that the equilibrium does not change much over the course of the reaction. Under this assumption, the relative concentrations can be framed in terms of partition functions, and the absolute rate constant can be approximated as: [3,10]

$$k = \kappa Q_t \frac{\mathbf{k}T}{\mathbf{h}} \times \frac{Q_{M^{\ddagger}}^{o} Q_N^{o} \cdots}{Q_{R^{\ddagger}}^{o} Q_X^{o} \cdots} e^{-E_{class}/RT} \frac{\alpha_R \alpha_X}{\alpha_{M^{\ddagger}} \alpha_N}$$

$$\ldots(1)$$

where κ is the transmission coefficient, $\mathbf{k}$ is the Boltzmann constant; $\mathbf{h}$ is Planck's constant, Q_t is the tunneling correction term, $Q_{M^{\ddagger}}^{o}$ stands for the partition function of the activation equilibria deprived of the decomposition mode, other $Q's$ and $\alpha's$ stand for the

3

partition function and activity coefficients of each specie in an idealized condition, in a gas phase reaction for example, E_{class} is the classical barrier from the bottom of the reactant to the saddle point (TS) at absolute zero. On the condition when the temperature is not too high that excited electronic states must be counted, or so low such that rotational partition function cannot be approximated as a continuum of states,[13] the transmission coefficient and $\alpha's$ can be dropped out. The partition function of the reactant R_1 can be written as a product of the translational, rotational and vibrational partition functions:

$$Q_1 = \frac{Q_{1,trans}}{V} Q_{1,rot} Q_{1,vib}$$

$$= \frac{(2\pi M_1\ kT)^{\frac{3}{2}}}{h^3} \times \frac{g_{1,el} g_{1,nuc}}{s_1} \times \frac{8\pi^2 (8\pi^3 I_{1,A} I_{1,B} I_{1,C})^{\frac{1}{2}}(kT)^{\frac{3}{2}}}{V}$$

$$\times \prod_i^{3N-6} e^{-\frac{\left(\frac{1}{2}\right)h\nu_i}{kT}} \left(1 - e^{-\frac{h\nu_i}{kT}}\right)^{-1}$$

$$\dots (2)$$

where M_1 denotes the molecular weight of the corresponding species; $g_{1,el}$, $g_{1,nuc}$, s_1 stand for electronic degeneracy, nuclear degeneracy and the symmetry number; $I_{1,A}, I_{1,B}, I_{1,C}$ (Note that the A, B, C denote three different rotational axes of a nonlinear chemical entity, in case a linear molecule, there are only two axes, where 3N-6 should be replaced with 3N-5.) stand for the three principle moments of inertia; ν_i stands for the vibrational frequency for vibrational mode i. The partition function of the corresponding activation equilibria $M_1^{\ddagger}$ has the same form; however, the imaginary frequency that results from the saddle point is removed from the vibrational contribution ($3N^{\ddagger} - 7$ should be replaced with $3N^{\ddagger} - 6$ for a linear molecule):

$$Q_1^{\ddagger} = \frac{(2\pi M_1^{\ddagger} kT)^{3/2}}{h^3} \times \frac{g_{1,el}^{\ddagger} g_{1,nuc}^{\ddagger}}{s_1} \times \frac{8\pi^2 (8\pi^3 I_{1,A}^{\ddagger} I_{1,B}^{\ddagger} I_{1,C}^{\ddagger})^{1/2}(kT)^{3/2}}{V}$$

$$\times \prod_i^{3N^{\ddagger}-7} e^{-\left(\frac{1}{2}\right)h\nu_i^{\ddagger}/kT}(1 - e^{-h\nu_i^{\ddagger}/kT})^{-1}$$

$$\dots (3)$$

The partition function for both substrate R_2 and the activation equilibria $M_2^{\ddagger}$ for the isotopologue can be written in a similar way. Taking the partition functions for the species in both reactions into equation (1), with E_{class} and $\alpha's$ cancelling out, the ratio of the rate constants of the two reactions is:

4

$$\frac{k_1}{k_2} = \frac{Q_{t,1}}{Q_{t,2}} \times \frac{Q_1^{\ddagger}/Q_1}{Q_2^{\ddagger}/Q_2} = \frac{Q_{t,1}}{Q_{t,2}} \times \frac{Q_1^{\ddagger}}{Q_2^{\ddagger}} \times \frac{Q_2}{Q_1} = \frac{Q_{t,1}}{Q_{t,2}} \left(\frac{k_1}{k_2}\right)_{semi}$$

$$\dots (4)$$

where $Q_{t,1}$ and $Q_{t,2}$ stand for the tunneling factors; *semi* denotes that the ratio is semi classical. This expression has separated the tunneling factor from the semi-classical contribution since they will be treated separately. Semi-classical here means that the quantization of vibrational level has been taken into account but not tunneling. The nuclear degeneracy factor is canceled when taking the ratio from the reactant to the activation equilibria, and the electronic degeneracy factor were canceled during taking the ratio of the rates since isotopologues have identical electronic energies and states. The symmetry factors rarely contribute to the isotope effects thus they are placed together with the semi classical KIE. Introducing $u_i = \boldsymbol{h}v_i^{\ddagger}/\boldsymbol{kT}$, the semi classical KIE ratio can be now expressed as a combination of three terms as in the following showed Bigeleisen-Mayer equation: MMI, EXC and ZPE. MMI is the combined molecular-mass and moments of inertia factors; EXC for excitation and ZPE for zero-point energy (for a linear molecule, $3N^{\ddagger} - 7$ and $3N - 6$ should be replaced with $3N^{\ddagger} - 6$ and $3N - 5$, respectively. The same change applies for a linear molecule in Equation 6 and Equation 7).

$$\left(\frac{k_1}{k_2}\right)_{semi} \times \frac{s_1^{\ddagger} \, s_2}{s_2^{\ddagger} \, s_1} = \left(\frac{M_1^{\ddagger}}{M_2^{\ddagger}} \times \frac{M_2}{M_1}\right)^{3/2} \times \left(\frac{I_{1,A}^{\ddagger} I_{1,B}^{\ddagger} I_{1,C}^{\ddagger}}{I_{2,A}^{\ddagger} I_{2,B}^{\ddagger} I_{2,C}^{\ddagger}} \times \frac{I_{2,A} I_{2,B} I_{2,C}}{I_{1,A} I_{1,B} I_{1,C}}\right)^{1/2} \quad \text{MMI}$$

$$\times \left(\prod_i^{(3N^{\ddagger}-7)} \frac{1 - e^{-u_{i,2}^{\ddagger}}}{1 - e^{-u_{i,1}^{\ddagger}}} \prod_i^{3N-6} \frac{1 - e^{-u_{i,1}}}{1 - e^{-u_{i,2}}}\right) \quad \text{EXI}$$

$$\times \left(\prod_i^{(3N^{\ddagger}-7)} \frac{e^{(1/2)u_{i,2}^{\ddagger}}}{e^{(1/2)u_{i,1}^{\ddagger}}} \prod_i^{3N-6} \frac{e^{(1/2)u_{i,1}}}{e^{(1/2)u_{i,2}}}\right) \quad \text{ZPE}$$

$$\dots (5)$$

By applying Teller-Redlich product theorem[14,15] to both substrates and the transition states, where $v_{im,1}^{\ddagger}$ and $v_{im,2}^{\ddagger}$ are imaginary frequencies lead to the elimination of the MMI term,

$$\left(\frac{M_1}{M_2}\right)^{3/2} \times \left(\frac{I_{1,A}I_{1,B}I_{1,C}}{I_{2,A}I_{2,B}I_{2,C}}\right)^{1/2} = \prod_j^N \left(\frac{m_{j,1}}{m_{j,2}}\right)^{3/2} \prod_i^{3N-6} \left(\frac{v_{i,1}}{v_{i,2}}\right)$$

$$\left(\frac{M_1^{\ddagger}}{M_2^{\ddagger}}\right)^{3/2} \times \left(\frac{I_{1,A}^{\ddagger}I_{1,B}^{\ddagger}I_{1,C}^{\ddagger}}{I_{2,A}^{\ddagger}I_{2,B}^{\ddagger}I_{2,C}^{\ddagger}}\right)^{1/2} = \frac{v_{im,1}^{\ddagger}}{v_{im,2}^{\ddagger}} \prod_j^N \left(\frac{m_{j,1}^{\ddagger}}{m_{j,2}^{\ddagger}}\right)^{3/2} \prod_i^{3N^{\ddagger}-7} \left(\frac{v_{i,1}^{\ddagger}}{v_{i,2}^{\ddagger}}\right)$$

$$\dots (6)$$

The Bigeleisen-Mayer equation can be rewritten as:

$$\left(\frac{k_1}{k_2}\right)_{semi} \times \frac{s_1^{\ddagger} s_2}{s_2^{\ddagger} s_1} = \frac{v_{im,1}^{\ddagger}}{v_{im,2}^{\ddagger}} \times \left(\prod_i^{3N^{\ddagger}-7} \frac{u_{i,1}^{\ddagger}}{u_{i,2}^{\ddagger}} \times \frac{e^{\left(\frac{1}{2}\right)u_{i,2}^{\ddagger}}}{e^{\left(\frac{1}{2}\right)u_{i,1}^{\ddagger}}} \times \frac{1-e^{-u_{i,2}^{\ddagger}}}{1-e^{-u_{i,1}^{\ddagger}}}\right)$$

$$\times \left(\prod_i^{3N-6} \frac{u_{i,1}}{u_{i,2}} \times \frac{e^{\left(\frac{1}{2}\right)u_{i,1}}}{e^{\left(\frac{1}{2}\right)u_{i,2}}} \times \frac{1-e^{-u_{i,1}}}{1-e^{-u_{i,2}}}\right)$$

$$\dots (7)$$

It is the equation employed for semi-classical KIE, and a Bell's multiplicative tunneling correction[16] as shown in equation (8) is usually applied to approach a better approximation. It is important to note that this correction assumes tunneling only in the direction of the reaction coordinate and only applies reliably in situations where tunneling is unlikely to play a major role in the reaction.[17,18]

$$\frac{Q_{t,1}}{Q_{t,2}} = \frac{u_{im,1}^{\ddagger}/\sin(u_{im,1}^{\ddagger})}{u_{im,2}^{\ddagger}/\sin(u_{im,2}^{\ddagger})}$$

$$\dots (8)$$

Within the semi-classical isotope effect for light isotopes, the EXC factor does not contribute much unless the temperature is very high that the first excitation state population is significant. The MMI term generally only contribute trivially to the isotope effect at room temperature but could be the single source of KIE at high temperatures. The ZPE term in equation (5) thus dominates in isotope effects for light isotopes such as hydrogen, deuterium and tritium, and was conveniently used as a good estimation. For heavier isotopes, e.g., ^{13}C, the contribution cannot be simply attributed to only one term and the full expression are generally used for a good approximation.

According to the Bigeleisen-Mayer equation and the Bell tunneling correction, we need to find the vibrational frequencies for all the normal modes for the reactant and the transition state. This is usually achieved by an optimization of stationary point geometries (reactant and saddle point) followed by frequency calculations. Varieties of simulation packages can perform these calculations at different level of theories. Density functional theory (DFT) has been widely employed due to its efficiency and accuracy compares to other methods such as Hartree-Fock or coupled cluster theory where compromises on either accuracy or efficiency have to be made.

1.4 Categories of KIE

In efforts to categorize KIEs, practitioners have chosen to make two general classes of KIE: primary and secondary KIEs. Primary KIEs are defined as arising from isotopic substitution at a position where bond breaking or bond making occurs. Secondary KIEs result from isotopic substitution at positions that don't experience bond breaking or bond making. Regarding the true origins of primary and secondary KIEs, zero-point energy has the dominant role in determining the magnitude of both classes with only rare exceptions. In organic chemical mechanism, ^{2}H and ^{13}C KIEs are the most frequently measured. Between these two types of KIEs, there is something of a division of labor. ^{13}C KIEs typically only become significant at positions of bond making and bond breaking and are therefore most useful in identifying positions of bond making or bond breaking in rate-limiting reaction steps. ^{2}H KIEs are more sensitive and more versatile. Primary ^{2}H KIEs can be used to identify influences from tunneling or gain detailed information about transition structure geometry. Together, primary and secondary KIEs work together to describe the key events that occur in rate- and product-determining steps and to provide structural information about the activated complexes for these reaction steps.

1.4.1 Primary Hydrogen KIE

The mass change in light elements can contribute substantially to ZPE difference in the ground states of reactants. For example, when deuterium replaced the hydrogen in a C-H bond, the reduced mass changed from 0.923 (μ_{C-H}) to 1.714 (μ_{C-H}), a factor of almost 2. This translates to the frequency from an average C-H stretch from 3000 cm^{-1} to around 2200 cm^{-1} for C-D bond according to $\nu = \sqrt{k/\mu}$ (compare to a measured sp3 C-H frequency of 2927 cm^{-1} and C-D 2170 cm^{-1}).[19] In the event of a chemical reaction where the vibrational frequency changes or diminishes at the transition state, the activation energy associated with different isotopologues can be different. This activation energy difference will be revealed by the reaction rate difference through the relationship KIE $\propto$ $e^{(-\Delta\Delta G^{\ddagger}/RT)}$, where $\Delta\Delta G^{\ddagger}$ is the free energy difference between the isotopologues from the reactant to the transition state.
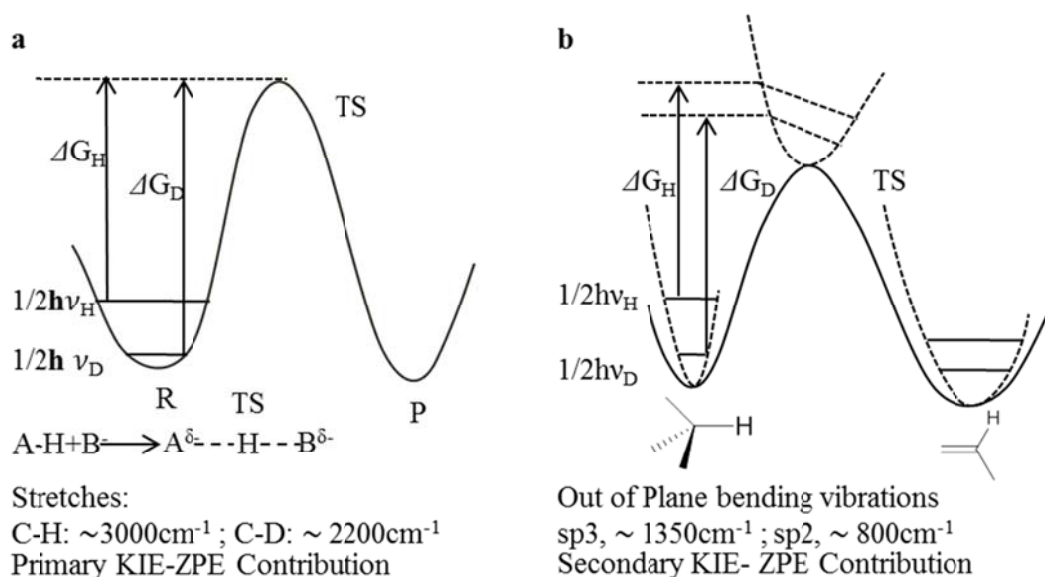
Figure 1: Kinetic isotope effect's origin from zero point energy. a) A complete bond breaking happens at the transition state causes the activation energy difference between C-H and C-D; b) A C-H or C-D bond that's involved in a hybridization of geometry change can vary its vibrational frequency, due to the width change of the potential well.

As shown in Figure 1a, where the isotope of interest is directly involved in the bond breaking and bond formation in the reaction, the KIE is called a primary kinetic isotope effect. For example, in the transition state of a hydride transfer or deprotonation process, the force constant of the stretching mode reduces or diminishes, which results in the ZPE difference between two isotopic reactants greatly contribute to the reaction rate difference. In this case, the activation energy for the perprotiated isotopologue will be smaller than the deuterated isotopologue, $k_H/k_D > 1$. We usually refer to a KIE greater than unity as a normal isotope effect (an inverse one otherwise). According to the Melander[20] and Westheimer[21] three center model for a linear hydrogen transfer reaction, it can reach the upper limit of the semi-classical prediction approximately 6.9 at a temperature of 25° for a C-H bond broken, using the vibrational frequency for C-H stretching as 3000 cm^{-1} and that of C-D bond as 2200 cm^{-1}. However, many reactions go beyond or fall below this limit. Tunneling has proven to contribute greatly to measured KIEs larger than the semi-classical limit; however, tunneling contributions should not be excluded when the KIE falls below it, because there are other factors can lower the KIE. Consider the transition state itself as a "molecule" that possesses $3N^{\ddagger} - 7$ real vibrational modes in total for a non-linear one, where $N^{\ddagger} = N_1 + N_2$, N_1 and N_2 are the number of atoms in two starting materials, which posess $[(3N_1 - 6) + (3N_2 - 6)$ real vibrational modes. There are five more real vibrational modes in the transition state than that are in the reactant, since only one stretching mode is converted into a translational one. Some of the ZPE was conserved in those additional modes, which results in less activation energy difference between isotopologues. Another reason why the measured KIE could be smaller is heavy

atom motion contribution. Although it generally increases the imaginary frequency, which also increases the tunneling contribution to the absolute rate, it usually decreases the ratio $v_{im,H}^{\ddagger}/v_{im,D}^{\ddagger}$ since it decreases the mass sensitivity of the atom being transferred. A third scenario that can result in a lowered KIE is caused by the asymmetry of the transition state. In a highly endergonic or exergonic reaction, if the transition state resembles the structure of a product or reactant, much of the ZPE can be conserved. A quantitative model was developed in the frame of Marcus theory[22] for this explanation. In cases where the transition state is not linear, for example, an intramolecular proton extraction forced to happen at a non-linear angle, a bending mode is converted into a translational one. It decreases the energy difference required to get to the transition state between different isotopologues, compared to what occurs when a stretching mode is being lost, since a bending mode has a much lower vibrational frequency.

1.4.2 Secondary Hydrogen KIE

Secondary KIE reflects the rate difference in the rate-determining step between isotopologues. It is caused by isotopes that are not directly involved in the bond breaking or bond formation in the transition state. A primary KIE can be understood as ZPE differences due to different reduced masses of bonds with different isotopes (e.g. C-H vs. C-D), which have the same force constants but different vibrational frequencies. A secondary KIE can be understood as if bonds with different reduced masses were affected due to a change in the force constant; such is the case with rehybridization or nonbonding steric interactions. It may not be obvious which type of interaction changed the force constant since both might be contributing at the same time. It is convenient to discuss them in bonding and non-bonding interactions caused isotope effects. Both effects involve the change of force constant. As an example in Figure 1b, where the hybridization of a carbon atom is changed from sp^3 to sp^2, the potential well for the bending mode becomes shallower. Thus the force constant becomes smaller. The vibrational frequency for the out of plane bending vibrations reduces from approximately 1350 cm^{-1} to 800 cm^{-1}. This reduction in vibrational frequency decreases the difference between the ZPE of a C-H bond and a C-D bond in the transition state. For this reason, the activation energy for the perprotiated isotopologue is higher than that of the deuterated isotopologue, $k_H/k_D > 1$. However, if the geometry changes from sp^2 to sp^3, the activation energy would cause k_H/k_D to be less than unity, which is an inverse isotope effect.
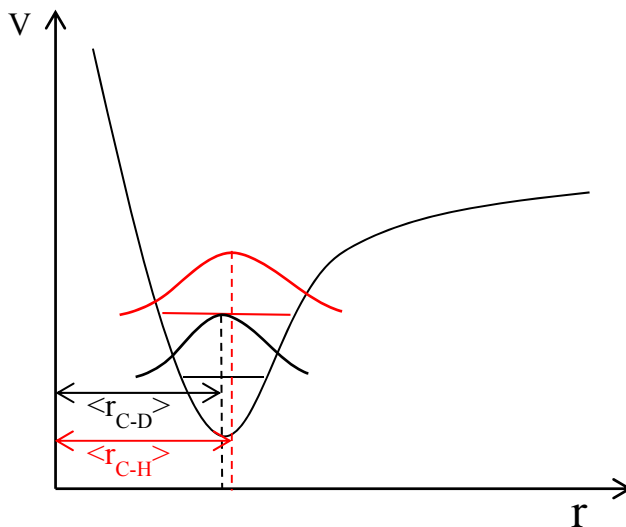
Figure 2: Difference of C-H and C-D bond on the vibrational potential well results in different effective average amplitudes for C-H and C-D vibrations.

Steric isotope effect arises with bonds with different isotopes experiencing different molecular crowding causing changes to force constant. The KIE observations are primarily focused on bonds with isotopes of hydrogen[23–28] in chemical reactions. The origin of hydrogen steric isotope effects can be explained by understanding that the C-H bond sits at a higher level than the C-D bond on the potential well of a quantum oscillator, which describes both C-H and C-D bond. This energy difference, as shown in Figure 2, results in a bigger dispersion of the wave function for a C-H bond compared to a C-D bond. It also results in a C-H bond experiencing more of the anharmonicity of the potential well than a C-D bond does. These differences cause the average amplitude of a C-H vibration larger than that of a C-D vibration. The difference in bond lengths is estimated[4,18,29] on the scale of 0.005 Å. However, highly accurate measurement of the molecular volume of benzene and benzene-d_6 by Dunitz and Ibberson[30] demonstrated that a C-H bond is not always longer than a C-D bond, due to temperature effects on the population of excited states, which could change the average amplitude of a bond. Recently, O'Leary, Meyer and co-workers[31,32] have used enthalpy/entropy ($\Delta H/\Delta S$) dissection of KIE contribution instead of the commonly known Bigeleisen-Mayer equation, to explain an abnormal deuterium steric KIE measured by Mislow and co-workers,[28] for the racemization of a doubly bridged diphenyl diketone. Instead of a real "single" normal steric KIE arising from ZPE differences, which is contradictory to the general notion that deuterium is smaller, they found that the ZPE contribution is indeed inverse but is being masked by an unusually large normal entropy term. This discovery suggests the relative "size" of a C-H and a C-D bond, reflected by an entropy term in KIE that is largely contributed by the excitation states of low frequency modes, can switch under some circumstances.

1.4.3 Heavy Atom Isotope Effect

Heavy elements such as carbon, oxygen, nitrogen, fluorine, phosphorus, sulfur and chlorine are commonly encountered in organic chemistry and biological processes that display isotope effects. Since the mass differences between isotopes of heavy elements are not substantial, the ZPE term does not necessarily dominant the isotope effect. The full expression of the Bigeleisen-Mayer equation for the semi-classical value and the tunneling correction term is generally applied. The calculation of those isotope effects does not require too much extra work, if the frequency calculation has already been performed to obtain the deuterium isotope effects. ^{13}C isotope effects are especially important in organic chemistry attributing to its general involvement in key steps. Although the natural abundance of ^{13}C is only around 1.1%, it allows accurate and site specific measurement with state-of-the-art NMR methods.

1.5 Isotope Effects Measurement Experiments

There are several types of experiments that can be carried out to obtain isotope effects. Each one can afford a unique set of results that is intended to explain a certain aspect of a reaction.[33] Consider deuterium isotope effects as an example as shown in Scheme 1, with an arbitrary C-H functionalization reaction. When the hydrogen in a C-H bond was replaced with a functional group (FG), experiment A requires two reactions being followed kinetically using appropriate analysis techniques. Two rate constants, k_{1-H} and k_{1-D} can be obtained by utilizing rate equations with the concentration of starting materials or products at various stages of the reaction. If there is any difference between the two rate constants, it is the only KIE experiment that can unequivocally prove the disassociation of a C-H bond occurs during the rate-determining step (RDS) in a stoichiometric reaction; or the "turnover limiting step" in a catalytic one.[33] Experiment B is a competitive experiment by putting both isotopologues in the same reaction. A ratio of rate constants k_{1-H}/k_{1-D} is obtained by measuring the fractional conversion (*F*), isotopologue ratio in the starting material (R_0) and re-isolated, unreacted starting material (*R*) (the derivation of how to derive the KIE from these measurable quantities will be shown in Chapter 2).[3] If this ratio is not in unity, it is an indicator that the C-H disassociation might be the RDS, although it is possible that steps prior to substrate binding could be limiting the rate of reaction. For example, such is the case with catalyst activation. Type C experiments can be used to detect isotope effects even after the RDS. The isotope effects can be obtained by directly measuring the concentration ratio of both products. It is important to note that the ratio measured in Experiment C is a compound KIE instead of a simple primary or secondary KIE. Experiments for heavy element isotope effects can be carried out in similar manners. Among the three types experiments, the non-competitive experiment requires fast and accurate measurement of the rate for reactions with different isotopologues, or multiple different initial concentration reactions to extract useful kinetic data. However, this approach is not always possible due to the

rate of reaction, and larger noise associated with in-situ measurements, not to mention the uncertainty brought by the reactions run in different micro environments, especially heterogeneous reactions. The second and third types of experiments, however, guarantee both isotopologues share exactly the same reaction conditions. It can also take advantages of accurate offline measurements. In the next section, we'll discuss the methods for isotope effect measurements utilized over the course of the history of KIE research.
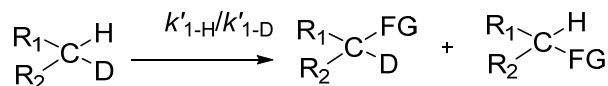
a Inter-molecular noncompetitive experiment
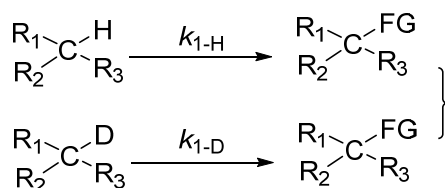
b Intra-molecular competitive experiment
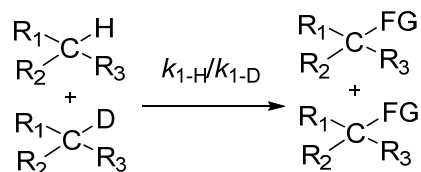
c Intra-molecular competitive experiment

Scheme 1: Different types of KIE experiments illustrated using an arbitrary C-H functionalization reaction. FG stands for functional group. a) An intermolecular, noncompetitive experiment where both isotopologues of a starting material react in different vessels, with two rate constants obtained separately. b) Two isotopologues of the starting material are subject to direct competition in the same experiment. A ratio of two rate constants is obtained. c) An intramolecular KIE experiment using a mono deuterium substituted substrate with either a C-H bond or a C-D bond being functionalized. In this case, a ratio of rate constants is obtained.

In order to obtain isotope effects, concentration ratios need to be measured using appropriate quantification techniques. Theoretically, any method that is able to quantify the concentration of both individual isotopologue, or the ratio of a mixture of isotopologues by utilizing the distinct properties they have, can be used. Numerous books[4,20] and review articles[18,34,35] are dedicated to all aspects of isotope effects and have summarized various methods extensively. Radioactive labeled isotopologues can be easily measured using a scintillator[36] by quantifying ionization energies such as with electrons, alpha particles or gamma ray. This method, which requires radioactive labeling, was employed more in the early stages of isotope effect exploration. However, some isotope effects can only be directly measured this way, such as KIEs for fluorine and phosphorus because they have only one stable isotope.

Mass spectroscopy is another method that has been used to quantify isotopologues. One method is whole molecule mass spectroscopy (WMS),[37] when the relative amount of isotopes are similar. This method is suitable for isotope pairs such as ^{35}Cl & ^{37}Cl, ^{79}Br & ^{81}Br. Since it works by detecting different m/z (mass/charge) ion pairs, the spectrometer quantifies different ions by varying the magnetic field (B) or the potential (V) according to $m/z = B^2 r^2 /2V$, to allow ions with different m/z ratios focusing on the detector sequentially so that the ion current can be measured at each m/z value. This approach creates problems when the ionization voltage becomes unstable during the time of shifting m/z values. It is possible that different isotopologues can have different fractionation thus the accuracy of this method is limited. To overcome these limitations, isotope-ratio mass spectrometry (IRMS)[38–40] was developed for high precision measurement. Although highly accurate, IRMS suffers from a limited scope of applications, due to the requirement of gas samples such as H_2, N_2, CO_2 and SO_2. Organic reactions such as the decarboxylation and nitrogen extrusion that generate gas molecules, which can be directly feed into a mass spectrometer, are suitable for this method. However, most organic reactions would be too complicated to utilize IRMS, due to the long degradation process to prepare appropriate gas samples. If the sample molecule was burned in oxygen to convert to CO_2 for measurement, the isotope effects for carbon would be averaged out over all sites, which returns little scientific value.[4]

Nuclear magnetic resonance (NMR) is by far the most powerful instrument in isotope effect analysis，as well as in general organic chemistry. The advantage of using NMR spectrum for quantification is that all signals are site specific. Isotope effects at different positions can thus be decoupled easily. In the early history of using NMR for KIE measurements, labeling was required to achieve a reasonable signal to noise ratio (S/N). With fast improving magnet and probe technology, natural abundance KIE measurements became a reality. For example, natural abundance ^2H KIE was first reported by Pascal and co-workers.[41] Singleton[42] has introduced the measurement of $^{13}C/^{12}C$ KIE with natural abundance in 1995, an idea comparing to the doubly labeled KIE experiment using mass spectroscopy introduced by O'Leary and Marliar[43] in 1978, but without the need for labeling. This method is capable of taking advantage of the wide range of chemical shifts of ^{13}C nuclei (0-220 ppm), which is very sensitive to the chemical environment.

New methods for various applications are being developed. Meyer and co-workers have used enantiotopic groups to detect the symmetry breaking event for asymmetric reduction of aryl ketone using DIP-chloride.[44] Another new method recently developed by Bennet and co-workers[45,46] utilizes the unique NMR peak patterns (splitting or chemical shift) from existence or lack of coupling between neighboring nuclei, to measure isotopes effects in enzymatic reactions in real time that could not be easily achieved previously, including NMR inactive nuclei pairs such as $^{18}O/^{16}O$.

In the history of employing KIE for mechanistic studies, reactions with multiple products have rarely been selected, although scenarios involving branching reaction have been discussed.[20] Probing reactions that generate side products using KIE measurements usually requires that conditions or substrates to be optimized to make the major product the only clean product. The mechanistic details, the geometry and energetics between different reaction pathways can only be indirectly explained by the difference of substrates or ligands. In the next chapter, we will introduce a method that can provide valuable information about the mechanism of reactions that lead to multi products. This method can also utilize the natural abundance of ^{13}C, which makes it convenient for the mechanistic investigation of reactions with complicated molecules.

1.6 References

(1)   Urey, H. C. *J. Chem. Soc.* **1947**, 562–581.

(2)   Bigeleisen, J.; Wolfsberg, M. In *Advances in Chemical Physics*; Prigogine, I., Ed.; Iterscience Publishers, Inc.: New York, 1958; Vol. 1, pp 15–76.

(3)   Melander, L.; Saunders, Wiliam H., J. *Reaction Rates of Isotopic Molecules*; John Wiley & Sons, Inc: New York, 1980.

(4)   Wolfsberg, M.; van Hook, W. A.; Paneth, P.; Rebelo, L. P. N. *Isotope Effects in the Chemical, Geological, and Bio Sciences*; Springer: New York, 2010.

(5)   *Isotope Effects in Chemistry and Biology*; Kohen, A., Limbach, H.-H., Eds.; Taylor & Francis: Boca Raton, FL, 2006.

(6)   Hammett, L. P. *J. Am. Chem. Soc.* **1937**, *59*, 96–103.

(7)   Blackmond, D. G. *Angew. Chem. Int. Ed.* **2005**, *44*, 4302–4320.

(8)   Polanyi, J. C.; Zewail, A. H. *Acc. Chem. Res.* **1995**, *28*, 119–132.

(9)   Ostrom, H.; Oberg, H.; Xin, H.; LaRue, J.; Beye, M.; Dell'Angela, M.; Gladh, J.; Ng, M. L.; Sellberg, J. A.; Kaya, S.; Mercurio, G.; Nordlund, D.; Hantschmann, M.; Hieke, F.; Kuhn, D.; Schlotter, W. F.; Dakovski, G. L.; Turner, J. J.; Minitti, M. P.; Mitra, A.; Moeller, S. P.; Fohlisch, A.; Wolf, M.; Wurth, W.; Persson, M.; Norskov, J. K.; Abild-Pedersen, F.; Ogasawara, H.; Pettersson, L. G. M.; Nilsson, A. *Science* **2015**, *347*, 978–982.

(10)   Glasstone, S.; Laidler, K. J.; Eyring, H. *The Theory of Rate Processes*; McGraw-Hill Book Company: New York, 1941.

(11)   Szabo, A.; Ostlund, N. S. *Modern Quantum Chemistry: Introduction to Advanced Electronic Structure Theory*, 1st ed.; McGraw-Hill: New York, 1989.

(12)   Anslyn, E. V.; Dougherty, D. A. *Modern Physical Organic Chemistry*; University Science Books: Sausalito, California, 2004; Vol. 43.

(13) McQuarrie, D. A.; Simon, J. D. *Physical Chemistry: A Molecular Approach*; University Science Books: Sausalito, California, 1997.

(14) Redlich, O. *Z. Phys. Chem. B* **1935**, *28*, 371–382.

(15) Cross, P. C.; E. Bright Wilson, J.; Decius, J. C. *Molecular Vibrations: The Theory of Infrared and Raman Vibrational Spectra*, Revised ed.; Dover Publications, Inc: New York, 1980.

(16) Bell, R. P. *Trans. Faraday Soc.* **1959**, *55*, 1.

(17) Northrop, D. B. *J. Am. Chem. Soc.* **1999**, *121*, 3521–3524.

(18) Meyer, M. P. *Adv. Phys. Org. Chem.* **2012**, *46*, 57−120.

(19) Lianca, C. Y.; Pearson, F. G.; Marchessault, R. H. *Spectrochim. Acta* **1960**, *17*, 568–571.

(20) Melander, L. *Isotope Effects on Reaction Rates*; Ronald, New York, 1960.

(21) Westheimer, F. H. *Chem. Rev.* **1961**, *61*, 265.

(22) Marcus, R. A. *J. Phys. Chem.* **1968**, *72* (9), 891–899.

(23) Melander, L.; Carter, R. E. *Acta Chem. Scand.* **1964**, *18*, 1138–1149.

(24) Carter, R. E.; Junggren, E. *Acta Chem. Scand.* **1970**, *24*, 633–643.

(25) Carter, R. E.; Junggren, E. *Acta Chem. Scand.* **1969**, *23*, 504–514.

(26) Carter, R. E.; Junggren, E. *Acta Chem. Scand.* **1968**, *22*, 503–508.

(27) Carter, R.; Liljefors, T. *Tetrahedron* **1976**, *32*, 2915–2922.

(28) Mislow, K.; Glass, M. A. W.; Hopps, B.; Simon, E.; Wahl, G. H. *J. Am. Chem. Soc.* **1964**, *86*, 1710.

(29) Bartell, L. S. *Tetrahedron Lett.* **1960**, No. 6, 13–16.

(30) Dunitz, J. D.; Ibberson, R. M. *Angew. Chem. Int. Ed.* **2008**, *47*, 4208–4210.

(31) O'Leary, D. J.; Rablen, P. R.; Meyer, M. P. *Angew. Chem. Int. Ed.* **2011**, *50*, 2564–2567.

(32) Fong, A.; Meyer, M.; O'Leary, D. *Molecules* **2013**, *18*, 2281–2296.

(33) Simmons, E. M.; Hartwig, J. F. *Angew. Chem. Int. Ed.* **2012**, *51*, 3066–3072.

(34) Paneth, P. *Talanta* **1987**, *34*, 877–883.

(35) Gu, H.; Zhang, S. *Molecules* **2013**, *18*, 9278–9292.

(36) Parkin, D. W. In *Enzyme Mechanism from Isotope Effects*; Cook, P. F., Ed.; Boca Raton, FL, USA, 1991; p 269–290.

(37) Zakett, D.; Flynn, R. G. A.; Cooks, R. G. *J. Phys. Chem.* **1978**, *82* (22), 2359–2362.

(38) Weiss, P. F. In *Enzyme Mechanism from Isotope Effects*; Cook, P. F., Ed.; CRC Press: Boca Raton, FL, USA, 1991; p 291–312.

(39) *Encyclopaedia of Analytical Science*; Townsend, A., Ed.; Academic Press Limited: London, UK, 1995.

(40) Gilbert, A.; Hattori, R.; Silvestre, V.; Wasano, N.; Akoka, S.; Hirano, S.; Yamada, K.; Yoshida, N.; Remaud, G. S. *Talanta* **2012**, *99*, 1035–1039.

(41) Pascal, R. A.; Baum, M. W.; Wagner, C. K.; Huang, D. *J. Am. Chem. Soc.* **1986**, No. 6, 6477–6482.

(42) Singleton, D. A.; Thomas, A. A. *J. Am. Chem. Soc.* **1995**, *117*, 9357–9358.

(43) O'Leary, M. H.; Marlier, J. F. *J. Am. Chem. Soc.* **1978**, *100*, 2582–2583.

(44) West, J. D.; Stafford, S. E.; Meyer, M. P. *J. Am. Chem. Soc.* **2008**, *130*, 7816–7817.

(45) Chan, J.; Lewis, A. R.; Gilbert, M.; Karwaski, M.-F.; Bennet, A. J. *Nat. Chem. Biol.* **2010**, *6*, 405–407.

(46) Chan, J.; Tang, A.; Bennet, A. J. *J. Am. Chem. Soc.* **2012**, *134*, 1212–1220.

Chapter 2: Development of Product-Specific Kinetic Isotope Effects

In Chapter 1, the principles of KIE measurement were discussed. One primary limitation to KIE measurement has been that KIE interpretation is difficult in reactions that do not proceed cleanly in high yield. We will now discuss the origins and development of product-specific KIEs, a mechanistic methodology that allows interrogation of multi-product reactions. Initially, isotopically labeled starting materials were used to measure isotope effects of reactions where a single, dominant product was formed, a spot to spot reaction. The derivation of these KIE's had been carried out by Bigeleisen and Wolfsberg.[1] The work was also presented by Melander and Saunders.[2] Initially, isotope effects were generally measured employing radiolabeled substrates and scintillation counting or high-resolution mass spectrometry. Singleton achieved simultaneously measurements of multiple sites, without the requirement of laborious labeling, using ^{13}C and ^{2}H at natural abundance.[3,4] It is important to note that the study of complicated mechanism has always been a goal of mechanistic research. Other probing methods such as direct kinetic analysis, have been applied to branching reactions where more than one pathway fractionates the isotopically labeled molecules.[2,5,6] These isotope effects, by definition, can be attributed to be product-specific. However, the ability of direct rate monitoring, in most cases, can only been applied to reactions of tailored systems with a relatively slow reaction rate. Although it should be stated that direct rate monitoring has improved greatly with faster and high throughput analysis techniques, such as NMR, GC-MS, LC-MS and React IR. Generally speaking, the information obtained from direct kinetic methods is limited to the rate-determining step which may or may not be the step where selectivity is concerned, such as the cases of diffusion processes or catalyst activation. KIE measurement is an advantageous mechanistic technique because accurate measurements can be done without the time constraints of most kinetic methods by using carefully reisolated starting material or product regardless of the rate of the reaction, even when fractionation occurs after the rate-determining step.[7–10] KIE methods applied to single pathway reactions account for isotopic fractionation by either analyzing the reisolated starting material or the purified single product. When a multi-pathway reaction was analyzed by the conventional method, accurate isotopic fractionation information would be obtained only if these multiple pathways share the same rate-determining step preceding product determination; otherwise, in the case of concurrent rate- and product-determining steps, the measured KIE would just be a weighted average. This approach, although useful in explaining some aspects of a reaction mechanism, does not provide much insight when the geometry and energetic landscape of multiple pathways are compared with respect to reactivity and selectivity origins.

Conventional KIE measurement with NMR utilizes the fact that atoms are conserved before and after a chemical reaction. In a single product reaction, the competing isotopes

in the starting material are partially converted to product. We can calculate the KIE using any three of the four factors that can be quantified, herein named as R_0, R, R_p, F, referring to the isotopic ratio in the starting material, reisolated starting material, product and the fractional conversion, respectively. Depending on the specific case, one of the two reciprocal quantities: R or R_p (isotopic ratio of the starting material or the product) is utilized to calculate the KIE. At low percent conversion, R_p is the preferred measurement; at a high percent conversion, R is preferred. It is due to the degree of enrichment of one isotope in either the product or the starting material. In the case of a multi-product reaction, of course, the isotopes are still conserved in the materials and the products. Therefore, there exists a way to calculate the fractionation of the different products which results in isotope effects for different reaction pathways. The presence or lack of an isotope effect at any given position can provide information regarding steps vital for the selectivity of a reaction. This ultimately allows us to compare the results with computationally modeled transition states for further mechanistic insights.

2.1 Conventional KIE derivation

The derivation here will include the conventional intermolecular kinetic isotope effect that has already been presented in the previous mentioned work for the continuity of this chapter.[2,3] All of the following derivation including the product-specific KIE itself can be found in the following publication.[11]

Assume a general chemical reaction

$$A + B + C + \cdots \xrightarrow{\;k\;} P_1 + P_2 + \cdots$$
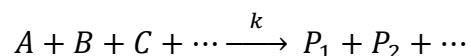
where A stands for the reactant which is partially labeled, $B, C, $ ...stand for other starting materials that are not isotopically labelled or sensitive. P_1, P_2, ...are products contain the isotopically labeled moiety in reactant A. For simplicity, we'll restrict ourselves to the case with only two products at this stage of the derivation. This could easily be expanded to situations where more than two products are being generated. Assuming first order kinetics[①] for reactant A where two isotopologues are competing in the reaction and the other reactants being involved in a similar manner (chemo-, regio-, diastereio- and enantio-selective reactions):

$$A^* + B + C + \cdots \xrightarrow{\;k^*\;} P_1^* + P_2^* + \cdots$$
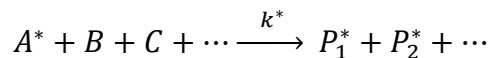
[①] For higher order kinetics, if one of the isotopologue only present in a trace amount, the treatment is very similar to first order, as demonstrated by Melander and Saunders;[2] If both isotopologues are present in a substantial amount, it is out of reach of this chapter. Such cases would not concern the studies in the following chapters.

where A^*, P_1^*, P_2^* stand for the heavier isotopologues of the starting material and corresponding products. The rate law for the depletion of A and A^* are:

$$\frac{d[A]}{dt} = k \,[\text{A}][\text{B}]^x[C]^y[...]^z$$

$$\frac{d[A^*]}{dt} = k^*[A^*][\text{B}]^x[C]^y[...]^z$$

Taken the ratio of these two equations,

$$\frac{d[A]}{d[A^*]} = \frac{k[A]}{k^*[A^*]}$$

Rearrange and integrate:

$$\frac{d[A]}{[A]} = \frac{k}{k^*} \times \frac{d[A^*]}{[A^*]}$$

to yield the rate ratio:

$$\frac{k}{k^*} = \frac{\ln([A]_t/[A]_{t0})}{\ln([A^*]_t/[A^*]_{t0})}$$

where t_0 and t denote the time when the reaction is initiated and stopped, respectively. This equation could also be expressed using the fractional conversion of each starting isotopologue:

$$\frac{k}{k^*} = \frac{\ln(1-F)}{\ln(1-F^*)}$$

This equation is generally served for the isotopic fractionation of the starting material. It applies when the percent conversion can be measured separately for both isotopologues. Now consider the ratios, we define R_0 and R as the ratio between isotopologues of the starting material and the reisolated starting material:

$$R_0 = \frac{[A]_{t0}}{[A^*]_{t0}} \text{ and } R = \frac{[A]_t}{[A^*]_t}$$

This relationship would afford:

$$[A^*]_{t0} = \frac{[A]_{t0}}{R_0} \text{ and } [A^*]_t = \frac{[A]_t}{R}$$

Since:

$$F = 1 - \frac{[A]_t}{[A]_{t0}} \quad and \quad F^* = 1 - \frac{[A^*]_t}{[A^*]_{t0}}$$

In case where one of the isotopologues is only present in a trace amount, for example, natural abundance ^{13}C or radioactive isotopes, the percent conversion of the abundant isotopologue would be very close to the percent conversion of the combined species. Define the percent conversion for both of the isotopologues as:

$$F_{all} = \frac{[A]_t + [A^*]_t}{[A]_{t0} + [A^*]_{t0}}$$

Then,

$$F \approx F_{all}$$

and we can express $1 - F^*$ as a function of $F, R \; and \; R_0$ by replacing $[A^*]_t$ with $[A]_t/R$ and $[A^*]_{t0}$ with $[A]_{t0}/R_0$:

$$1 - F^* = (1 - F_{all}) \frac{R_0}{R}$$

The kinetic isotope effect could be expressed as:

$$\frac{k}{k^*} = \frac{\ln(1 - F)}{\ln(1 - F^*)} = \frac{\ln[(1 - F_{all})]}{\ln[(1 - F_{all}) R_0/R]}$$

It is important to note that, in cases where ^{13}C is measured at natural abundance levels by NMR, the ratio of $^{12}C/^{13}C$ cannot be directly measured. Instead, a reference carbon position that is considered to not be involved in the fractionation event, is defined as a standard reference.[3,12] The relative concentration of other carbon positions are obtained by comparing the integration of its signal to that of the standard position. This integration ratio is thus a relative one. If we define R'_0 and R' as $^{13}C/^{12}C$ at the beginning of the reaction and the end of the reaction, we can rewrite the expression for ^{13}C isotope effects as:[4]

$$KIE = \frac{^{12}k}{^{13}k} = \frac{\ln(1 - {}^{12}F)}{\ln(1 - {}^{13}F)} = \frac{\ln(1 - F_{all})}{\ln[(1 - F_{all}) R'/R'_0]}$$

The error for each measurement could be determined by propagation of the standard deviation of the integrated value for each quantity from multiple NMR spectra:

$$\Delta\text{KIE} = \sqrt{\left(\frac{\partial \; KIE}{\partial \; F_{all}} * \Delta F_{all}\right)^2 + \left(\frac{\partial \; KIE}{\partial \; R'} * \Delta R'\right)^2 + \left(\frac{\partial \; KIE}{\partial \; R'_0} * \Delta R'_0\right)^2}$$

$$\frac{\partial \, KIE}{\partial \, F_{all}} = \frac{-1}{(1 - F_{all}) * \ln[(1 - F_{all}) \, R'/R'_0]} + \frac{\ln(1 - F_{all}) * F_{all} * R'/R'_0}{\{\ln[(1 - F_{all}) \, R'/R'_0]\}^2}$$

$$\frac{\partial \, KIE}{\partial \, R'} = \frac{-\ln(1 - F_{all})}{R' * \{\ln[(1 - F_{all}) \, R'/R'_0]\}^2}$$

$$\frac{\partial \, KIE}{\partial \, R'_0} = \frac{\ln(1 - F_{all})}{R'_0 * \{\ln[(1 - F_{all}) \, R'/R'_0]\}^2}$$

Multiple repetitions of the same experiment are generally performed to achieve better precision, the final value utilized for mechanism investigation is an error-weighted average of measured KIEs.[13] Let w_i be the weighting factors for value KIE_i,

$$w_i = 1/\Delta KIE_i{}^2$$

Then the weighted average is:

$$\overline{KIE} = \frac{w_1 * KIE_1 + w_2 * KIE_2 + \cdots + w_i * KIE_i}{w_1 + w_2 + \cdots + w_i}$$

Let's consider another scenario where both isotopologues exist with a substantial concentration, for example, proton and deuterium labeled materials. If the percent conversion of the two isotopologues can be measured separately, then the following equation can be directly used for KIE calculation.

$$KIE = \frac{k}{k^*} = \frac{\ln(1 - F)}{\ln(1 - F^*)}$$

However, if the percent conversion can only be measured or is easier to measure as a whole for both isotopologues, substitution of $[A^*]_t$ with $[A]_t/R$ and $[A^*]_{t0}$ with $[A]_{t0}/R_0$ in the expression for F_{all} affords:

$$F_{all} = 1 - \frac{[A]_t \left(1 + \frac{1}{R}\right)}{[A]_{t0} \left(1 + \frac{1}{R_0}\right)} = 1 - (1 - F) \frac{\left(1 + \frac{1}{R}\right)}{\left(1 + \frac{1}{R_0}\right)}$$

Thus:

$$1 - F = (1 - F_{all}) \frac{(1 + 1/R_0)}{(1 + 1/R)}$$

Similarly:

$$1 - F^* = (1 - F_{all}) \times \frac{(1 + R_0)}{(1 + R)}$$

Now the intermolecular KIE could be expressed as:

$$KIE = \frac{k}{k^*} = \frac{\ln(1-F)}{\ln(1-F^*)} = \frac{\ln[(1-F_{all})\,(1+1/R_0)/(1+1/R)]}{\ln[(1-F_{all})\,(1+R_0)/(1+R)]}$$

The error propagation is carried out in the same manner as previously shown to derive the error-weighted average.

$$\Delta KIE = \sqrt[2]{\left(\frac{\partial\, KIE}{\partial\, F_{all}} * \Delta F_{all}\right)^2 + \left(\frac{\partial\, KIE}{\partial\, R} * \Delta R\right)^2 + \left(\frac{\partial\, KIE}{\partial\, R_0} * \Delta R_0\right)^2}$$

$$\frac{\partial\, KIE}{\partial\, F_{all}} = \frac{-1}{(1-F_{all}) * \ln[(1-F_{all})\,(1+R_0)/(1+R)]}$$
$$+ \frac{1}{(1-F_{all}) * \{\ln[(1-F_{all})\,(1+R_0)/(1+R)]\}^2}$$

$$\frac{\partial\, KIE}{\partial\, R} = \frac{1/R^2}{(1+1/R) * \ln[(1-F_{all})\,(1+R_0)/(1+R)]}$$
$$+ \frac{1}{(1+R) * \{\ln[(1-F_{all})\,(1+R_0)/(1+R)]\}^2}$$

$$\frac{\partial\, KIE}{\partial\, R_0} = \frac{-1/R_0^2}{(1+1/R_0) * \ln[(1-F_{all})\,(1+R_0)/(1+R)]}$$
$$+ \frac{-1}{(1+R_0) * \{\ln[(1-F_{all})\,(1+R_0)/(1+R)]\}^2}$$

2.2 Product-specific KIE derivation

Section 2.1 is primarily concerned with isotopic fractionation of the starting material. The only species of concern is the substrate which is isotopically labeled, *A*. Contributions from all other species cancel out in the determination of the KIE as a rate constant ratio. In the following derivation, other reactants are omitted for simplicity. Now consider the rate constants for the formation of each product:

$$A \xrightarrow{k_1} P_1 \; and \; A \xrightarrow{k_2} P_2$$

$$A^* \xrightarrow{k_1^*} P_1^* \; and \; A^* \xrightarrow{k_2^*} P_2^*$$
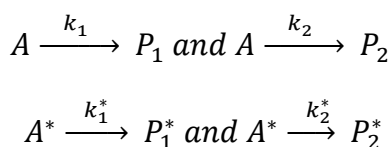
The rate equations for the formation of each product from the unlabeled A are:

$$\frac{d[P_1]}{dt} = k_1 [A] \text{ and } \frac{d[P_1]}{dt} = k_2 [A]$$

Integration of the products affords:

$$\int d[P_1] = k_1 \int_0^t [A]dt = [P_1]$$

$$\int d[P_2] = k_2 \int_0^t [A]dt = [P_2]$$

Take the ratio of those two expressions we can get:

$$\frac{k_1}{k_2} = \frac{[P_1]}{[P_2]}$$

Similarly for the labeled A^*:

$$\frac{k_1^*}{k_2^*} = \frac{[P_1^*]}{[P_2^*]}$$

Now, since the intermolecular KIE can be expressed as:

$$KIE_{inter} = \frac{k}{k^*} = \frac{k_1 + k_2}{k_1^* + k_2^*}$$

Replacing k_2 by $k_1 * [P_2]/[P_1]$ and k_2^* by $k_1^* * [P_2^*]/[P_1^*]$, the intermolecular KIE could be written as:

$$KIE_{inter} = \frac{k_1 + k_2}{k_1^* + k_2^*} = \frac{k_1 (1 + \frac{[P_2]}{[P_1]})}{k_1^*(1 + \frac{[P_2^*]}{[P_1^*]})}$$

Thus the product specific KIE for P_1 can be expressed with KIE_{inter} and product ratio terms. R_p and R_p^* stand for the ratio of unlabeled and labeled products, P_2 to P_1 and P_2^* to P_1^*, respectively.

$$KIE_{P_1} = \frac{k_1}{k_1^*} = KIE_{inter} \times \frac{1 + \frac{[P_2^*]}{[P_1^*]}}{1 + \frac{[P_2]}{[P_1]}} = KIE_{inter} \times \frac{1 + R_p^*}{1 + R_p}$$

Note that the two product ratios are directly measured, the error propagation for the product-specific KIE is:

$$\Delta KIE_{P_1} =$$

$$\sqrt[2]{\left(\frac{\partial \ KIE}{\partial \ KIE_{inter}} \times \Delta KIE_{inter}\right)^2 + \left(\frac{\partial \ KIE}{\partial \ R_p^*} \times \Delta R_p^*\right)^2 + \left(\frac{\partial \ KIE}{\partial \ R_p} \times \Delta R_p\right)^2}$$

The product-specific KIE can also be written as:

$$KIE_{P_1} = \frac{k_1}{k_1^*} = KIE_{inter} \times \frac{\frac{[P_1^*] + [P_2^*]}{[P_1^*]}}{\frac{[P_1 \ ] + [P_2 \ ]}{[P_1 \ ]}}$$

For reactions that generate more than two products, it is easy to observe that if we have product P_i formed with its associated rate constant k_i , then the product-specific KIE for P_i would be:

$$KIE_{P_i} = \frac{k_i}{k_i^*} = KIE_{inter} \times \frac{\frac{\sum_{i=1}^{j}[P_i \ ]}{[P_i \ ]}}{\frac{\sum_{i=1}^{j}[P_i^*]}{[P_i^*]}}$$

Or:

$$KIE_{P_i} = \frac{k_i}{k_i^*} = KIE_{inter} \times \frac{\sum_{j=1}^{j}(\frac{[P_j \ ]}{[P_i \ ]})}{\sum_{j=1}^{j}(\frac{[P_j^*]}{[P_i^*]})} = KIE_{inter} \times \frac{\sum_{j=1}^{j} R_{ji}}{\sum_{j=1}^{j} R_{ji}^*}$$

Where R_{ji} and R_{ji}^* are the ratio of the *j*th product to product *i* for unlabeled and labeled products. This formula shows that the product-specific KIE can be expressed as a product of the intermolecular KIE and sets of product ratios. This method can, in principle, be extended to reactions that yield more than two products. The product ratio can be measured by various analytical methods, as long as it can afford the corresponding ratio. Currently, it would be easier with NMR if multiple positions are concerned. With natural abundance ^{13}C isotope effects, the product ratio can be determined for each specific carbon since they experience different degrees of fractionation. NMR cannot directly measure the concentration of ^{12}C, therefore the ratio of peak integrations corresponding to different products at a standard carbon site was used for all ^{12}C ratios. The standard

24

carbon is selected in the manner applied to the Singleton method, a position where fractionation is unlikely to occur. The primary limitation is the measurement of product ratios, which depends upon the amount of product being assayed and the ability to resolve all positions of all products and reactants in the ^{13}C NMR spectrum. In the next two chapters, conventional and product-specific KIE methods are employed to give insight into the mechanism of rhodium catalyzed C-H functionalization and cobalt catalyzed [2+2] and Alder-ene reaction.

2.3 References

(1)   Bigeleisen, J.; Wolfsberg, M. In *Advances in Chemical Physics*; Prigogine, I., Ed.; Iterscience Publishers, Inc.: New York, 1958; Vol. 1, pp 15–76.

(2)   Melander, L.; Saunders, Wiliam H., J. *Reaction Rates of Isotopic Molecules*; John Wiley & Sons, Inc: New York, 1980.

(3)   Singleton, D. A.; Thomas, A. A. *J. Am. Chem. Soc.* **1995**, *117*, 9357–9358.

(4)   Singleton, D. A.; Szymanski, M. J. *J. Am. Chem. Soc.* **1999**, *121*, 9455–9456.

(5)   Thibblin, A.; Bengtsson, S.; Ahlberg, P. *J. Chem. Soc., Perkin Trans. 2* **1977**, 1569–1577.

(6)   Thibblin, A.; Ahlberg, P. *J. Am. Chem. Soc.* **1977**, *99*, 7926–7930.

(7)   Simmons, E. M.; Hartwig, J. F. *Angew. Chem. Int. Ed.* **2012**, *51*, 3066–3072.

(8)   Brown, S. N.; Myers, A. W.; Fulton, J. R.; Mayer, J. M. *Organometallics* **1998**, *17*, 3364–3374.

(9)   Sibbald, P. A.; Rosewall, C. F.; Swartz, R. D.; Michael, F. E. *J. Am. Chem. Soc.* **2009**, *131*, 15945–15951.

(10)   Zhu, H.; Clemente, F. R.; Houk, K. N.; Meyer, M. P. *J. Am. Chem. Soc.* **2009**, *131*, 1632–1633.

(11)   Xiang, S.; Meyer, M. P. *J. Am. Chem. Soc.* **2014**, *136*, 5832–5835.

(12)   O'Leary, M. H.; Marlier, J. F. *J. Am. Chem. Soc.* **1978**, *100*, 2582–2583.

(13)   Mandel, J. *The Statistical Analysis of Experimental Data*; Dover Publications, Inc, New York: Washington, D.C., 1964.

Chapter 3: Mechanistic Study of

Cobalt Catalyzed [2+2] Cycloaddition and Alder-ene Reaction

3.1 Background and Previous Work

Elements such as cobalt, iron and other first row transition metals have been drawing more attention due to their abundance and low cost when compared to heavier precious metal elements such as palladium, ruthenium and rhodium. With similar electronic configuration in the periodic table between the ones in the same column, they are all capable of catalyzing a variety of reactions. However, the associated catalysts developed for the first-row transition metals Co, Fe and Ni have not been as successful as their precious metal competitors. With the increasing demand of cheaper and environmentally sustainable catalytic systems, first-row transition metal catalysts are under intensive developing. For example, cobalt has been found to be a versatile metal in catalyzing chemical reactions such as cycloaddition, coupling and ring expansion reactions.[1] However, the diverse nature of the reactivity also poses those cobalt-catalyzed reactions with side reactions that lower the yield and selectivity.[1–7] Traditional mechanistic probes are limited to rate law determination, crystal structures, thermal chemistry on a few clean reaction systems and thus computational efforts are also largely trying to reproduce these data. These approaches have been no doubt generating valuable data as will be reviewed later; however, the most valuable information in the transition states has not been approached frequently using the powerful tool of kinetic isotope effect, which can be coupled with advanced computational chemistry tool to explain the reactivity and selectivity accurately and quantitatively. The underlying reason is that conventional KIE methods only allow clean reactions to be studied, where only the information of a single step in a reaction can be obtained by analyzing the reisolated starting material or the solely product.[8–11] This issue can be addressed now using our newly developed product-specific KIE method, which can accommodate multiple products in theory as long as the ratio of products can be analyzed.

In this Chapter, we will try to understand the mechanism of cobalt complexes catalyzed reactions recently developed in Hilt's group.[12–14] By using different ligands, two distinct products were generated from the same starting materials. When dppp (1,3-bis(diphenylphosphino)propane) or dppe (1,2-bis(diphenylphosphino)ethane) were used as ligands, the reaction generates preferentially either [2+2] or Alder-ene products, respectively[14] as shown in Scheme 1. As the ultimate goal of physical organic chemistry is to understand the factors affecting reactivity and selectivity, totally different behavior of the same reaction system caused by a difference of one methylene tether between dppp and dppe ligand drew our attention naturally. Which factor is governing the reaction, electronic or geometry factor (biting angle, steric hindrance) of the ligands given that they are the only noticeable difference?

The hypothesis provided by Hilt and co-workers[14] (Scheme 2) for reaction in Scheme 1a will be tested using product-specific ^{13}C and ^{2}H isotope effects, which would provide rich information about the transition states, rate- and product- determining steps. It would be optimal to test reaction B also; however, the slow reaction rate and possible multiple trimerization products of this reaction make it more economical and feasible to study when the analytic power becomes stronger in the future. Instead, a different starting material, norbornene (see Scheme 4) will be used.[13,14] Coupled with either dppp or dppe as the ligand, these two reactions would generate the same product due to the unlikelihood of β hydrogen transfer according to Bredt's rule,[15–17] which states that a double bond cannot be formed at a bridgehead in a bridged ring system. In this case, isotope effects shown in processes with different ligands can provide us insights into the nature of how the two ligands interacting differently with other parts of the complex in their transition states.
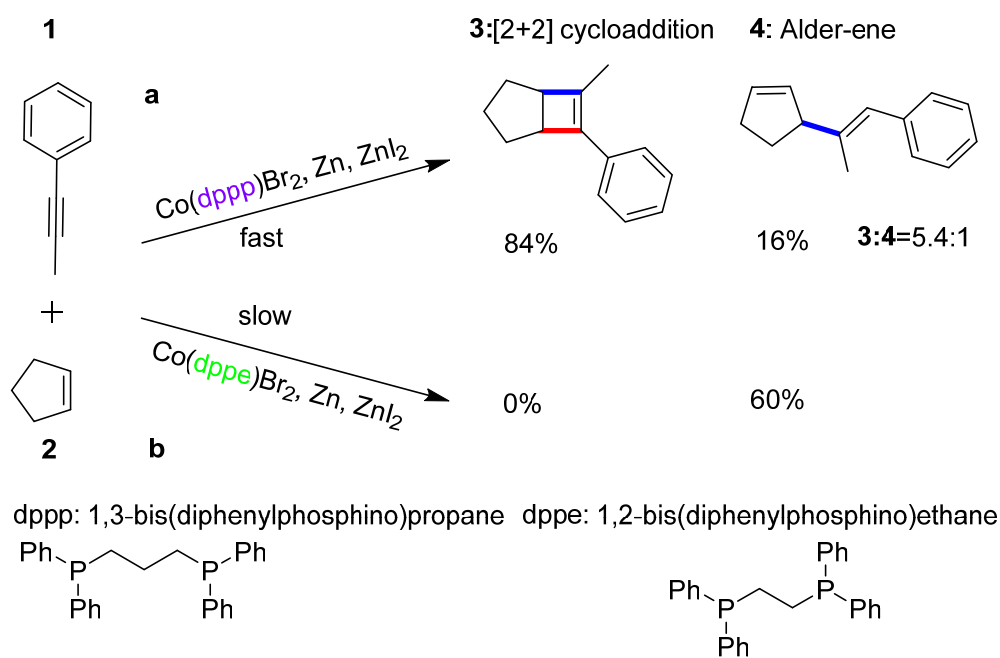
Scheme 1: a) CoBr$_2$(dppp) catalyzed [2+2] cycloaddition and Alder-ene reaction. b) CoBr$_2$(dppe) catalyzed Alder-ene reaction only generates Alder-ene product without 100% yield[14] (the possibly side products are trimerization products such as 1,3,5- or 1,2,4-triphenylbnzene.)

As shown in Scheme 2, cyclopentene and 1-phenylpropyne are thought to form complex I_1 then convert to intermediate I_2. This intermediate will either go through reductive elimination to form the [2+2] product **2** or a β-hydride transfer to I_3, which finally leads to product **3** that resembles an ene reaction product. It would be ideal to test the existence of I_2 and I_3, and their plausibility of involvement in the catalytic cycle. Prior to a discussion of results, however, past mechanistic studies on similar Co-catalyzed couplings serve to inform mechanistic expectations.
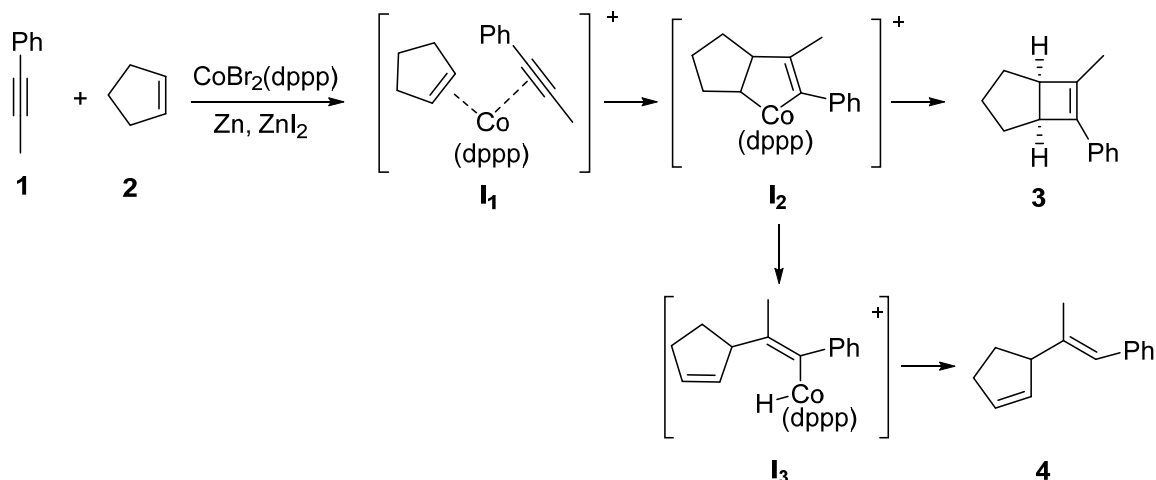
Scheme 2: Putative reaction mechanism proposed by Hilt and co-workers[14]

3.2 General Mechanistic Considerations

The role of each component plays in the reaction needs to be considered. Cobalt bidentate compounds such as $CoBr_2(dppp)$ and $CoBr_2(dppe)$, which are used as catalysts for this study, were initially prepared and characterized by Horrocks, Hecke and Hall in 1966[18] when they found these compounds bear a pseudo-tetrahedral conformation. Zinc is used as a reductant to produce low valent cobalt. The use of cobalt(I) complexes as catalysts for coupling reactions date back to Lyons and co-workers.[19,20] Their catalytic system is composed of cobalt(III) acetylacetonate, $[Co(acac)_3]$, diethylaluminum chloride (Et_2AlCl). The aluminum reagent reduces Co(III) to Co(I)), whose dppe complex catalyzes [2+2+2] cycloaddition reactions between norbornadiene and acetylenic hydrocarbons. This catalytic system overcame the hurdle of low reactivity encountered by electron withdrawing free, unactivated propyne. The combination of $[CoI_2(PPh_3)_2]$ and zinc powder was developed by Cheng and co-workers[21] resulted in higher activity than when acetoacetate (acac) was used as a catalyst ligand. Hilt[22] found that the replacement of reducing agent Zn by other reagents such as borohydrides and aluminum hydrides only afford little Diels-Alder product, except alanes (DIBAL, diisobutylaluminum hydride). That is when they introduced a Lewis acid ZnI_2 into the catalytic system and used it in varieties of reactions catalyzed by low valent cobalt catalyst such as homo Diels-Alder reaction,[22,23] reductive coupling reactions of alkenes and alkynes,[2,6] cycloaddition,[7,12–14] Alder-ene reaction.[14,24,25] At the meantime, they found that there is an induction period which depends on the reductant being used. It is somewhat long with zinc. This is confirmed in our study when using zinc powder as received; however, if zinc powder is treated with dilute hydrochloride acid and thoroughly dried prior to use, the induction period becomes insignificant compared to about 30 minutes when left untreated. This result also confirms the reductant role of zinc powder since it is related to the available

nonoxidized zinc. The Lewis acid have two functions as pointed out by Cheng and co-workers.[2] On one hand, it can remove one halogen coordinator (Br^-, I^-) from the reduced cobalt complex, to form a more active cationic cobalt complex with an empty coordination site. On the other hand, it can possibly activate the dienophile in Diels-Alder reaction. The functions of Zn and ZnI_2 have been confirmed by Hilt, Schafer[26] and coworkers by studying the gas phase catalyst complexes using electrospray ionization mass spectrometry (ESI-MS). The study employs [$CoBr_2(dppe)$] as the pre-catalyst for the formation of Diels-Alder product between isoprene and phenyl acetylene in acetonitrile (ACN). The major forms of the catalyst complexes they found experimentally are [Co(II) Br(dppe)]$^+$ and [Co(I)(dppe)]$^+$ before and after reduction, respectively. The active catalyst exists in the form of Co(I) is in line with their calculation result that the enthalpy of formation for a [Co(II)(dppe)isoprene] complexes is much lower than that [Co(I)Br(dppe)isoprene].[26,27] Based on this information, a catalytic cycle was proposed for this reaction. It starts from an 18 electron solvated cobalt complex, [Co(II)Br(dppe)(ACN)$_3$], which is then reduced by the Zn/ZnI$_2$ system. The reduced cobalt complex incorporates both of the starting materials (preferably with isoprene compares to the phenyl acetylene) leading to the formation of a cobaltacycle. The cobaltacycle will release the product, and the catalyst is regenerated at the same time.
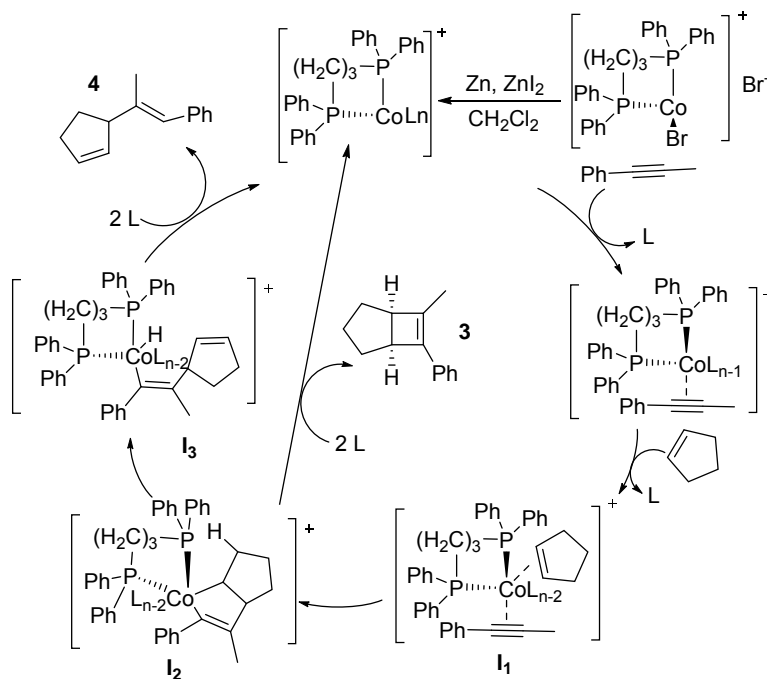
Scheme 3: A proposed catalytic cycle for the Alder-ene and [2+2] cycloaddition reaction catalyzed by CoBr$_2$(dppp) based on reviewed literature.

Here is a catalytic cycle (Scheme 3) we propose based on previous studies. A few features in this cycle need to be compared to the isoprene-phenyl acetylene substrates system. First of all, in the context of competing for coordination sites that leading to

reaction, the solvent should be able to dissolve the catalyst but not act as a good coordinator, such as dichloromethane or 1,2-dichloroethane but not tetrahydrofuran, for instance.[21] Dichloromethane was used for this reaction instead of a coordinative solvent like acetonitrile, which was employed in the previously discussed study of intermediates.[14,26] Thus the likelihood of coordination is not as high as acetonitrile, although dichloromethane has been shown to be incorporated into the coordination sphere of other metals.[28,29] This issue will have to be addressed computationally. Secondly, we propose the phenyl propyne coordinates prior to cyclopentene, analogous to the isoprene-phenyl acetylene system. One reason is that alkynes generally form more stable π-complexes than alkenes; however, the bidentate nature of a diene might reverse preferential coordination such that cyclopentadiene is preferred. During a mechanistic study of triphenylphosphine coordinated cobalt, which involved formation and reaction of cobaltacyclopentadiene and cobaltacyclopentene by Wakatsuki,[30] the complex $[(\eta^5\text{-}C_5H_5)(PPh_3)Co(CO_2Me\text{-}C\equiv C\text{-}CO_2Me)]$ was found to react with alkene but not the other way around if the alkene was coordinated first. This preference or affinity is potentially relevant to deuterium isotope effects which we will discuss later. Although in the same study they found that the coordination of the alkyne requires departure of the triphenylphosphine ligand, since coordination sites are limited due to the existence of the η^5-cyclopentadiene ligand; it is not necessary with the dppp as the only ligand since there is enough space and coordination sites. In the same reference, experimental results show that the bulkier group preferably resides close to the cobalt center when cobaltacyclopentene ring was formed, which is consistent with the placement of the phenyl-bearing carbon adjacent to the Co in the cobaltacyclopentene intermediate (**I₂**). Regarding chemo-selectivity, dppp and dppe ligands render different electronic effects upon the Co center via bite angle. These ligands also provide a different steric environment for the coupling partners, altering the preferences for the Alder-ene pathway and the [2+2] pathway. Given the sum of previous mechanistic work, it would not be an unreasonable idea to assume that the reaction is under kinetic control. When dppp is used, the hydride transfer occurs preferentially. When dppe was used, both reaction channels slow down (evidenced by prolonged reaction time), the cobalt complex might be too rigid to allow the β-hydride transfer to occur in a rate that's comparable to the [2+2] pathway.

3.3 ^{13}C Kinetic Isotope Effects[31]

The materials in this section were adapted with permission from "Xiang, S.; Meyer, M. P. *J. Am. Chem. Soc.* **2014**, *136*, 5832–5835, Copyright 2014, American Chemical Society". The traditional intermolecular KIE was measured in the same way described in Singleton's original report[11] as shown in Equation 1. Equation 1 is suitable for reactions that can be taken cleanly to high conversion (more than 80%). *F* stands for percent conversion; *R* and R_0 stand for the relative ^{13}C composition at each specific site in the

starting material and reisolated starting material. However, some reactions can only go to low percent conversion, or there are significant side reactions at prolonged reaction time. In this case, Equation 2 is preferred for measurements at low percent conversion. F still stands for the percent conversion. R_0' can be measured from starting material although it could also be measured from the reisolated product by taken the reaction to full conversion with different condition thus the product will yield the same information as the starting material. R' measures the ^{13}C composition in the product in the low percent conversion reaction. It should be noted that both Equation 1 and Equation 2 provide us the same information upon accurate measurement. The product-specific KIE was calculated based on KIE_{Inter} and product ratio at each specific carbon position where the index i permutes through all products and j indicates the product of interest (see Chapter 2 for details). The ^{13}C ratio are measured from quantitative ^{13}C NMR spectrum. ^{12}C ratio are either measured from quantitative proton spectrum; or from a chosen carbon site on the ^{13}C spectrum assumed to not participate in a way such that it experiences. This assumption is also inherent in the Singleton method. For the purpose of this work, the ^{13}C KIE for product **3** and **4** can be calculated by Equation 4 and Equation 5.

$$KIE_{Inter} = \frac{\ln(1-F)}{\ln[(1-F)\,R/R_0]} \cdots\cdots (1)$$

$$KIE_{Inter} = \frac{\ln(1-F)}{\ln\left(1 - F\dfrac{R'}{R_0'}\right)} \cdots\cdots (2)$$

$$KIE(P_j) = KIE_{Inter} \times \frac{\left(\sum_{i=1}^{n}[^{13}P_i]\right)/[^{13}P_j]}{\left(\sum_{i=1}^{n}[^{12}P_i]\right)/[^{12}P_j]} \cdots\cdots (3)$$

$$KIE(3) = KIE_{Inter} \times \frac{\left([^{13}3]+[^{13}4]\right)/[^{13}3]}{\left([^{12}3]+[^{12}4]\right)/[^{12}3]} \cdots\cdots (4)$$

$$KIE(4) = KIE_{Inter} \times \frac{\left([^{13}3]+[^{13}4]\right)/[^{13}4]}{\left([^{12}3]+[^{12}4]\right)/[^{12}4]} \cdots\cdots (5)$$
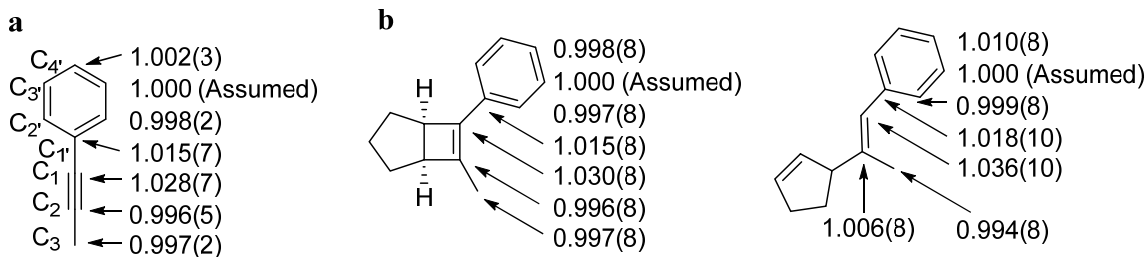

Figure 1: a) Conventional intermolecular ^{13}C KIEs, and b) product-specific ^{13}C KIEs for the reaction of cyclopentene and 1-phenyl-1-propyne catalyzed by CoBr$_2$(dppp)

The conventional intermolecular KIEs are shown in Figure 1a and the product-specific KIEs are shown in Figure 1b. The statistical errors are somewhat large, but this work represents a proof of principle that will find greater utility when NMR hardware and software can yield more precise estimates of isotopic content. Also, the product distribution of this specific reaction exhibits a significant preference for the formal [2+2] cycloaddition product, which creates a challenge in estimating isotopic content with equivalent degrees of certainty. This problem is naturally avoided in reactions that yield nearly 1:1 product mixtures as demonstrated in Chapter 4, which describes rhodium catalyzed C-H functionalization. However, the product-specific KIE can still provide us important information because it can augment the information provided by isotope effects over conventional KIE measurements.[32–34] If there is a common intermediate after the rate-determining step leading to different products, the product-specific KIE will show further fractionation on the base of the intermolecular KIE. If the rate- and product-determining step are the same step, then the intermolecular KIE will be a weighted average of the intrinsic KIE of both processes. In either case, the measurement of isotope effects on not only the unreacted starting material, but also on products where potentially further fractionation could happen after the rate-determining step will allow us to differentiate various mechanistic possibilities.

It is quite obvious from Figure 1 that the conventional KIEs are very similar to the product specific KIEs, namely, C_1 on the reisolated starting material and two products possess significant KIEs but lack of KIE at C_2 position. Although greater precision on measurements would possibly make the case clearer, the similarity of these KIEs makes it unlikely that: (1) **3** and **4** are originated from different regioisomers of I_2; (2) C-C and Co-C bond formation occur synchronously during rate-limiting formation of I_2; and (3) I_1 π-complex formation is rate-limiting. The first scenario would result in KIEs at either C_1 or C_2 position on starting material **1** with different magnitude. In cases of synchronous transition states, the KIE measured on the starting material at both C_1 and C_2 site should be closer and fall in between the product-specific KIEs of the two products on both carbon C_1 and C_2, which reveal traces of further fractionation from the common intermediate. Finally, rate limiting formation of I_1 is likely to generate very small KIEs on both C_1 and C_2 with similar magnitude. The measured product specific KIEs would only provide the ratio of KIEs for the two different pathways; however, it provides vital information that reflects the energy barrier, bond strength difference between two pathways during the product-determining step.

While it is only possible to eliminate unlikely pathways based on any mechanistic method, for a moderately complicated reaction, we can draw some preliminary conclusions based on the isotope effects observed relating to our hypothesis shown in Scheme 2 and Scheme 3. The significant intermolecular KIE at C_1 position and the lack of it at position C_2 suggests a highly asynchronous transition state that the C-C bond

formation is lagging behind the leading formation of the Co-C bond when forming the cobaltacyclopentene. In cases of highly asynchronous concerted transition states, Houk and co-workers[35] have demonstrated that the sites experience earlier bond formation will have a higher KIE than that of the later one. It can be understood in the way that the C-C bond is formed after Co-C bond formation on the downhill slope of the potential energy surface.

No significant further fractionation happened at C_1 position between **3** and **4** is less anticipated. This means, C_1 is not much involved in the product-determining step no matter how different those two pathways are. It is possible that similar to the lack of KIE at C_2 during the formation of cyclocoaltapentene ring I_1, C_1 is not much involved in the transition state from I_2 to **3** or I_2 to I_3; it is rather a consequence of β-hydride elimination that is determining the product distribution. Alternatively, this could also be a consequence of early transition states from I_2 to both **2** and I_3. One other possibility is that, the reductive elimination of I_3 to **4** on the Alder-ene pathway could also serve as the product-determining step. It is equivalent to say that the two reductive eliminations (I_2->**3** and I_3->**4**) are competing in the product determination and likely resulting in similar fractionation on C_1.

One of the key intermediates in the putative mechanism shown in Scheme 1 is the cobaltacyclopentene I_1. The evidence of this intermediate in similar coupling reactions was from confirmed X-ray structures of the stoichiometric reaction between Co(I)-alkyne complexes with various alkenes as discussed in the introduction section.[30] These complexes structurally resemble the cobaltacyclopentadiene which was confirmed as on pathway intermediates in alkyne trimerization reactions catalyzed by cobalt.[36,37] DFT calculations also identify these metallacycles as intermediates.[38–40] These arguments make it likely for I_2 to exist as a common intermediate on the pathway leading to both products. Substantial fractionations at the aromatic quaternary center $C_{1'}$ suggests some form of interaction between this carbon and the cobalt center. Possessing such a KIE means a bond breaking at some point along the reaction pathway. There are two possibilities at least to count this behavior. This carbon could directly bond to the cobalt center either at the rate-determining step, or the conjugation between this carbon and the closely bonded C_1 was broken which caused by the geometric requirement of ligands and itself during the rate-determining step. Currently, most of the computational research regarding cobaltacyclopentene and cobaltacyclopentadiene intermediates have been focusing on model structures which lack of complexities might been experienced here. However, as demonstrated by X-ray, the only phenyl substituent ring is out of the plane with the π-system in the C=C double bond internal to the complex.[30] This can be revealed from the optimized geometry of the cobaltacyclopentene intermediate preliminary calculation at B3LYP level of theory with 6-31G basis set using Gaussian 09.[41] As shown in Figure 3, the dihedral angle between the double bond to the phenyl ring is about 54.6°

in the intermediate as well as the products, although smaller, 49.3° and 16.9° for Alder-ene product and [2+2] products, respectively. Future frequency calculation would certainly yield more information regarding the origin of the isotope effects on $C_{1'}$, and the correct prediction, if carried out, would enrich the detail of the mechanism of regarding the transition state leading to $\mathbf{I_1}$.

While intermolecular KIEs measures the rate difference between individual isotopologues when mass sensitive vibrations are involved in the rate-limiting step after substrate binding, intramolecular KIEs can measure the fractionation when symmetry is broken at steps not necessarily limited to rate-determining steps on symmetric sites. For this reason, intramolecular KIE was measured for the cyclopentene moiety given that the symmetry it has, although intermolecular KIE could also provide valuable information. The intramolecular KIEs are relative by definition and are the inverse of the integrations at corresponding sites. If there is no further fractionation after the irreversible symmetry breaking, the intramolecular KIEs reveals the relative bond strength in the event of bond breaking and formation. However, if there's further fractionation due to different processes of the non-equivalent carbons that were symmetric, the results of the product-specific KIEs might not be immediately interpretable.[42–44] As shown in Figure 2a, the intramolecular ^{13}C KIE at site a' and b' are 1.050 and 1.078, which is very large for ^{13}C KIEs in the traditional sense. In this case, since it is highly possible, according to the putative mechanism, that the two vinyl carbons experience different downstream fractionation on the already fractionated intermediate $\mathbf{I_2}$. We could explore the intramolecular KIE of the formation of $\mathbf{I_2}$ by taken the weighted average of the ^{13}C integration of the products at the corresponding carbon sites. As shown in Figure 2a, the intramolecular KIEs are $\int a / \int a'$ and $\int b / \int b'$, respectively. Equation 6 is an example for the calculation of intramolecular KIE at site a' shown in Figure 2b for the common intermediate; and it was similarly done for site b'. The intramolecular KIE results are shown in Figure 2b. There is a substantial KIE at a' position in $\mathbf{I_2}$ and is consistent with a highly asynchronous transition state with prior Co-C bond formation. It is not intuitively interpretable for the intramolecular KIEs at site b' since it has not yet in direct bond breaking or formation. However, it is possible that the breaking of hyperconjugation is experienced by a different degree on b and b'. This behavior resulted a normal KIE at b' site, although the details need more investigation, since breaking of hyperconjugation generally strengthens the partially broken C-H bond, which should lead to an inverse KIE. In order to fully utilize these measured KIEs, computational chemistry tools will be employed in the future for accurate modeling for relative energy of the two competing transition states and frequency of related vibrational models.

For a summary, ^{13}C product-specific KIE coupled with conventional KIE have provided us insights that allow safely ruling out a large number of hypotheses, and it provides checkpoints for developing computational chemistry models. In the following section, we

will use deuterium substituted cyclopentene to investigate the hypothesized reaction pathway further.

$$KIE_{intra}(a') = \frac{([3]/[4]) \int 3 - a + \int 4 - a}{([3]/[4]) \int 3 - a' + \int 4 - a'} KIE(4)$$

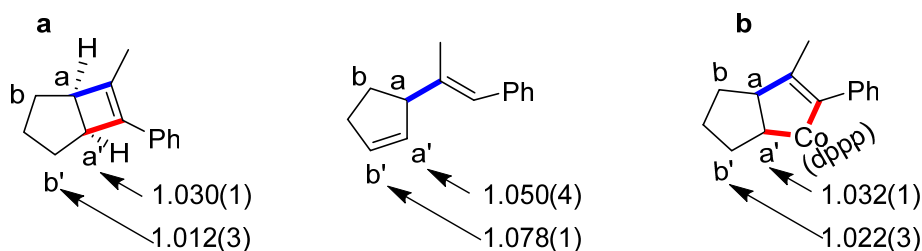$$= KIE_{Inter} \times \frac{([^{13}3] + [^{13}4])/[^{13}4]}{([^{12}3] + [^{12}4])/[^{12}4]} \cdots\cdots (6)$$

Figure 2: a) Intramolecular KIE for Alder-ene product and [2+2] product; b) Intramolecular KIEs for the rate-determining step leading to the common intermediate, I_2.

3.4 ^2H Kinetic Isotope Effects

Allylically mono-deuterated cyclopentene was synthesized[45,46] and subjected to reaction with 1-phenyl-1-propyne, under the same condition as the ^{13}C intermolecular KIE experiments. The substitution of a hydrogen atom by deuterium breaks the symmetry of the cyclopentene, which allows us to test the interaction between these hydrogens with other parts of the molecule in the transition states. In this case, several kinds of interactions may exist during the reaction pathway such as steric effects, hyperconjugation and agostic effects (a hydrogen bonded to a metal center and another carbon at the same time).[47] The products were assigned by comparing the deuterium spectrum of the mixture of deuterated products to the proton spectrum of the unlabeled product, which was assigned by using HSQC, HMBC and NOESY and 1-D NOESY spectra. The measurements were a challenge due to two reasons. For one, the proton signals for multiple nuclei in the products are largely overlapped due to similar chemical shifts; for another, fast decaying deuterium signals lead to wide linewidth on ^2H spectrum; Despite challenges, the deuterium spectra were used for integration to avoid peak contamination presented on proton spectra. Statistical reliable integrations are made by utilizing the deconvolution tool provided in Topspin software by Bruker. The exact geometry and coordination pattern for I_2 is not known yet. However, it would be reasonable to assume the hydride transfer happens on the hydrogen atom endo to the cobalt, as shown in Figure 3a based on proximity, where the distance between cobalt and hydrogen is 2.889 Å.
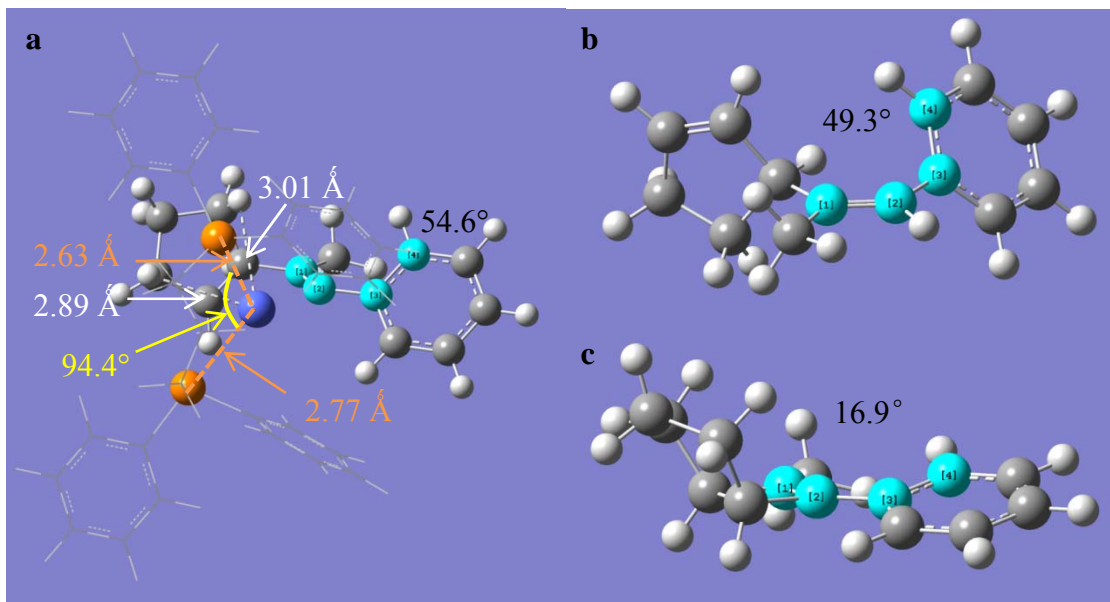
Figure 3: Preliminary data for geometry optimized with B3LYP functional with 6-31G basis set using Gaussian 09. a) cobaltacyclpentene intermediate. The dihedral angle between the phenyl ring and the double bond on the cobaltcyclopentene ring is about 54.6°.The atoms of dppp ligand are shown in gray except for the two phosphorous atoms; b) the Alder-ene product; c) [2+2] cycloaddition product. The later two also show this dihedral angle presents in A, 49.3° and 16.9°, respectively. They are smaller than that of the Alder-ene product. On structure A, the distance between the cobalt center to the endo hydrogen on the same side is around 2.89 Å, which is shorter than that of the other side, 3.01 Å. Assuming the hydride endo to the cobalt would be transferred, and the geometry does not change upon deuterium substitution.

Based on this hypothesis and the postulated reaction mechanism, we can trace each of the eight products back to its corresponding intermediates as I_{2a}, I_{2b}, I_{2c}, I_{2d} as shown in Figure 4. For simplicity, the intermediates I_3 for all Alder-ene products are omitted. It does not in anyway lowering their possibility as the product-determining step (PDS), since where two processes could possibly be the PDS: hydride transfer on I_2 or reductive elimination on I_3. However, this allows us to treat all the I_2 isotopologues in an intuitive way and study the preference for hydrogen or deuterium at each position. All the I_2 isotopologues are formed irreversibly from their corresponding I_1 complexes which were postulated in equilibrium with substrates 1 and 2_D. Lacking the detailed steps and rate constants for each step involved, all the rate constants shown in Figure 4 are assumed to be compound rate constants possibly involving more than one fundamental step. In order to study the relative rates of the formation four I_1 intermediates, the relationship between the four rate constants k_{2a}, k_{2b}, k_{2c}, and k_{2d}, will be derived. Useful ratios of these rate constants will also be discussed. Taking I_{2a} as an example, the rate law could be expressed as shown in Equation 7. Where "L" stands for ligands and "…" stands for species unknown. These unknown factors are presumed to be the same for formation of all intermediates, although not based on solid evidence but rather a reasonable assumption. We could similarly get the expression for the formation of I_{2b} as in Equation 8. Take the ratio of both equations and integrate on both sides affords Equation 9.
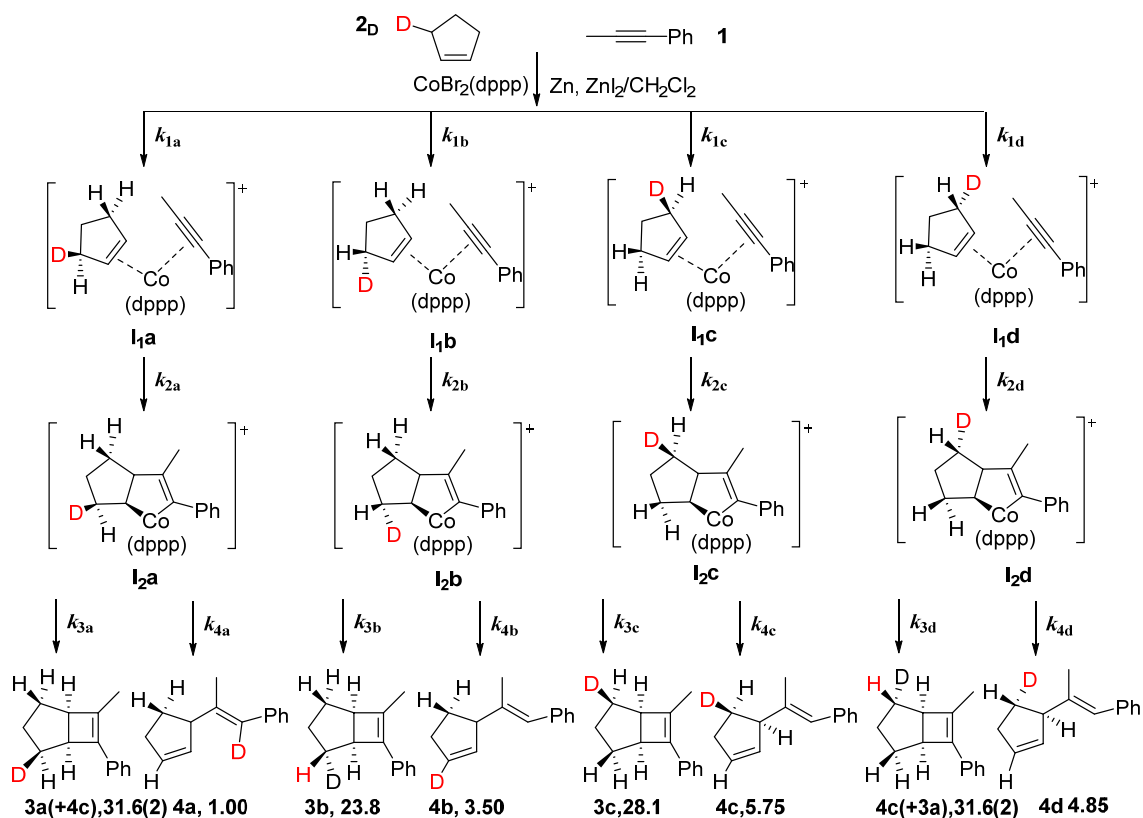
Figure 4: Product distribution for the reaction between mono-deuterium substituted cyclopentene and 1-phenyl-1-propyne. Assuming the hydride transfer from the hydrogen endo to the cobalt center in intermediate I_2, and the geometry does not change upon deuterium substitution.

$$d[I_{2a}] = -k_{2a}[I_{1a}][L_1]^x[L_2]^y \dots \mathrm{d}t$$

$$= -k_{2a}[L_1]^x[L_2]^y \dots \times -k_{1a}[\mathbf{1}][\mathbf{2_D}][L_1]^m[L_2]^n \dots \mathrm{d}t$$

$$= k_{1a}k_{2a}[\mathbf{1}][\mathbf{2_D}][L_1]^h[L_2]^l \dots \mathrm{d}t$$

$$= k_{1a,2a}[\mathbf{1}][\mathbf{2_D}][L_1]^h[L_2]^l \dots \mathrm{d}t \;\cdots\cdots (7)$$

$$d[I_{2b}] = k_{1b,2b}[\mathbf{1}][\mathbf{2_D}][L_1]^h[L_2]^l \dots \mathrm{d}t \;\cdots\cdots (8)$$

$$\frac{d[I_{2a}]}{d[I_{2b}]} = \frac{k_{1a,2a}}{k_{1b,2b}} \Rightarrow k_{1b,2b}\int d[I_{2a}] = k_{1a,2a}\int d[I_{2b}] \cdots\cdots (9)$$

$$\frac{k_{1a,2a}}{k_{1b,2b}} = \frac{[\mathbf{3a}]+[\mathbf{4a}]}{[\mathbf{3b}]+[\mathbf{4b}]} \cdots\cdots (10)$$

Since intermediates I_2 irreversibly convert to the corresponding products, the integration of their concentrations over time would be the same for their corresponding products.

Thus we can get Equation 10 for the ratio between $k_{1a,2a}$ and $k_{1b,2b}$, the combined rate constants for coordination and the formation of cobaltacyclopentene ring.

As shown in Figure 4 and Figure 9, the deuterium signals for product 3a and 4c cannot be separated on the ^{2}H NMR spectrum, due to their overlap at 1.75 ppm. We will take a look at products derived from $\mathbf{I_{2b}}$ and $\mathbf{I_{2d}}$ at first. The product ratio without deuterium substation is about 5.36. A substitution at a position on the cobalt side would only result in secondary KIEs. The ratio 3b/4b=(23.8/3.50)/5.36=6.8/5.36=1.27 is a combination of secondary isotope effects experienced by the [2+2] cycloaddition and the Alder-ene pathway. The other one, 3d/4d=(23.7/4.85)/5.36=4.89/5.36=0.91, is also a combination of secondary isotope effects of both pathways. Since electronic factors are the only likely source of isotope effects from $\mathbf{I_{2d}}$ to its products 3d and 4d, we can use this ratio as a calibration, in a way that the product ratio 3c/4c to be the same as 3d/4d. With this in mind, the integration of 3a+4c can be split into 25.8 and 5.75 for 3a and 4c, respectively. The product distribution with this assumption is displayed in Figure 5. The ratio (3a/4a)/5.36, 4.81 is a combination of secondary KIE for [2+2] pathway and a primary KIE for Alder-ene pathway. Since secondary deuterium KIEs are usually in the range from 0.75 to 1.25, the primary KIE for the Alder-ene process falls in between 3.8 on the low end and 6.0 on the high end, which is in a reasonable range. All isotope effects displayed here cannot be interpreted in any conventional way; however, a model that can accurately predict the product ratio of 3b/4b and 3d/4d should also provide reasonable value for product ratio 3c/4c. In this sense, a check for product ratio 3a/4a can also be made, which might experience agostic effects in addition to mass effects experienced by the formation of all intermediates and products.
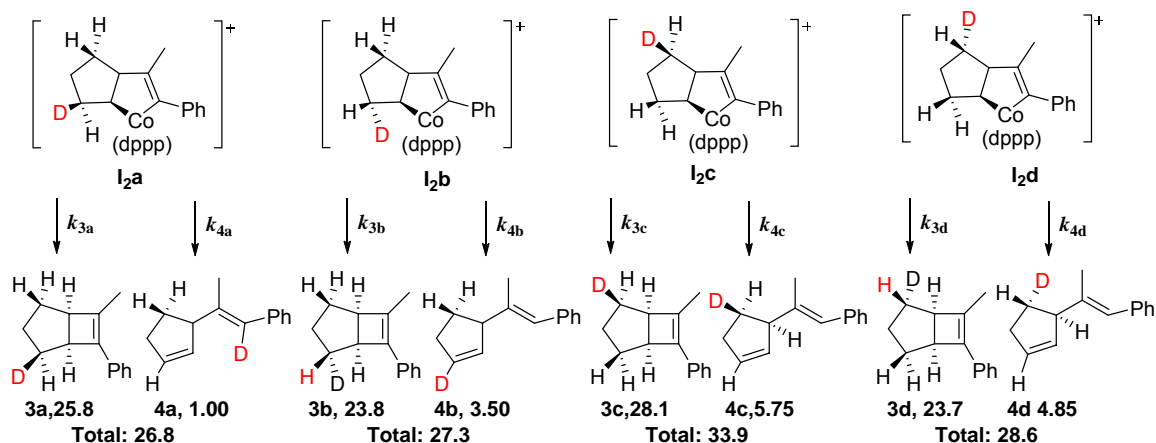

Figure 5: Product distribution for the reaction between mono-deuterium substituted cyclopentene and 1-phenyl-1-propyne, with the assumption that there's no KIE between the processes from $\mathbf{I_{2c}}$ and $\mathbf{I_{2d}}$ to their corresponding products. Note: without deuterium substitution, the weighted average of product ratio is 5.36.

3.5 Reaction of norbornene with 1-phenyl-1-propyne

By exploring reactions generating same products that are catalyzed by same transition metal but different ligands, we can determine whether a different mechanism or just different electronic or steric factors that are affecting the catalyst behavior. The reaction takes significantly longer for the one with dppe as a ligand than that of dppp (30 min done versus 60 min for ~60% conversion). To avoid complication of side products generation over prolonged reaction time, both reactions for measurements were taken to low percent conversion. The condition for dppp only used 20% of norbornene compared to that of 1-phenyl-1-propyne. The differences employed here is to ensure low percent conversion for the dppp one and enough percent conversion for the dppe ligated catalyst version. The percent conversion is the ratio of norbornene to 1-phenyl-1-propyne as started in the dppp case since it is 100% reaction for the norbornene. For dppe, approximately equal amounts of both starting materials were used. The percent conversion was calculated from the ratio between the product to unreacted 1-phenyl-1-propyne on ^{1}H NMR spectrum. It may seem odd to use different concentrations of norbornene to start with in two different reactions for comparison; however, the symmetry of norbornene guaranteed that the intramolecular KIE would provide enough information, and the change of concentration would not matter. It is possible in some reactions that KIE changes upon condition change.[48] For example, an oxidation of phenyl ethylalcohol with different concentrations of ligand[49] and oxidation of benzyl alcohol oxidized with a different concentration in toluene.[50] However, the reaction conditions used here can ensure that, when intermolecular KIE is desired for the Ph-C≡C-CH$_3$, same concentrations are used in reactions with different ligands; and when intramolecular KIE is pursued, the symmetry of norbornene matters, not the absolute concentration of itself. Equation 2 was used for both of the reactions. The intramolecular KIE at each position is just the inverse of their ^{13}C integration ratio, to that of the corresponding symmetric carbon in norborene.
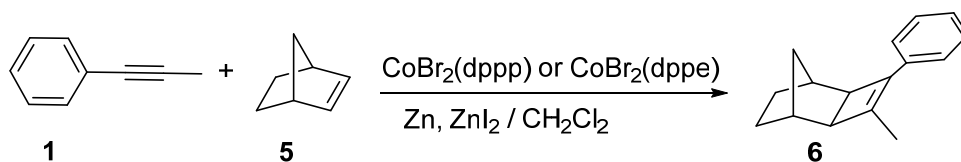
Scheme 4: Reaction between norbornene and 1-phenyl-1-propyne using CoBr$_2$(dppp) or CoBr$_2$(dppe) as the catalyst

The ^{13}C isotope effect results are displayed in Figure 6. The KIEs on the 1-phenyl-1-propyne carbons are intermolecular KIEs (calculated by Equation 2); while the ones on the norbornene moiety are intramolecular isotope effects. We notice the isotope effect pattern observed here on the 1-phenyl-1-propyne, do not resemble the ones measured when using cyclopentene as the alkene starting material. There are few noticeable

differences: 1) There's no significant isotope effect on C_1 and $C_{1'}$ position; 2) There is a small inverse isotope effect on C_2 position; 3) There's a large inverse isotope effect on the methyl carbon C_3 for the product wit dppe as the ligand, but not on the one with dppp; 4) The intramolecular isotope effect on $C_{5'}$ for the product with dppe ligand bigger than that with dppp.
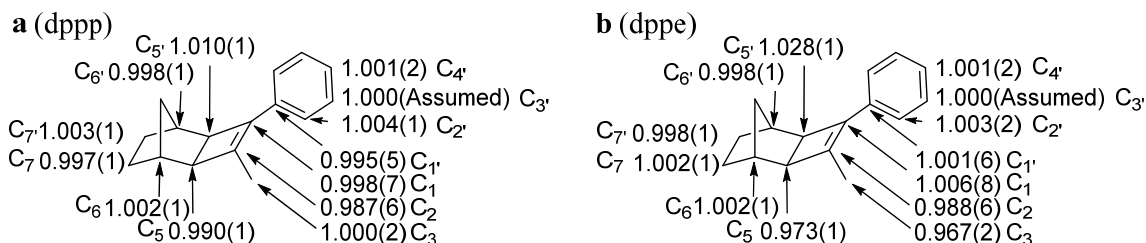
a (dppp)
$C_{5'}$ 1.010(1)
$C_{6'}$ 0.998(1)
1.001(2) $C_{4'}$
1.000(Assumed) $C_{3'}$
1.004(1) $C_{2'}$
$C_{7'}$1.003(1)
C_7 0.997(1)
0.995(5) $C_{1'}$
0.998(7) C_1
0.987(6) C_2
C_6 1.002(1)
C_5 0.990(1)
1.000(2) C_3

b (dppe)
$C_{5'}$ 1.028(1)
$C_{6'}$ 0.998(1)
1.001(2) $C_{4'}$
1.000(Assumed) $C_{3'}$
1.003(2) $C_{2'}$
$C_{7'}$ 0.998(1)
C_7 1.002(1)
1.001(6) $C_{1'}$
1.006(8) C_1
0.988(6) C_2
C_6 1.002(1)
C_5 0.973(1)
0.967(2) C_3

Figure 6: ^{13}C isotope effects measured for cobalt catalyzed reactions using a) dppp, and b) dppe as ligands. The isotope effects on the 1-phenyl-1-propyne are intermolecular KIE calculated with Equation (2), and the ones on norbornene are intramolecular isotope effects calculated by taken the inverse ratio of the ^{13}C integration with the corresponding symmetric carbon originated from the cyclopentene moiety.

Table 1: Isotope effects measured with their standard errors at each position of the product from the reaction with dppp as the ligand. The values for $C_{5'}$, $C_{6'}$ and $C_{7'}$ are not displayed since they are just reciprocals to the values of C_5, C_6 and C_7, respectively. These values are employed to calculate the weighted average and weighted error.

Inter	Expt.1	Expt.2	Expt.3	Expt.4	Expt.5	Err.1	Err.2	Err.3	Err.4	Err.5
C_1	0.977	1.006	0.981	1.014	1.032	0.014	0.015	0.015	0.020	0.018
C_2	0.985	1.001	0.980	0.995	0.977	0.013	0.014	0.013	0.015	0.013
C_3	1.018	1.002	0.993	0.987	1.002	0.004	0.005	0.003	0.004	0.005
$C_{1'}$	0.983	1.000	0.978	1.007	1.021	0.011	0.011	0.011	0.016	0.014
$C_{2'}$	1.003	1.001	0.998	1.005	1.011	0.003	0.004	0.003	0.003	0.003
$C_{3'}$	1.000	1.000	1.000	1.000	1.000	0.000	0.000	0.000	0.000	0.000
$C_{4'}$	1.002	0.998	0.999	1.003	1.005	0.005	0.005	0.005	0.006	0.005
Intra	Expt.1	Expt.2	Expt.3	Expt.4	Expt.5	Err.1	Err.2	Err.3	Err.4	Err.5
C_5	1.010	1.007	1.013	1.007	1.008	0.005	0.003	0.002	0.004	0.004
C_6	0.997	0.998	0.996	0.998	0.999	0.003	0.003	0.003	0.002	0.003
C_7	0.996	0.998	0.997	0.998	0.998	0.001	0.002	0.002	0.002	0.003

The most challenging question here is the existence of an inverse intermolecular ^{13}C isotope effect on the 1-phenyl-1-propyne moiety. Inverse ^{13}C isotope effects are not as common as normal isotope effects. The first thing is to check how credible the data set itself is. Five independent reactions were carried out for measurements, and the results are shown in Table 1 and Table 1. Unfortunately, the quality of the intermolecular KIE data does not appear to be good enough to support any arguments. For example, the KIE for C_1 position (first entry, Table 1) on the product from the reaction with dppp ranges from inverse to normal (0.977 to 1.032), as well as the one with dppe (first entry, Table 1). Similar variations were found on C_2 and C_3. It is likely that either the spectra are

40

suffering from phasing problem, which cannot be tackled easily or some unknown factor during the reaction was playing a role in it. The author has tried different parameters for processing, but statistical trustworthy data had not been obtained.

Table 2: Isotope effects measured with their standard errors at each position for dppe ligated pathway. The values for $C_{5'}$, $C_{6'}$ and $C_{7'}$ are not displayed since they are just reciprocals to the values of C_5, C_6 and C_7, respectively. These values are employed to calculate the weighted average and weighted error.

Inter	Expt.1	Expt.2	Expt.3	Expt.4	Expt.5	Err.1	Err.2	Err.3	Err.4	Err.5
C_1	1.029	0.990	1.015	1.008	0.973	0.017	0.019	0.018	0.017	0.022
C_2	0.979	0.996	0.994	0.986	0.985	0.013	0.014	0.013	0.014	0.012
C_3	0.961	1.014	0.957	0.982	0.960	0.005	0.011	0.005	0.004	0.004
$C_{1'}$	1.007	0.995	1.006	1.000	0.997	0.012	0.013	0.013	0.011	0.012
$C_{2'}$	1.007	1.000	1.001	1.004	1.006	0.004	0.004	0.003	0.004	0.004
$C_{3'}$	1.000	1.000	1.000	1.000	1.000	0.000	0.000	0.000	0.000	0.000
$C_{4'}$	1.001	1.000	0.998	1.002	1.003	0.005	0.005	0.007	0.005	0.005
Intra	Expt.1	Expt.2	Expt.3	Expt.4	Expt.5	Err.1	Err.2	Err.3	Err.4	Err.5
C_5	1.033	1.028	1.027	1.032	1.024	0.003	0.003	0.002	0.003	0.003
C_6	1.004	1.002	1.003	1.001	1.002	0.003	0.002	0.002	0.002	0.003
C_7	1.005	1.001	1.002	1.002	1.001	0.003	0.002	0.002	0.003	0.003

However, in the case of a real inverse ^{13}C isotope effect, it could be either EIE (equilibrium isotope effect) or KIE. EIE works in a way such that the heavier isotope prefers to reside on the higher frequency bond.[51] Saunders have measured the EIE for 2,3-dimethyl-2-[2-^{13}C]-butylium ion (a carbonium ion) in the range of 1.0115 to 1.0197 for $K_{13/12}$ when temperature changed from -62 °C to -104 °C using NMR.[52] Another Inverse ^{13}C EIE has been reported for the ionization of triphenyl chloride in liquid sulfur dioxide at 0 °C, a process closely related to a S_{N1} heterolysis with a magnitude of 0.983(3) by Kresage and co-workers.[53,54] A very small inverse ^{13}C KIE has also been reported for the solvolysis of 1-(4'-methyl- pheny1)-1-bromoethane in methanol with a magnitude of 0.9995(5). In the latter two cases, the inverse isotope effects were explained in a way that the zero point energy lost during breaking of a C-X (X=Cl, Br) bond was over compensated by the increase of the force constant between the C-C bond, which linked the primary carbon and the aromatic ring. This bond strengthen effect is realized by hyperconjugation between the phenyl ring(s) and the ionized carbon, supported by bond length shortening of the three C-C single bond in triphenylmethyl perchlorate crystal structure.[73] In the current case with 1-phenyl-1-propyne, it is not absolutely impossible that, the breaking of a π bond in the C≡C triple bond in exchange of another strained C-C single bond when forming the four member ring, which results a tighter environment. However, such argument has to be treated cautiously when lack of other evidences.

Although the intermolecular isotope effects are not up for quantitative interrogation, in this case, the intramolecular isotope effects are less likely to be affected by either

experimental condition or integration complication. Since there is only one product for norbornene, it is not likely the symmetrical positions would go through other fractionation that would make the intramolecular competition complicated by intermolecular competition, as discussed in the reaction between 1-phenyl-1-propyne and cyclopentene. The ^{13}C peaks associated with the symmetric carbons are closely spaced on the carbon spectrum of the product, which make them less prone to phase or baseline issues. As shown in Figure 6, the intermolecular for $C_{5'}$ position on the dppp and dppe pathways are 1.010(1) and 1.028(1), respectively. Referring to the mechanism for the cyclopentene reaction, the $C_{5'}$-Co bond was formed prior to the formation of C_5-C_2, which resulted in the enrichment of ^{12}C at $C_{5'}$. The different magnitude was likely due to the different electronics and steric restriction posed by the different ligands.
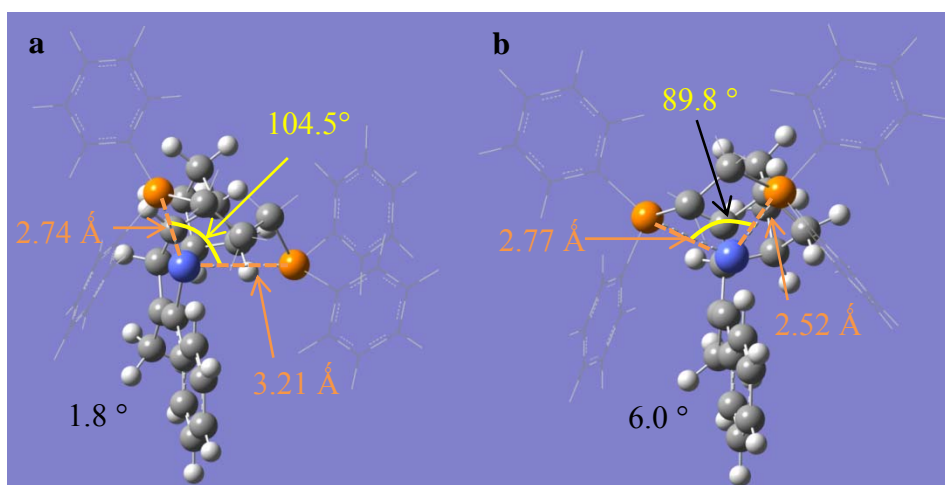
Figure 7: B3LYP/6-31G level optimized intermediate **I$_2$** when using norbornene as the alkene for [2+2] cycloaddition. a) dppp as the ligand; b) dppe as the ligand.

Though a full set of KIE calculation is not available yet, the structure of norbornene and 1-phenyl-1-propyne coordinated cobalt complex for both dppp and dppe ligated versions were optimized, using hybridized functional B3LYP with basis set 6-31G as shown in Figure 7. The hypothesis that the biting angle affects the transition state could be revealed here. First of all, a significant difference, by comparing both structures to the structure of coaltacyclopentene in Figure 7, is that the phenyl ring resides nearly on the plain of the C=C double bond internal to the cobaltacyclopentene ring. This means the conjugation of between the triple bond and aromatic ring in 1-phenyl-1-propyne is not completely lost, which results in no KIE or a small KIE. Now comparing the difference between the two in Figure 7, one more methylene tether on dppp allows the biting angle to be 104.5° while only 89.5° for that of dppe. Comparing to the cyclopentene one in Figure 7 the biting angle for dppp is only 94.4°, which is much less than 104.5° for dppp but closer to 89.5° for dppe ligand. However, this is not strange in a way that, one more methylene tether allowed more flexibility for the catalyst to accommodate substrate of different geometric requirements. The flexibility can also be evidenced by the distance change

between cobalt and phosphorous on the alkene side on the dppp ligated complex: for cyclopentene, 2.63 Å; for norbornene: 3.01 Å. The small biting angle for the dppe ligated complex make it possible that the active substrate experience more strain, which could affect the vibrational frequency of sensitive bonds in the transition state. The other differences is that the methyl group does slightly deviate from the conjugation plane, 1.8° for dppp cobalt complex and 6.0° for dppe one, which could result in different measured KIEs for the methyl carbon.

3.6. Summary and Future Work

In summary, the hypothesis for $CoBr_2(dppp)$ catalyzed [2+2] and Alder-ene reaction between cyclopentene and 1-phenyl-1-propyne has been tested using both ^{13}C and ^{2}H isotope effects. Combined with conventional KIE methods, product-specific KIE is capable of ruling out multiple hypotheses and providing compelling evidence for one likely theory. Both $CoBr_2(dppp)$ and $CoBr_2(dppe)$ have been used to test the reaction between norbornene and 1-phenyl-1-propyne. Although only the intramolecular KIE was being explained in our confidence, it does support the hypothesis that the Co-C bond formation leading the C-C bond formation when cobaltacyclopentene ring is formed. However, the power of this method is not fully revealed until coupled with further detailed computational study, which would utilize the rich information of experimentally measured ^{13}C and ^{2}H isotope effects. Further studies would try to reproduce these isotope effects using DFT methods, which can often accurately predict isotopes effect if appropriate functional and geometry are used, with a sufficiently large basis set. These calculations would confirm us about the details of a hypothesized mechanism of the reaction, if our hypothesis were close enough. With enough accumulated experimental and computational data, it would allow us to predict the behavior of related substrates, ligands and the product distribution. The extension of this method to more systems would certainly make us benefit from a complete picture when investigating reactions with multiple pathways.

3.7 Experimental Section

3.7.1 Syntheses

3.7.1.1 Synthesis of the catalyst $Co(dppp)Br_2$ and $Co(dppe)Br_2$

The catalyst $Co(dppp)Br_2$ was synthesized following the procedure published by Hall and co-workers.[18] Into a mixture of 1,2-bis(diphenylphosphino)propane (dppp, 2.93 g, 7.12 mmol) and isopropanol (150 ml) in a 500 ml two neck RBF charged with a condenser, Cobalt(II) bromide (2.21 g, 10.01 mmol) in 50 ml was added. After refluxing overnight and a hot-filtration, the green solid was washed with isopropanol (10 ml*3), diethyl ether (10 ml*3) and dried in *vacuo* for 10 hours. 3.96 g product was received. Yield:88%. Catalyst $Co(dppe)Br_2$ was synthesized in the same manner as $Co(dppp)Br_2$.

3.7.1.2 Synthesis of 3-bromo-cyclopent-1-ene[55]
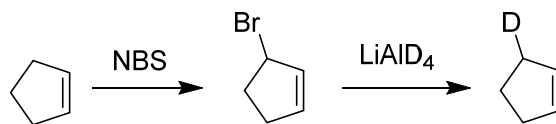
Into a flame dried 3-neck RBF charged with a thermocouple and two long condensers on top, AIBN (0.2 g, 1.24 mmol), CCl_4 (30 ml), cyclopentene (10 g, 146.8 mmol) and NBS (6.5 g, 36.8 mmol) were added under N_2 protection. The mixture was heated to 70 ^{0}C. The reaction mixture was stopped and cooled down immediately after the disappearing of the vigorously boiling cyclopentene layer. The mixture was filtered through a thin layer of silica, and 3-bromo-cyclopent-1-ene was distilled under N_2 protection. The product was used immediately after distillation. Yield: 64%.

3.7.1.3 Synthesis of 3-deuterio-cyclopent-1-ene

Lithium aluminum deuteride (570 mg, 13.6 mmol) was added into a flame dried 25 ml 2-neck RBF charged with a distillation head and receiving flasks, followed by addition of 10 ml dry 2-methyl THF. 3-bromo-cyclopent-1-ene (2.0 g, 13.6 mmol) was added, and the mixture was taken to reflux. The product 3-deuterio-cyclopent-1-ene was collected in the receiving flasks. 1.35 g mixture of 3-deuterio-cyclopent-1-ene and 2-methyl THF was received. 436 mg of 3-deuterio-cyclopent-1-ene presented in the solution, according to NMR analysis. Yield: 32%. ^{1}H NMR (400 MHz, $CDCl_3$): 5.72 (t, 2H); 2.29 (m, 3H); 1.9 (m, 2H). ^{2}H NMR(400 MHz, $CHCl_3/CDCl_3$): 2.29, singlet.

3.7.2. Structure determination and assignment

3.7.2.1 Carbon assignment for 1-phenyl-1-propyne (**1**), 6-methyl-7-phenylbicyclo[3.2.0] hept-6-ene (**3**) and (E)-(2-(cyclopent-2-en-1-yl)prop-1-en-1-yl)benzene (**4**).

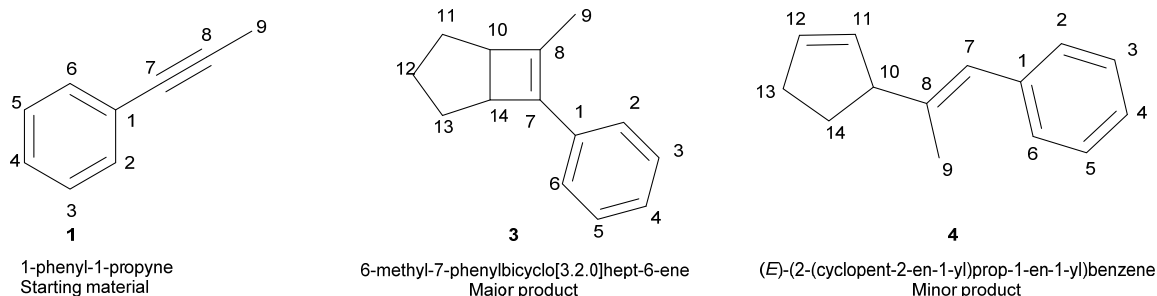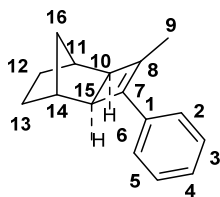Graph 1. Chemical structures and labeling of **1**, **3** and **4** for assignment

Table 3: Carbon assignment of **1, 3** and **4**.

Assignment for **1**		Assignment for **3**		Assignment for **4**	
Chemical Shift(ppm)	Assigned to carbon	Chemical Shift(ppm)	Assigned to carbon	Chemical Shift(ppm)	Assigned to carbon
4.3	9	14.0	9	16.1	9
79.9	7	23.5	12	29.6	14
85.9	8	24.8	11	32.7	13
124.2	1	26.0	13	55.5	10
127.6	4	43.7	14	124.0	7
128.3	3,5	46.7	10	126.0	4
131.6	2, 6	125.9	2, 6	129.0	2, 6
		126.4	4	132.4	12
		128.5	3, 5	133.6	11
		135.5	1	128.2	3, 5
		137.3	7	138.8	1
		139.3	8	142.2	8

3.7.2.2 Carbon assignment for (1S,2R,5S,6R)-3-methyl-4-phenyltricyclo[4.2.1.0^{2,5}]non-3-ene (**6**)

(1*S*,2*S*,5*S*,6*R*)-2,3,5-trimethyl-4-phenyltricyclo[4.2.1.0^{2,5}]non-3-ene (**6**)

Figure 8: Chemical structures and labeling of the [2+2] cycloaddition product **6** from the reaction of 1-phenyl-1-propyne (**1**) and norbornene

Table 4: Carbon assignment for **6**. The assignment was done in 1,1,2,2-tetrachloroethane-d$_2$, the same solvent used for quantitative measurement.

Chemical shift (ppm)	Assignment to carbon
139.493	8
138.127	7
135.516	1
128.240	3,5
126.233	4
125.703	2,6
49.132	10
46.355	15
34.695	14
33.487	11
30.587	16
28.491	12
28.358	13
13.979	9

3.7.2.3 Assignment of peaks on the ^2H spectrum of the product mixture from the reaction of d_1-cyclopentene and 1-phenyl-1-propyne

The deuterium peaks in the mixture were assigned to different compounds according to proton assignment on the non-deuterated [2+2] cycloaddition product and Alder-ene product.
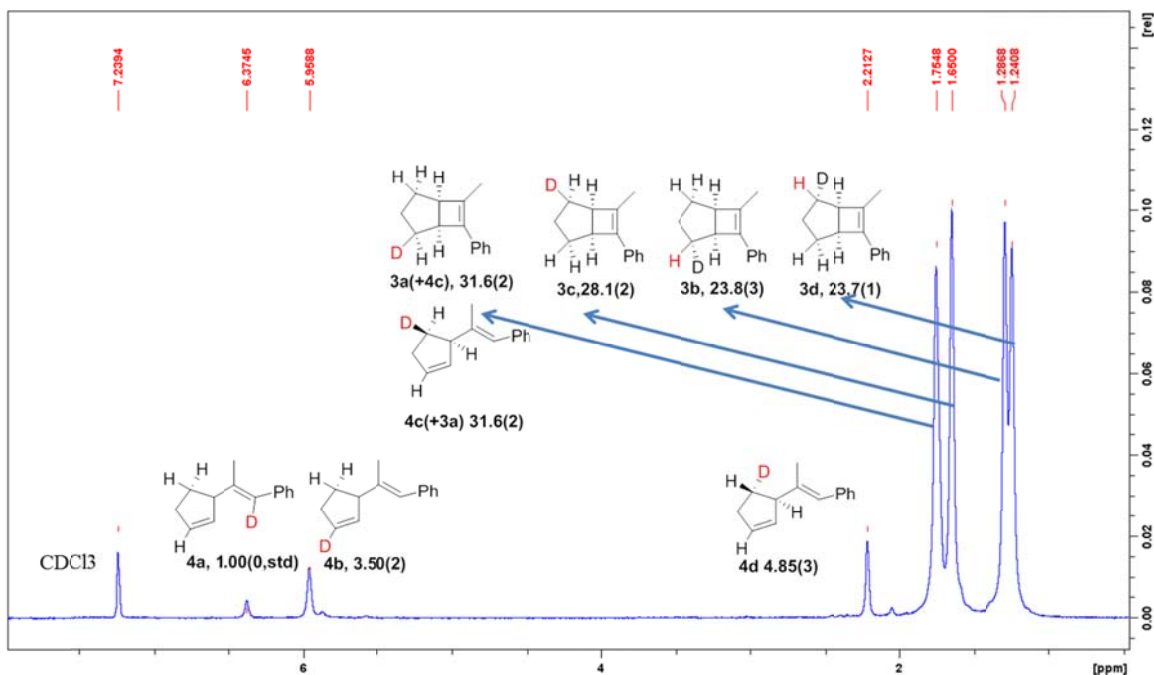

Figure 9: Assignment of peaks to corresponding products from the reaction between d_1-cyclopentene and 1-phenyl-1-propyne. Product 3a and 4a overlapped at 1.75 ppm.

3.7.3 KIE measurement conditions and raw data

All quantitative NMR has been done on Bruker 600 MHz magnet charged with a carbon optimized cryoprobe. All the quantitative NMR has been done in CDCl₃ at 5 °C for optimal separation of peaks. Sample Information: see "General procedure for carrying out high conversion reaction."

3.7.3.1 Measurement conditions and raw data of ^{13}C KIE for Co(dppp)Br₂ catalyzed [2+2] cycloaddition and Alder-ene reaction[14]

A 25 ml RBF was flame dried under nitrogen protection (vacuum and refill cycle, five times) with a heat gun. ZnI₂ (1.185 g, 3.71 mmol) was added into the flask under nitrogen and flame dried in the flask again at approximately 300 °C. Zinc dust (243 mg, 3.712 mmol) and Co(dppp)Br₂ (1.171 g, 1.856 mmol) were added under nitrogen protection. After three vacuum and nitrogen refilling cycles, 1-phenyl-1-propyne (1.078 g, 1.000 ml,

9.28 mmol) , cyclopentene (0.632 g, 0.820 ml, 9.28 mmol) and 10 ml anhydrous CH_2Cl_2 were added under nitrogen protection. The mixture was stirred under nitrogen for 50~55 min. 0.1 ml of the mixture was loaded onto a pipette column with 2 cm of silica gel and flushed with $CDCl_3$ into a 5 ml vial. Most CH_2Cl_2 in the 5 ml vial was vacuumed away at 20 °C under 5 inHg pressure. The resulting mixture was analyzed by ^1H NMR to get percent conversion and major/minor product ratio. The rest of the reaction mixture was immediately loaded onto a 2-inch diameter column with 15 inch silica gel and eluted with pentane and diethyl ether (95:5). Two products and the unreacted starting material was collected. The solvent was removed in *vacuo*. A mixture of the two products and the unreacted starting material in approximately 1:1:1 ratio was subject to NMR analysis.

^1H NMR

Acquisition parameter: swipe width (sw): 14 ppm; center of spectrum (o1): 4.15 ppm; number of scans (ns): 16; dummy scans (ds): 4; acquisition time (aq): 3.89 s; FID resolution: 0.26 Hz; d1: 30 s; size of FID (TD): 64k. Processing parameter: zero filling to 128k points; line broadening: 0 Hz. The spectra were manually phased, and a polynomial baseline correction was applied for the whole spectrum. S/N ratio for smallest peak: >3000

^{13}C NMR

Acquisition parameter: sweep width (sw):258.4 ppm; center of spectrum (o1): 73.51 ppm; number of scans (ns): 100; dummy scans (ds): 4; acquisition time (aq):3.36 s; FID resolution: 0.26 Hz; d1: 80 s; size of FID (TD): 256k; Processing parameter: zero filling to 512k points; line broadening: 0.2 Hz. The spectra were manually phased, and a polynomial baseline correction was applied for the whole spectrum. S/N ratio for smallest peak: >1000

For raw data, see support information of the published article. [31]

3.7.3.2 Measurement condition and raw data of ^2H isotope effects for Co(dppp)Br$_2$ catalyzed [2+2] cycloaddition and Alder-ene reaction

ZnI_2 (60 mg, 0.1 mmol) was added into a 5 ml glass vial charged with a stir bar. After flame dried under N_2 protection, Co(dppp)Br$_2$ (70 mg, 0.1 mmol), Zn (13 mg, 0.2 mmol), were quickly added into the vial, and the solid mixture was purged with N_2 for 5 min. CH_2Cl_2 (0.6 ml) was added into the mixture, and the vial was placed in a water bath of 40 ^0C under N_2. Then a mixture of 3-deuterio-cyclopent-1-ene (34 mg, 0.5 mmol) (2-methyl THF present as in the distillation mixture) and 1-phenyl-1-propyne (58 mg, 0.5 mmol) was added. The mixture was stirred for 1 hour before it was quenched with 2 ml of pentane. The quenched mixture was filtered through a short pipette column with about 3mm silica gel and washed with pentane (1 ml*3). The solvent was removed in *vacuo*. The resulted residue was used in NMR analysis for product ratio.

^{2}H NMR

Acquisition parameter: sweep width (sw):16.0 ppm; center of spectrum (o1): 4.0 ppm; number of scans (ns): 2400; dummy scans (ds): 4; acquisition time (aq):1.5 s; FID resolution: 0.67 Hz; d1: 2 s; size of FID (TD): 4428; Processing parameter: zero filling to 16k points; line broadening: 0 Hz. The spectra were manually phased, and a polynomial baseline correction was applied to the whole spectrum. S/N ratio: for smallest peak: 40; for highest peak: 1000.

Table 5. Original deconvoluted integration values for each peak on the ^{2}H spectra of the product mixture from the reaction between d1-cyclopentene and 1-phenyl-1-propyne. The first peak was used as the standard. The error was the standard deviation measured from eight FIDs of the same sample.

Chemical Shift (ppm)	Expt.1	Expt.2	Expt. 3
6.37	1.00(std)	1.00(std)	1.00(std)
5.96	3.51 ± 0.04	3.52 ± 0.04	3.47 ± 0.04
2.21	4.85 ± 0.05	4.80 ± 0.05	4.91 ± 0.06
1.75	31.5 ± 0.3	31.8 ± 0.3	31.4 ± 0.3
1.65	28.2 ± 0.2	28.4 ± 0.2	27.8 ± 0.3
1.28	23.7 ± 0.2	23.9 ± 0.3	23.7 ± 0.3
1.24	23.6 ± 0.3	23.7 ± 0.1	23.1 ± 0.2

3.8 References

(1)   Hess, W.; Treutwein, J.; Hilt, G. *Synthesis* **2008**, *2008*, 3537–3562.

(2)   Chang, H. T.; Thiruvellore, T. J.; Wang, C. C.; Cheng, C. H. *J. Am. Chem. Soc.* **2007**, *129*, 12032–12041.

(3)   Schmidt, A.; Hilt, G. *Org. Lett.* **2013**, *15*, 2708–2711.

(4)   Bohn, M. A.; Schmidt, A.; Hilt, G.; Dindaroğlu, M.; Schmalz, H.-G. *Angew. Chem. Int. Ed.* **2011**, *50,* 9689–9693.

(5)   Arndt, M.; Dindarolu, M.; Schmalz, H. G.; Hilt, G. *Synthesis* **2012**, *44*, 3534–3542.

(6)   Wei, C.; Mannathan, S.; Cheng, C. *J. Am. Chem. Soc.* **2011**, *133*, 6942–6944.

(7)   Wei, C. H.; Mannathan, S.; Cheng, C. H. *Angew. Chem. Int. Ed.* **2012**, *51*, 10592–10595.

(8)   Bigeleisen, J.; Wolfsberg, M. In *Advances in Chemical Physics, Volume 1*; Debye, I. P. and P., Ed.; John Wiley & Sons, Inc.: Hoboken, NJ, USA, 1957.

(9)   Bigeleisen, J.; Mayer, M. G. *J. Chem. Phys.* **1947**, *15*, 261–267.

(10)   Bigeleisen, J.; Wolfsberg, M. In *Advances in Chemical Physics*; Prigogine, I., Ed.; Iterscience Publishers, Inc.: New York, 1958; Vol. 1, pp 15–76.

(11)   Singleton, D. A.; Thomas, A. A. *J. Am. Chem. Soc.* **1995**, *117*, 9357–9358.

(12)   Hilt, G.; Treutwein, J. *Angew. Chem. Int. Ed.* **2007**, *46*, 8500–8502.

(13)   Treutwein, J.; Hilt, G. *Angew. Chem. Int. Ed.* **2008**, *47*, 6811–6813.

(14)   Hilt, G.; Paul, A.; Treutwein, J. *Org. Lett.* **2010**, *12*, 1536–1539.

(15)   Bredt, J.; Bredt, J. *Ann. Der Chemie* **1924**, *437*, 1–13.

(16)   Shea, K. J. *Tetrahedron* **1980**, *36*, 1683–1715.

(17)   Tani, K.; Stoltz, B. M. *Nature* **2006**, *441*, 731–734.

(18)   Horrocks, W.; Van Hecke, G. R.; Hall, D. *Inorg. Chem.* **1966**, *6*, 694–699.

(19)   Lyons, J. E.; Myers, H. K.; Schneider, A. *J. Chem. Soc., Chem. Comm.* **1978**, No. 15, 636–638.

(20)   Lyons, J. E.; Myers, H. K.; Schneider, A. *Ann. N. Y. Acad. Sci.* **1980**, *333*, 273–285.

(21)   Duan, I.-F.; Cheng, C.-H.; Shaw, J.-S.; Cheng, S.-S.; Liou, K. F. *J. Chem. Soc., Chem. Comm.* **1991**, No. 19, 1343–1347.

(22)   Hilt, G.; du Mesnil, F.-X. *Tetrahedron Lett.* **2000**, *41*, 6757–6761.

(23)   Hilt, G.; Lüers, S. *Synthesis* **2003**, No. 12, 1784–1786.

(24)   Hilt, G.; Erver, F.; Harms, K. *Org. Lett.* **2011**, *13*, 304–307.

(25)   Erver, F.; Hilt, G. *J. Org. Chem.* **2012**, *77*, 5215–5219.

(26)   Fiebig, L.; Kuttner, J.; Hilt, G.; Schwarzer, M. C.; Frenking, G.; Schmalz, H.; Scha, M. *J. Org. Chem.* **2013**, *78*, 10485–10493.

(27)   Morschel, P.; Janikowski, J.; Hilt, G.; Frenking, G. *J. Am. Chem. Soc.* **2008**, *130*, 8952–8966.

(28)   Newbound, T. D.; Colsman, M. R.; Miller, M. M.; Wulfsberg, G. P.; Anderson, O. P.; Strauss, S. H. *J. Am. Chem. Soc.* **1989**, *111*, 3762–3764.

(29)   Visentin, T.; Kochanski, E.; Moszynski, R.; Dedieu, A. *J. Phys. Chem. A* **2001**, *105*, 2031.

(30)   Wakatsuki, Y.; Aoki, K.; Yamazaki, H. *J. Am. Chem. Soc.* **1979**, *101*, 1123–1130.

(31)   Xiang, S.; Meyer, M. P. *J. Am. Chem. Soc.* **2014**, *136*, 5832–5835.

(32)   Melander, L.; Saunders, Wiliam H., J. *Reaction Rates of Isotopic Molecules*; John Wiley & Sons, Inc: New York, 1980.

(33)   Thibblin, A.; Bengtsson, S.; Ahlberg, P. *J. Chem. Soc., Perkin Trans. 2* **1977**, 1569–1577.

(34) Thibblin, A.; Ahlberg, P. *J. Am. Chem. Soc.* **1977**, *99*, 7926–7930.

(35) Hock, K. N.; Gustafson, S. M.; Black, K. A. *J. Am. Chem. Soc.* **1992**, *114*, 8565–8572.

(36) McAlister, D. R.; Bercaw, J. E.; Bergman, R. G. *J. Am. Chem. Soc.* **1977**, *99*, 1666–1668.

(37) Wakatsuki, Y.; Nomura, O.; Kitaura, K.; Keiji, M.; Yamazaki, H. *J. Organomet. Chem.* **1983**, *105*, 1907–1912.

(38) Hardesty, J. H.; Koerner, J. B.; Albright, T. A.; Lee, G. Y. *J. Am. Chem. Soc.* **1999**, *12*, 6055–6067.

(39) Gandon, V.; Agenet, N.; Vollhardt, K. P. C.; Malacria, M.; Aubert, C. *J. Am. Chem. Soc.* **2006**, *128*, 8509–8520.

(40) Agenet, N.; Gandon, V.; Vollhardt, K. P. C.; Malacria, M.; Aubert, C. *J. Am. Chem. Soc.* **2007**, *129*, 8860–8871.

(41) Gaussian 09, Revision B.01. M. J. Frisch, G. W. Trucks, H. B. Schlegel, G. E. S.; M. A. Robb, J. R. Cheeseman, G. Scalmani, V. Barone, B. M.; G. A. Petersson, H. Nakatsuji, M. Caricato, X. Li, H. P. H.; A. F. Izmaylov, J. Bloino, G. Zheng, J. L. Sonnenberg, M. H.; M. Ehara, K. Toyota, R. Fukuda, J. Hasegawa, M. Ishida, T. N.; Y. Honda, O. Kitao, H. Nakai, T. Vreven, J. A. Montgomery, J.; J. E. Peralta, F. Ogliaro, M. Bearpark, J. J. Heyd, E. B.; K. N. Kudin, V. N. Staroverov, T. Keith, R. Kobayashi, J. N.; K. Raghavachari, A. Rendell, J. C. Burant, S. S. Iyengar, J. T.; M. Cossi, N. Rega, J. M. Millam, M. Klene, J. E. Knox, J. B. C.; V. Bakken, C. Adamo, J. Jaramillo, R. Gomperts, R. E. S.; O. Yazyev, A. J. Austin, R. Cammi, C. Pomelli, J. W. O.; R. L. Martin, K. Morokuma, V. G. Zakrzewski, G. A. V.; P. Salvador, J. J. Dannenberg, S. Dapprich, A. D. D.; O. Farkas, J. B. Foresman, J. V. Ortiz, J. C.; Fox, and D. J. Gaussian, Inc.: Wallingford CT, 2010.

(42) Grdina, S. B.; Orfanopoulos, M.; Stephenson, L. M. *J. Am. Chem. Soc* **1979**, *101*, 3111–3112.

(43) Singleton, D. A.; Szymanski, M. J. *J. Am. Chem. Soc.* **1999**, *121*, 9455–9456.

(44) Giagou, T.; Meyer, M. P. *J. Org. Chem.* **2010**, *75*, 8088–8099.

(45) Becker, N.; Carreira, E. M. *Org. Lett.* **2007**, *9*, 3857–3858.

(46) Jacquet, O.; Bergholz, T.; Magnier-Bouvier, C.; Mellah, M.; Guillot, R.; Fiaud, J. C. *Tetrahedron* **2010**, *66*, 222–226.

(47) Brookhart, M.; Green, M. L. H.; Parkin, G. *Proc. Natl. Acad. Sci. U.S.A.* **2007**, *104*, 6908–6914.

(48) Simmons, E. M.; Hartwig, J. F. *Angew. Chem. Int. Ed.* **2012**, *51*, 3066–3072.

(49) Mueller, J. A.; Jensen, D. R.; Sigman, M. S. *J. Am. Chem. Soc.* **2002**, *124*, 8202–8203.

(50) Steinhoff, B. A.; Stahl, S. S. *Org. Lett.* **2002**, *4*, 4179–4181.

(51) Hascall, T.; Rabinovich, D.; Murphy, V. J.; Beachy, M. D.; Friesner, R. A.; Parkin, G. *J. Am. Chem. Soc.* **1999**, *12*, 11402–11417.

(52) Saunders, M.; Kates, M. R.; Walker, G. E. *J. Am. Chem. Soc.* **1981**, *103*, 4623–4624.

(53) Kresge, A. J.; Lichtin, N. N.; K. N. Rao. *J. Am. Chem. Soc.* **1963**, *85*, 1210–1211.

(54) Kresge, A. J.; Lichtin, N. N.; Rao, K. N.; Weston, R. E. *J. Am. Chem. Soc.* **1965**, *87*, 437–445.

(55) Brennan, M. B.; Claridge, T. D. W.; Compton, R. G.; Davies, S. G.; Fletcher, A. M.; Henstridge, M. C.; Hewings, D. S.; Kurosawa, W.; Lee, J. A.; Roberts, P. M.; Schoonen, A. K.; Thomson, J. E. *J. Org. Chem.* **2012**, *77*, 7241–7261.

Chapter 4: Investigation of Rhodium Catalyzed C-H Functionalization

4.1 Introduction to C-H Functionalization and the Current State on the Mechanistic Research of Rhodium Catalyzed C-H Functionalization

Carbon-Hydrogen (C-H) bond functionalization involves the cleavage of a C-H bond and the formation of C-X bond, "X" refers to other heavy atoms or functional groups. This process is often named C-H functionalization (Scheme 1). Various approaches have been developed for the realization of this transformation.[1–10] Its broad applications can be found in pharmaceutical industry as well as general synthetic chemical industry.[1,11]
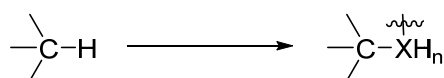
Scheme 1: C-H Functionalization

Recently developed methods can substantially shorten the synthetic routes for a complicated compound.[12,13] Among those transformations, donor/acceptor rhodium carbene complexes have been developed and widely applied for their high regio- and stereo-selectivity in C-H insertion and cyclopropanation.[14–18] The understanding of the mechanism[7,16,19–22] is of great importance for future catalyst design. The product-specific KIE method developed in Chapter 2 can elucidate structural and energetic information regarding the rate-determining step (RDS) and the product-determining step (PDS) in multi-channel reactions that generate two or more products. With both experimental KIE measurements and theoretical KIE calculations, this chapter will try to uncover the mechanism of the following dirhodium tetracarboxylate catalyzed C-H insertion.

Unexpected results were observed when reactions were carried out between **4** ((*E*)-methyl 2-diazo-4-phenylbut-3-enoate) derived rhodium carbenoids, and **1** (*4*-methyl-*1,2*-dihydronaphthalene) or **5** (*3*-methyl-*1H*-indene), as shown in Scheme 2 and Scheme 3, respectively. The carbenoid is formed in situ by adding **4** into the mixture of **1** or **5** with a catalytic amount of $Rh_2(OAc)_4$ in dichloromethane. While compound **1** generates two diastereomeric isomers for C-H insertion, compound **5** afforded a single diastereomer of possible cyclopropanation products, despite the similarities in the structure of the starting materials. These two reactions, C-H insertion, and cyclopropanation appear side by side for numerous substrates. Product distribution is highly dependent upon substrate identity. The primary concern of this chapter will be the details of the diastereo-selectivity on the C-H insertion process. A short discussion of cyclopropanation of compound **5** will also be included.

The C-H insertion reaction in Scheme 2 catalyzed by achiral catalyst $Rh_2(OAc)_4$ generates two diastereomers in approximately a 2.2:1 ratio between **2**_{*HH*} and **3**_{*HH*}. When

this reaction was purified immediately over a silica gel column after the dropwise addition of **4** into the mixture of **1**$_{HH}$ and Rh$_2$(OAc)$_4$ in CH$_2$Cl$_2$, the ratio between **2**$_{HH}$
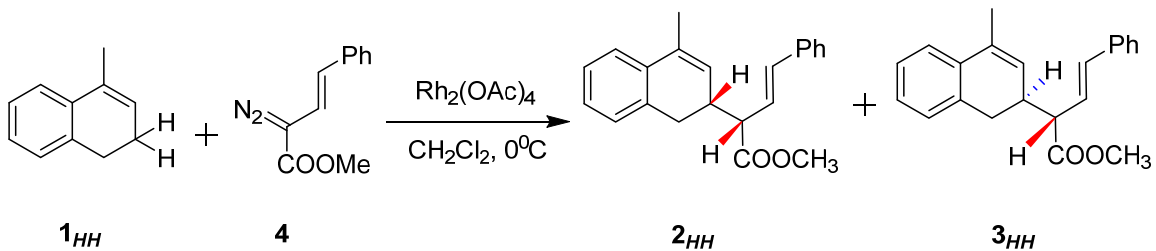
Scheme 2：C-H insertion of 4-methyl-1,2-dihydronaphthalene (enantiomers are not shown)
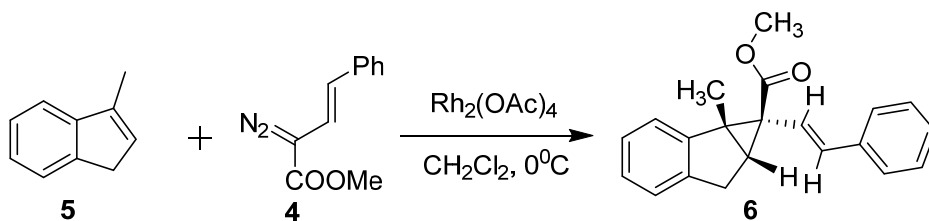
Scheme 3：Cyclopropanation of 3-methyl-1H-indene (enantiomers are not shown)

and **3**$_{HH}$ was observed to increase over time steadily when monitored by NMR. Over the course of approximately two hours, the final ratio of 2.2:1 was reached. An intermediate **2'**$_{HH}$ was observed and characterized via NMR. It quantitatively converts to **2**$_{HH}$ over a few hours at room temperature. When the same experiment was performed with chiral catalyst Rh$_2$(S-DOSP)$_4$ in dichloromethane or 2,2-dimethylbutane (DMB),[14] this conversion was more easily observed. It is due to the fact that only **2**$_{HH}$ and **2'**$_{HH}$ are formed, without the complication of **3**$_{HH}$. As shown in Figure 1a, for example, the decreasing integration of the singlet methyl group at 1.5 ppm is accompanied with an increasing integration of the triplet methyl group at 2.2 ppm. Upon comparison of the conversion between **7** and **8** observed by Davies group,[14] as shown in Scheme 4, the intermediate is likely to be the product formed by a C-H Activation/Cope rearrangement (CHCR) process as proposed by Davies and co-workers. This event is currently described as C-H insertion, despite the fact that the fundamental mechanistic event is thought to be achieved in discrete steps involving hydride transfer. Henceforward this process will be referred to as C–H insertion to be in accord with current literature practices. The stabilization created by the conjugation of the phenyl group to the double bond from the conversion of **2'**$_{HH}$ to **2**$_{HH}$ makes it easier, compared to the conversion from **7** to **8,** as shown in Scheme 4, where a much higher temperature is required. Since both chiral and achiral rhodium catalysts generate one product going through the CHCR process, a

summary of mechanistic studies on rhodium carbenoids involving C-H insertion will serve as a start for the mechanistic discussion of this chapter.
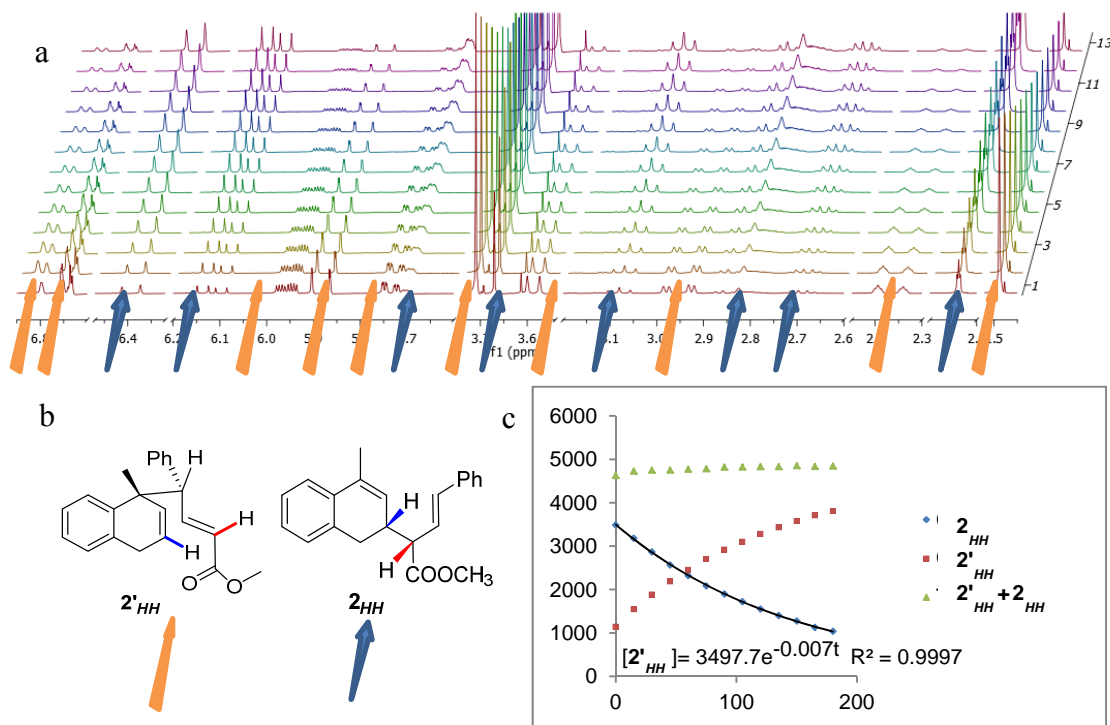

Figure 1: NMR evidence for the conversion between intermediate ($2'_{HH}$) and product (2_{HH}). a) The brown arrows indicate the decrease of intensity of the peaks that belong to 2_{HH} and the blue arrows indicate the increase of the intensity for $2'_{HH}$. b) Structures of $2'_{HH}$ and 2_{HH}. c) The semi-quantitative integration of the methyl groups of $2'_{HH}$ to 2_{HH} indicates the quantitative conversion by noticing their summation is a constant over time.
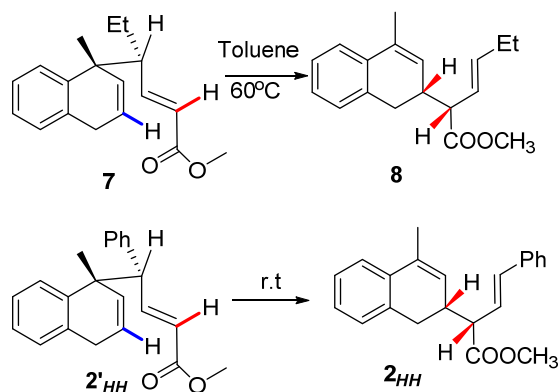
Scheme 4: Conversion between intermediate ($2'_{HH}$) and product (2_{HH}). a) An example from Davies' article.[14] With an ethyl group, compound **7** is relatively stable. It goes through a retro-Cope rearrangement only at an elevated temperature. b) With a phenyl group, this process for compound $2'_{HH}$ to 2_{HH} happens at room temperature.

54
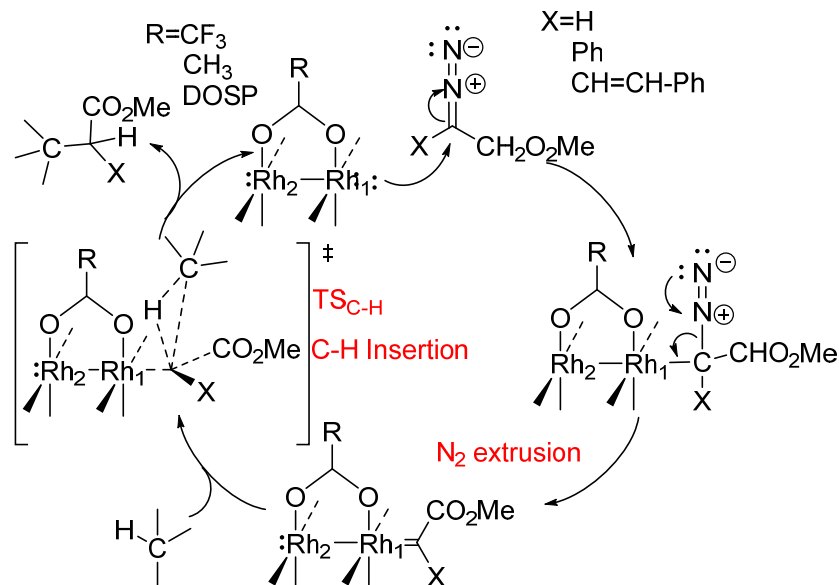
Scheme 5: Catalytic cycle for rhodium carboxylate catalyzed C-H insertion

Investigation of rhodium carbenoids involving C-H insertion and cyclopropanation is prevalent in mechanistic literature.[16,19,23–27] As shown in Scheme 5, the general catalytic cycle starts with the formation of the rhodium carbenoid complex by nitrogen extrusion from a diazo compound. This rhodium carbenoid approaches and breaks a C-H bond, with the formation of a C-C bond and another C-H bond at the same time. The energetic profile of rhodium carbenoid formation and its stability have been thoroughly discussed.[16] The structure of the transition state (TS$_{(C-H)}$ in Scheme 5) controls the stereo-selectivity and is of great interest. Early mechanistic study for rhodium catalyzed C-H insertion uses acceptor only diazo compounds (the carbenoid only attaches to electron withdrawing groups) such as ethyl diazoacetate for generation of carbenoids. Costa[28], Doyle[29] and their co-workers have shown that catalyst with electron-donating ligand allows the carbene to stay intact with the rhodium, thus providing more regio-selectivity. On the other side of the complex, with the three centered (C(Rh)-H-C) model,[29] an electron deficient ligand on rhodium reduces the electron density on the carbenal carbon. This deficiency in electron density allows the hydride transfer to happen at an earlier stage with lower selectivity. For the same reason, the electron rich C-H bond is more easily functionalized. Adams'[26] model study on a rhodium catalyzed C-H insertion with 1-methyl-1-(diazoacetyl)-cyclohexane derivatives has also demonstrated the positive effects on stereo-selectivity from electron donating ligands on the catalyst, as well as electron donating group (EDG) α- to the site of insertion. The measured deuterium isotope effects on intra- and inter- molecular C-H insertion by Costa[28] and Adams'[26] are between 1.2 to 2.5, depending on the ligand used. The low primary KIE is in accord with the use of more reactive carbenes, which are frequently described as "acceptor only carbenes" where "X" denotes hydrogen, as shown in Scheme 5. Mechanistically, these

small isotope effects are likely due to the early transition states. Adams' explanation does not conflict with Doyle's three center transition state; however, their research states that existing evidence cannot offer a clear resolution between a concerted and stepwise mechanism. This conclusion is supported by Tabor's observation[30] of carbon configuration retention, or a hydride transfer initiated, stepwise transition state. DFT calculations made by Nakamura and co-workers[31] also suggest a three center concerted, but a synchronous transition state, with leading hydride transfer and lagging C-C bond formation. These mechanistic studies can partially explain[32] existing stereo-selectivity and serve as a preliminary information to guide the formation of mechanistic hypotheses that will be explored in detail below.

Increasing demand for higher diastereo-selectivity, led the Davies group to develop donor/acceptor type carbene precursor (where "X" refers to phenyl, phenylvinyl) and chiral rhodium catalyst (e.g. $Rh_2(S\text{-DOSP})_4$) for both C-H insertion[14,33–35] and cyclopropanation.[23,36] With numerous examples, Davies and Morton[16] have shown that rhodium catalyzed C-H insertion, especially with donor/acceptor carbenoids mediated C-H insertion, does not require directing groups for selectivity. The electronic and steric factors are thus likely responsible for observed selectivity profiles. The site selection for C-H insertion sterically favors primary C-H bonds due to the bulkiness of the catalyst; it electronically favors tertiary C-H bond formation because it can better stabilize positive charge formation at the carbon center. For chemo-selectivity, the electron-rich alkene favors cyclopropanation over C-H insertion. However, the alkene is also likely to go through C-H insertion if sterically hindered (e.g. tri-substituted alkene). Computational mechanistic studies have been carried out for both C-H insertion[20,21,25] and cyclopropanations.[19,20]

CHCR, short for combined C-H insertion/Cope rearrangement process, was thought to be the key to the high diastereo-selectivity observed in rhodium catalyzed C-H insertion, as has been proposed by Davies and co-workers.[25] With a few possibilities, the focus of the discussion in the references has been on how to differentiate the following two pathways in Scheme 6, which will also be the focus of this chapter. In a simplified model, pathway "a" started with a hydride transfer to form a zwitterion which couples to form the product (we call this product CHCR product corresponding to *2′$_{HH}$* in Scheme 4). Pathway "b", on the other hand, is a seven centered, concerted transition state directly leading to the product. By performing DFT calculations with B3LYP functional in gas phase on a model system consist of dirhodium tetraformate and cyclohexadiene, a concerted, but highly asynchronized transition state was located: the transition state was found to be initiated with a hydride transfer, and then C-C bond formation before the carbon centers go through rehybridization to form a zwitterion intermediate. This process was called CHCR because the reaction was described as starting with C-H insertion that is interrupted by a Cope rearrangement. In our reaction (Scheme 2), this CHCR product will

thereafter go through a retro-Cope rearrangement to form the C-H insertion product **2**$_{HH}$ at room temperature. Their calculation on CHCR process is also consistent with direct C-H insertion pathway investigated earlier.[21,31,32] It was reasoned that the two pathways share the same transition state because they lie on the same potential energy surface without an intermediate in between, this is a bifurcation mechanism explained in the reference.[37–42] However, computational investigation of this phenomenon is not a viable task due to complication with potential energy surface shape and Newtonian dynamics.[43,44]
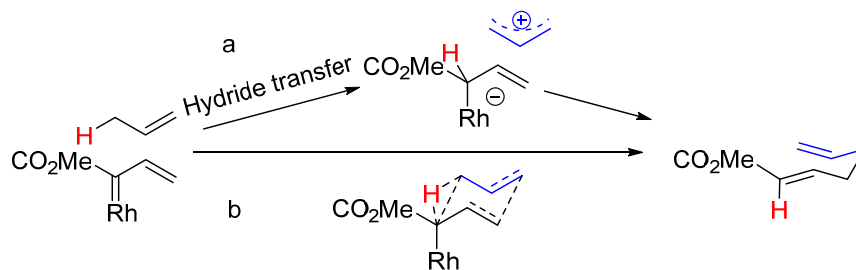
Scheme 6: Mechanistic proposals for the formation of CHCR product. a) A stepwise transition state with two steps: hydride transfer leading to zwitterion formation, and coupling of zwitterion to form the final product; b) a concerted seven-centered mechanism.

Computational chemistry has advanced mechanistic study significantly, which was recognized by Pople and Kohn being awarded a Nobel Prize in 1998 for their contribution to the field. It has been widely used for elucidation of organic mechanisms,[45] especially when coupled with experiment evidence. Despite computational advances, the task of achieving optimization of all transitions states and intermediates possible in a reaction is still a challenging task, especially with relatively complex systems. However, hypothetical transition states and intermediates based on experimental evidence are still vital to the elucidation of a reasonable mechanism. Without experimental evidence, the mechanism of a reaction under research can only be narrowed down to multiple closely related, computationally indistinguishable pathways, due to the accuracy of current methods or incomplete searches of possible chemical entities.[46] For example, the CHCR process and the direct C-H insertion cannot currently be accurately distinguished using purely computational approaches.[21,31,32]

Transition state theory[47] has been played an enormously important role in predicting chemical mechanisms. However, the geometry of a transition state for a reaction, which is crucial to understand chemical reactivity and selectivity, cannot be directly viewed by instruments with the technology available, except for some very few simple systems.[48,49] Kinetic isotope effects (KIEs) have been proven valuable for describing the key features of transition structures.[50–53] Deuterium and ^{13}C isotope effects in chemical reactions are widely used for mechanistic studies since their development by Bigeleisen.[54] Singleton's

natural abundance ^{13}C KIE method[55] has made it easy for general use of ^{13}C KIEs, due to its negation of the need for laborious labeling of reaction substrates.

Before further discussion of using product-specific KIE methods developed in Chapter 2, it is important to understand that even a sizable ^2H or ^{13}C KIE does not mean that the bond breaking or making event measured is the rate-determining step (RDS) of the reaction. The KIE measured could be a step after the RDS. For example, if the substrate only binds to the catalyst after the RDS, which could be due to catalyst activation or solvation,[53] a KIE would mostly likely be measured, but would not be the RDS of the reaction. This article will focus on the step where a C-H bond is cleaved, and a C-C bond is formed, which may or may not be the RDS for the overall reaction. An observed ^2H or ^{13}C KIE indicates that the step could be the rate-limiting step after the RDS as well as RDS itself. We will use the rate-limiting step to differentiate from RDS in this chapter. In the current case, the extrusion of N_2 gas is likely the RDS as suggested by the calculation of Hansen, Autschbach and Davies.[21] For intermolecular competition experiments with only one product involved, the isotopic fractionation information obtained from measuring the reisolated starting material would tell us whether there is a bond breaking or formation, and whether it is the rate-limiting step. We could get the same information from measuring the isotope content of the product. The logic behind this method is that the information presented in the starting material is reciprocal to that of the product. An isotope concentration measurement on either species would be enough to know whether or not the isotopic fractionation occurred during the rate-limiting step. However, this is not the case if there are multiple products formed. There are two different scenarios that explain the behavior of a KIE. In one case, when the rate-limiting step and product-determining step (PDS) are the same, we can measure two sets of different KIEs for the two products. In another case, the products share the same rate-limiting step but a different product-determining step, the two products can have the same KIE on some sites (for ^{13}C) but different on others. In either case, the information we get from the reisolated starting material could tell us nothing than net isotopic fractionation occurred. That explains the need for investigating multi-product reactions using product-specific KIE.

4.2 Intermolecular ^2H KIE Experiments for $Rh_2(OAc)_4$ Catalyzed C-H Insertion

In order to obtain the associated isotope effects that allow us to compare to modeled transition state states, the following inter-molecular KIE experiments were carried out. As shown in Scheme 7 and Scheme 7, the intermolecular deuterium KIE experiments between the perprotiated and the mono-deuterated, di-deuterated starting material were carried out under the same condition as shown in Scheme 2. From those experiments, primary KIE and secondary KIE for both processes can simultaneously be obtained by utilizing product-specific KIE methods.
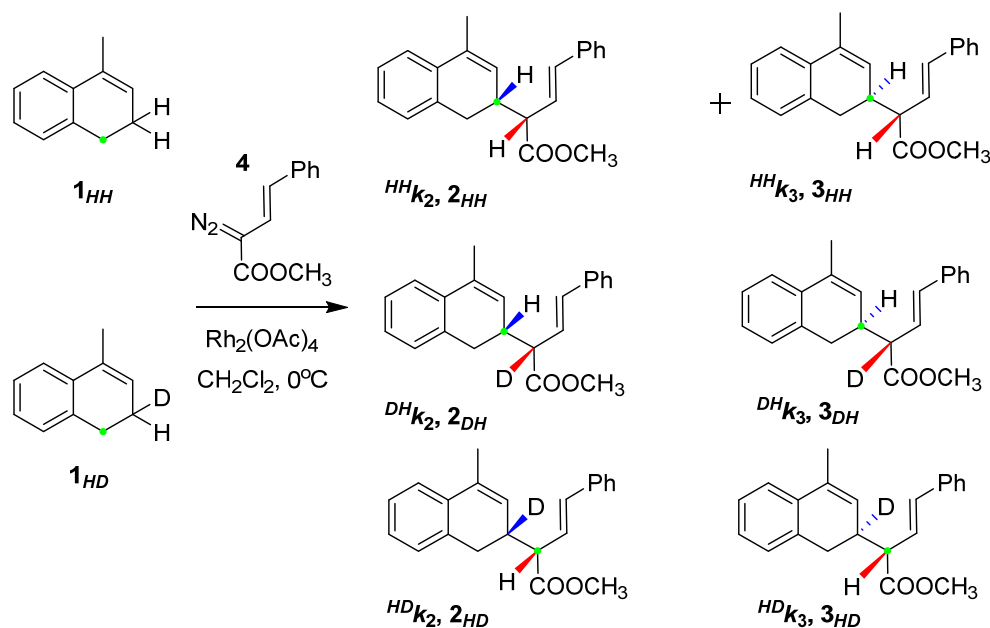
Scheme 7: Intermolecular KIE experiment between the perprotiated (1_{HH}) and mono-deuterated (1_{HD}) isotopologues. 1_{HH} generates two diastereomers and 1_{HD} generates four products. Each product has its rate constant. The first letter indicates the atom being transferred and the second refers to the atom retained. The green-dot labeled carbons are chosen for measurement using ^{13}C spectrum.

$$KIE_{inter}(HH/HD) = \frac{^{HH}k}{^{HD}k} = \frac{\ln(1 - F_{HH})}{\ln(1 - F_{HD})} = \frac{\ln\left[(1 - F_{all})\left(1 + \frac{1}{R_0}\right)/\left(1 + \frac{1}{R}\right)\right]}{\ln[(1 - F_{all})(1 + R_0)/(1 + R)]} \cdots\cdots (1)$$

$$\frac{^{HH}k_2}{^{HD}k_2} = KIE_{inter}(HH/HD) \times \frac{([2_{HD}] + [2_{DH}] + [3_{HD}] + [3_{DH}])/[2_{HD}]}{2 \times ([2_{HH}] + [3_{HH}])/[2_{HH}]} \cdots\cdots (2)$$

It is possible to put all three starting materials in one pot and obtain the ratios between all the different rate constants in the course of one experiment. However, the limited resolution of all eight products by either chromatography or spectroscopy is a significant limitation for accurate and precise quantification. Due to this limitation, our two experiments were carried out separately. The ratio of different products are quantified using quantitative ^{13}C NMR. A number of product ratios and kinetic isotope effects were calculated. In Equations (1) and (2), R_0 and R stand for the ratio of $1_{HH}/1_{HD}$ in the starting material mixture and reisolated starting material, respectively. k_{HH} and k_{HD} stand for the overall rate of reaction for the two isotopologues, respectively. It is important to notice that 1_{HD} is a mixture of two enantiomers. Since the products for 1_{HD} are two pairs of diastereomers and only one pair for 1_{HH}, there will be a factor of 2 when the product specific KIE is calculated, according to the derivation of Chapter 2. As shown in Scheme 7 and Scheme 7, the letters in the products and rate constants are assigned that the first one stands for the atom being transferred and the second one being retained. k_2 and k_3 are rate constants for CHCR process and direct C-H insertion process, respectively. For

example, $^{HD}k_2$ stands for the rate constant for the formation of 2_{HD} with a hydrogen atom being transferred and deuterium retained through the CHCR process.

The product specific KIE between the formation of product 2_{HH} and 2_{HD} is shown in Equation (2). Similarly, other ratios could be obtained by arranging the corresponding rate constants and product ratios. All the measurement results are displayed in Table 1. From Entry 1, 2 and 3, depends on the transferred atom and the retained one, the ratios between any two processes are different, although slightly but statistically significant. Entry 1 shows that, for reactant 1_{HH}, the product ratio between CHCR process and direct C-H insertion is 2.19(1). However, when H was transferred from reactant 1_{HD} to form 2_{HD} and 3_{HD}, this ratio becomes 2.14(1); when D was the transferred atom, this ratio becomes 2.06(2). The energy perturbation by replacing a hydrogen with a deuterium on the potential energy surface of the reaction pathway is very small compared to the energy of the overall reaction, which is ca. 10 kcals/mol.[21,25] The pathway each isotopologue travels is assumed not to change significantly upon isotopic substitution. This means, for example, 2_{HH}, 2_{HD} and 2_{DH} take the same CHCR route to form. The potential energy surfaces for all the species with different isotopes along the way to the product are the same. This is also the assumption on the direct C-H insertion process for the formation of 3_{HH}, 3_{HD} and 3_{DH}. With that assumed, the small differences between the product ratios can be attributed to the zero point energy (ZPE) change due to isotopic substitution, as will be discussed below.

Table 1: Intermolecular KIE measured from competition experiments between 1_{HH} and 1_{HD} using $Rh_2(OAc)_4$ as the catalyst. The values from entry 1 to 5 are ratios directly measured from NMR spectra. Values for entry 7 to 10 are calculated according to the product-specific KIE formula. 1^0 stands for primary, and 2^0 stands for secondary.

Entry	Rate Ratios	Values	Products	Explanation
1	$^{HH}k_2/^{HH}k_3$	2.19(1)	$2_{HH}/3_{HH}$	CHCR/CH-1_{HH}-H transfer
2	$^{HD}k_2/^{HD}k_3$	2.14(1)	$2_{HD}/3_{HD}$	CHCR/CH-1_{HD} -H transfer
3	$^{DH}k_2/^{DH}k_3$	2.06(2)	$2_{DH}/3_{DH}$	CHCR/CH-1_{HD} -D transfer
4	$^{HD}k_3/^{DH}k_3$	3.71(3)	$2_{HD}/2_{DH}$	H/D transfer-1_{HD} -CHCR process
5	$^{HD}k_2/^{DH}k_2$	3.55(4)	$3_{HD}/3_{DH}$	H/D transfer-1_{HD} -CH process
6	$^{HH}k_2/^{DH}k_2$	3.74(1)	$2_{HH}/2_{DH}$	CHCR process-1^0 KIE-H/D transfer-1_{HH}&1_{HD}
7	$^{HH}k_2/^{HD}k_2$	1.00(1)	$2_{HH}/2_{HD}$	CHCR process-2^0 KIE-H/D retain-1_{HH}&1_{HD}
8	$^{HH}k_3/^{DH}k_3$	3.55(1)	$3_{HH}/3_{DH}$	CH process-1^0 KIE-H/D transfer-1_{HH}&1_{HD}
9	$^{HH}k_3/^{HD}k_3$	1.00(1)	$3_{HH}/3_{HD}$	CH process-2^0 KIE-H/D retain-1_{HH}&1_{HD}
10	$KIE_{inter}^{Acetate}$(HH/HD)	1.57(2)		Compound KIE between 1_{HH}&1_{HD}

A reasonable mechanism should be able to account for all observed experimental results. As entry 6 and 8 show in Table 1, the primary KIEs for CHCR and direct C-H insertion processes are 3.74(1) and 3.55(1), respectively. Any difference between those two values

means that they do not share the same transition states from starting materials to products. Although product ratio changes with deuterium substitution on the substrate has been observed in some systems with dynamic effects, such a system does not require different geometry changes for different products.[39,56] In our case, two different geometries are required for the formation of these two diastereomers. This contradicts with previously discussed bifurcation mechanism proposed by Davies and co-workers.[25] Their study shows the two processes, CHCR and direct C-H insertion, share the same potential energy surface for the hydride transfer but separate along the reaction coordinate to form different products. This mechanism suggests that we should get the same KIE for the formation of both products since they share the same transition state. There are at least two possibilities to address this discrepancy between the different KIEs observed in our investigation and the earlier suggested bifurcation mechanism.
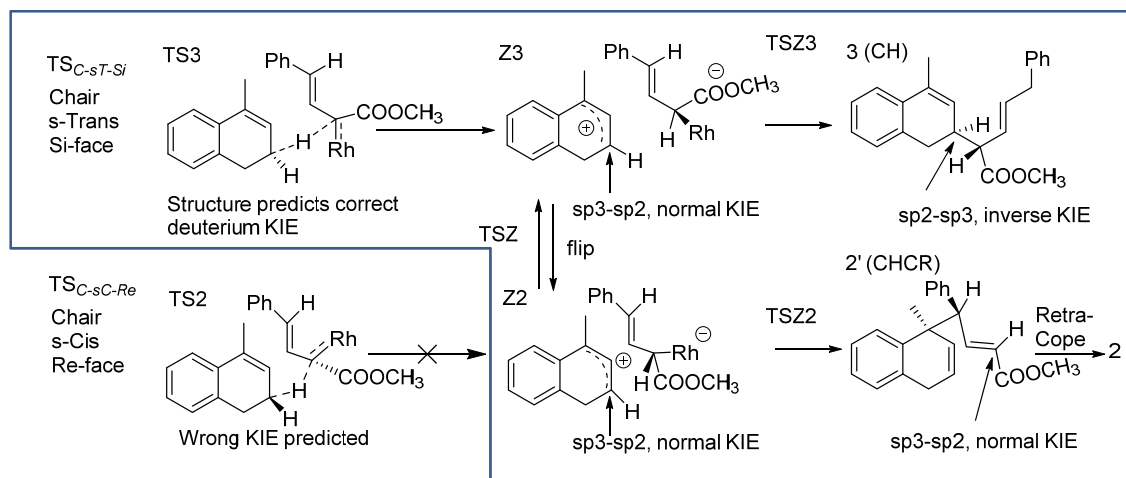
Scheme 8: Two possible scenarios for two products to have different KIEs. 1) Two transition states directly lead to their corresponding products: **TS3(->Z3)->3** and **TS2(->Z2)->2**. 2) Starting from either **TS3** or **TS2** to form a zwitterion (**Z3** or **Z2**) that can interconvert to another one, and then form the corresponding products. KIE calculations have suggested that **TS3**, the one with the chair and s-trans conformation, is likely the common transition state. The working mechanism is framed in the blue box. The hybridization change along the reaction was also labeled.

Intuition suggests that there are two distinct hydride transfer transition states to initiate the formation of the CHCR and direct C-H insertion product, respectively. Although distinct, they would result in very closely measured KIEs. Another hypothesis is that that one hydride transfer transition state leads to the formation of a zwitterion intermediate, which interconverts between two different conformations that can lead to different products. Different zwitterions are subjected to different isotopic fractionation when forming the CHCR and direct C-H insertion products. Those two scenarios are illustrated in Scheme 8. The first one would be two different routes for two different products: **TS3(->Z3)->3**, **TS2(->Z2)->2**, respectively; the second would start from either **TS2** or **TS3**, then the formation of either **Z2** or **Z3** (**Z** for zwitterion). **Z3** and **Z3** can inter- convert between each other but only lead to their corresponding products, **3** and **2'**

(quantitatively converts to **2**). Of course, if there are two hydride transfer transition states that generate the exact KIE for both products, we would not be able to tell if there are any intermediates involved or not. However, if there's only one hydride transfer transition state that corresponds to the KIE values measured, it is likely that both processes share the same hydride transfer transition state, with different intermediates before final product formation.

To tell the difference between those two scenarios, two sets of boat and chair hydride transfer transition states, with s-cis and s-trans conformation in each set, were optimized and the corresponding KIE for each one of them was calculated.[①] The calculations were carried out using M052X functional with 6-31g+(d,p) basis set for the second-row elements and effective core potential for rhodium(MWB28) using Gaussian 09.[57] Solvent model SMD was employed with dichloromethane. The results are summarized in Figure 2. It is no surprise that the two chair-TSs have lower energy than the calculated boat transition states. Without correcting for tunneling, the calculation often underestimates the value of the KIE. We found that three of the transition states have already produced a KIE value far greater than the measured values of 3.74 and 3.55, for CHCR and direct C-H insertion processes, respectively. Only the TS with a chair and s-trans conformation predicted the correct ^{2}H primary KIE and more closely reproduced a ^{2}H KIE of 3.43 with tunneling correction. KIE computed employing DFT have proven to be very accurate, so it is reasonable to assume that there's only one hydride transfer state leading to the formation of both products. To explain the different KIEs for the two different diastereomers, different routes must be taken after the first transition state (Although the possibility that there are other common transition states before the reaction coordinate goes to two different routes cannot be ruled out, it is not necessary to assume such events). Next, we will try to explore the hypothesis for further details on the basis that there is one common hydride transfer transition states, to explain the difference in primary KIEs between the two different routes.

The CHCR product displayed a primary KIE of 3.74, which is higher than that of the direct C-H insertion process, 3.55. This difference can be rationalized assuming a hybridization change from zwitterion to the product is occurring, as shown in Scheme 8. After hydride transfer, zwitterion **Z2** converts to the CHCR product **2'**. During this process, the C-H bond with the hydrogen being transferred goes through a rehybridization from sp3 to sp2, which is associated with a normal KIE where species with ^{1}H reacts faster than ^{2}H. Comparing this to the route the direct C-H insertion products take, from **Z3**->**3**, the C-H bond with the transferred hydrogen does not go through this rehybridization. We propose that this is where the differences in KIEs measured between the two products come from. On the other hand, on the retained hydrogen, there's an inverse KIE associated from **Z3**->**3** but not from **Z2**->**2**. These two

secondary KIEs at the second step are likely the source of the KIE difference between the two processes.

It is important to understand that product-specific KIE cannot be interpreted in the same way as conventional KIEs. The conventional KIEs are obtained by comparing the ratio of the partition function of the transition state ensemble to that of the starting materials for isotopic molecules. We would not be able to measure a difference in rates if the involved atoms go through another transition state with lower energy than the one that determines the KIE in an intermolecular KIE experiment. Product-specific KIE can measure the energetic differences even after the RDS if followed by a PDS different from the RDS. The isotopic fractionation for the PDS is thus reflected in the product-specific KIE and does not reflect the fractionation for a single step.
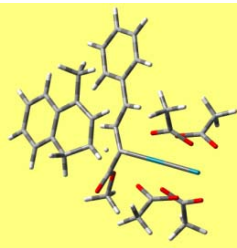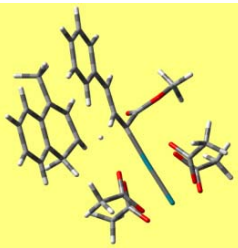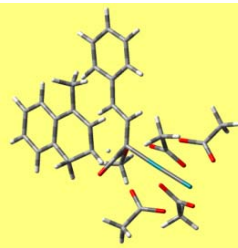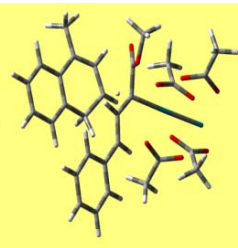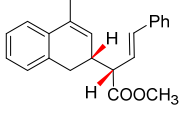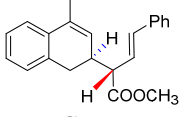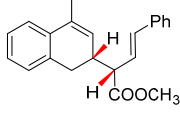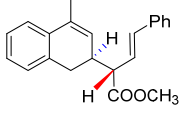
Starting Conformation	Chair, s-Cis	Chair, s-Trans	Boat, s-Trans	Boats-Cis
Optimized TS				
Corresponding Product	CHCR	CH	CHCR	CH
Relative Energy(kcal/mol)	0	0.83	4.47	6.79
$1°\ ^2$H KIE (Without/With Tunneling Correction)	4.40/4.8	3.37/3.4	4.34/4.6	4.20/4.5
$2°\ ^2$H KIE	1.07/1.1	1.06/1.0	1.05/1.0	1.02/1.0

Figure 2: Computational results for hydride transfer with four conformations. The four transition states were arranged from low energy to high energy by setting the first one to zero. The corresponding products were assumed according to the conformation of the transition state (The IRC calculations did not lead directly to products). The primary and secondary deuterium KIEs were calculated with and without a bell tunneling correction.

To better understand how exactly the product ratio changes when the site of insertion is isotopically labeled, the following energy diagram in Figure 3 based on mechanism discussed earlier will be used for illustration. The chair, s-trans hydride transfer transition state leads to zwitterion **Z3**, which can convert to **Z2**. Those two species are in equilibrium. For now, there's no exact information regarding the relative energy of **Z2** and **Z3**. A Curtin-Hammett scenario is assumed here. Starting material 1_{HH} is used to establish a ratio between 2_{HH} and 3_{HH}, measured as 2.19 as entry 1 shown in Table 1.

Now, consider changing the transferred atom from hydrogen to deuterium, as shown in Scheme 8 for the formation of **3**. Since there's no hybridization change on the anion from **Z3**->**3**, the vibrational frequency for both C-H bond and C-D bond do not change substantially during **TSZ3**. That means the activation energy for the deuterium substituted substrate will experience the same activation energy as it would with a hydrogen. However, this is different from **Z2**->**2**. Since the hybridization changed from sp3 to sp2, the vibrational well become looser in the **TSZ2** thus the vibrational frequency difference between the C-H bond and the C-D bond become smaller than they are in **Z2**. A higher activation energy for the deuterium substituted isotopologue is expected. According to the Curtin-Hammett principle, the product ratio depends on the relative energy of **TSZ3** and **TSZ2**. Thus the deuterated isotopologue will favor the direct C-H insertion product. This explains why the product ratio between **2**$_{DH}$ and **3**$_{DH}$ observed was reduced to 2.06 as shown in entry 3 in Table 1. Similarly, when the retained atom is deuterium, from **Z3** to **TSZ3**, the cation experiences a rehybridization from sp2 to sp3, this is associated with an inverse KIE. This process lowers the energy required for **TSZ3** compared to that of **TSZ2**, which is unchanged. It also results in a product ratio drop between **2**$_{HD}$ and **3**$_{HD}$, from 2.19 to 2.14, as shown in entry 2, Table 1.
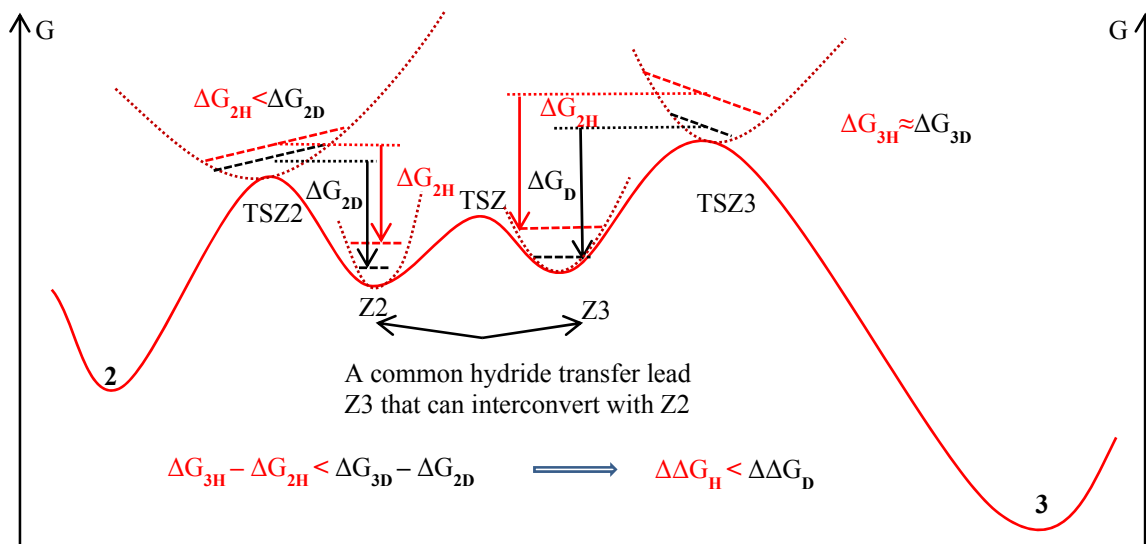

Figure 3: Energy diagram for rhodium catalyzed C-H insertion-isotopic substitution. The reaction was initiated with a hydride transfer from the naphthalene moiety; and then forms zwitterion which can rearrange to two different conformational isomers leading to two distinct products.

The same effect was when carrying out the intermolecular KIE experiment between **1**$_{HH}$ and **1**$_{DD}$, as shown in Scheme 9. The equations used to calculate the intermolecular KIE is:

$$KIE_{inter}(HH/DD) = \frac{^{HH}k}{^{DD}k} = \frac{\ln(1 - F_{HH})}{\ln(1 - F_{DD})} = \frac{\ln\left[(1 - F_{all})\left(1 + \frac{1}{R_0}\right)/\left(1 + \frac{1}{R}\right)\right]}{\ln[(1 - F_{all})(1 + R_0)/(1 + R)]} \quad \cdots\cdots (3)$$

where R_0 and R stand for the ratio of $\mathbf{1_{HH}/1_{DD}}$ in the starting material mixture and reisolated starting material. ^{HH}k and ^{DD}k stand for the overall rate of reaction for the two isotopologues, respectively. The product specific KIE is:

$$\frac{^{HH}k_2}{^{DD}k_2} = KIE_{inter}(HH/DD) \times \frac{([\mathbf{2_{DD}}] + [\mathbf{3_{DD}}])/[\mathbf{2_{DD}}]}{([\mathbf{2_{HH}}] + [\mathbf{3_{HH]}}])/[\mathbf{2_{HH}}]} \quad \cdots\cdots\cdots (4)$$
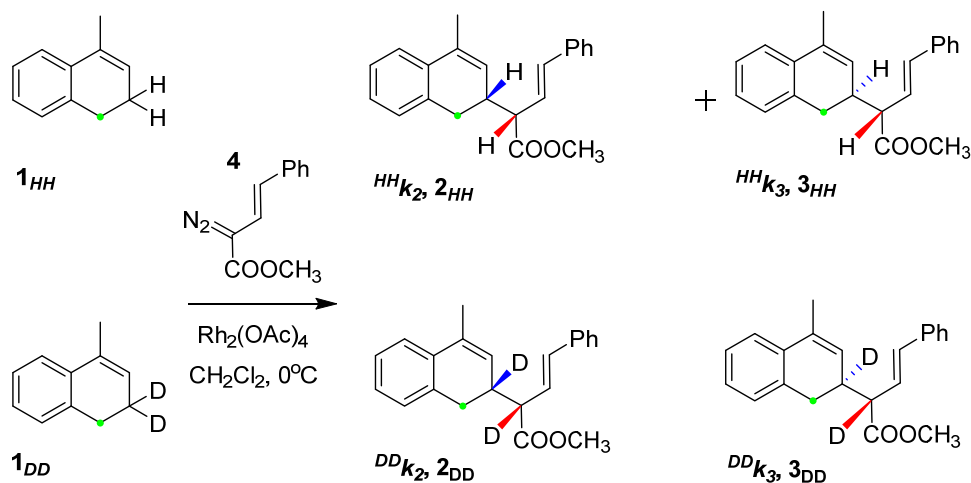
Scheme 9: Intermolecular KIE experiment between the perprotiated ($\mathbf{1_{HH}}$) and di-deuterated ($\mathbf{1_{DD}}$) isotopologues. Each starting material generates two products with their specific rate constants. The green-dot labeled carbons are chosen for measurement using ^{13}C spectrum.

Table 2: Intermolecular KIE measured from competition experiments between $\mathbf{1_{HH}}$ and $\mathbf{1_{DD}}$ using Rh$_2$(OAc)$_4$ as the catalyst. Values for entry 1 and 2 are directly measured from experiment while 3 and 4 are calculated using product-specific KIE formula.

Entry	Rate Ratios	Values	Products	Explanation
1	$^{HH}k_2/^{HH}k_3$	2.19(1)	$\mathbf{2_{HH}/3_{HH}}$	CHCR/CH-$\mathbf{1_{HH}}$ -H transfer
2	$^{DD}k_2/^{DD}k_3$	2.03(1)	$\mathbf{2_{DD}/3_{DD}}$	CHCR/CH-$\mathbf{1_{DD}}$ -D transfer
3	$^{HH}k_2/^{DD}k_2$	3.98(4)	$\mathbf{2_{HH}/2_{DD}}$	H/D transfer-$\mathbf{1_{HD}}$&$\mathbf{1_{DD}}$-CHCR process
4	$^{HH}k_3/^{DD}k_3$	3.78(4)	$\mathbf{3_{HH}/3_{DD}}$	H/D transfer-$\mathbf{1_{HD}}$&$\mathbf{1_{DD}}$-CH process
5	$KIE_{inter}^{Acetate}(HH/DD)$	3.89(4)		Compound KIE between $\mathbf{1_{HH}}$ and $\mathbf{1_{DD}}$

The results are summarized in Table 2. As shown in entry 1 and 2, the diastereomeric ratio $\mathbf{2_{HH}/3_{HH}}$, 2.19, is bigger than that of $\mathbf{2_{DD}/3_{DD}}$, 2.03. If we take a closer look, take the ratio between the values in entry 1 and entry 2 (2.19/2.14=1.02); and the ratio between values in entry 1 and entry 3 (2.19/2.06=1.06), which accounts for the rate contribution

from a retained deuterium and a transferred deuterium atom, respectively. The multiplication of those two ratios: 1.02*1.06=1.08 is in good agreement with the one ratio between $2_{HH}/3_{HH}$ and $2_{DD}/3_{DD}$, 2.19/2.03=1.08.

The rule of geometric mean[58,59] can be used to compare the intermolecular KIE between 1_{HH} and 1_{DD}, $\text{KIE}_{inter}^{\text{Acetate}}$(HH/DD) as shown in Table 1, and that of 1_{HH} and 1_{HD}, $\text{KIE}_{inter}^{\text{Acetate}}$(HH/HD) as shown in Table 1. The rule of geometric mean states that the isotope effect displayed by each isotopic substitution is independent of other isotope effects. As shown in Figure 2, the computed tunneling correction to the semi-classical KIE is not a substantial value, which means the substitution of a secondary deuterium does not significantly affect the imaginary frequency[59,60] of the transferred atom. For this reason, we could test the computational results by applying the rule of geometric mean as shown in Equation 5 and 6. Since there's no statistical observable secondary KIE on the retained atom, solving equation 5 give us a primary KIE of 3.87, which matches very well with the compound KIE from equation 6. Since the secondary KIE in Equation 5 is essentially unity based on our assumption, that makes the primary KIE measured from both experiments consistent. Their adherence to the rule of geometric mean suggests that there is no significant tunneling occurring during reaction,[58,60,61] which is consistent with our computation results.

$$\text{KIE}_{inter}^{\text{Acetate}}\left(\frac{\text{HH}}{\text{HD}}\right) = \frac{2k_{HH}}{k_{DH} + k_{HD}} = \frac{2}{\frac{k_{DH}}{k_{HH}} + \frac{k_{HD}}{k_{HH}}} = \frac{2}{\frac{1}{1°\text{KIE}} + \frac{1}{2°\text{KIE}}} = 1.57 \cdots\cdots (5)$$

$$\text{KIE}_{inter}^{\text{Acetate}}\left(\frac{\text{HH}}{\text{DD}}\right) = \frac{k_{HH}}{k_{DD}} = \frac{k_{HH}}{k_{DH}} \times \frac{k_{HH}}{k_{HD}} = 1°\text{KIE} \times 2°\text{KIE} = 3.89 \cdots\cdots (6)$$

4.3 Investigation on the Relative Barrier Heights on PDS for CHCR and Direct C-H Insertion Processes

To probe the relative barrier heights of the two different processes experienced, the $Rh_2(OAc)_4$ catalyzed C-H insertion experiments were conducted at different temperatures ranging from -10 °C to 100 °C in 1,2,3-trichloropropane. This solvent was chosen because it remains in a liquid state over a wide range of temperatures (-14 °C-156 °C); and that it has a similar dielectric constant (7.5) compared to dichloromethane (9.14). The generally expected result, if there's no mechanism change with the change of solvent, is that the diastereomeric ratio would be bigger at lower temperatures and smaller at elevated temperatures. The given the diastereomeric ratio equals to $\exp(-\Delta\Delta G(\mathbf{TSZ2}, \mathbf{TSZ3})/RT)$, where $\Delta\Delta G(\mathbf{TSZ2}, \mathbf{TSZ3})$ is the barrier difference between the two transition states leads to the final CHCR and direct C-H insertion product, as shown in Figure 3. The experimental results are plotted as diastereomeric ratio (dr.) vs. temperature (T), or the Arrhenius plot according to Equation (7), ln (dr.) vs. inverse temperature (1/T) as shown in Graph 1a and Graph 1b, respectively.

The data sets were originally collected from 0 °C to 100 °C. Due to the strange behavior observed at lower temperatures, repeated experiments were carried out again at 0 °C, 20 °C and 40 °C, which showed no substantial deviation from values measured previously. A final measurement at -10 °C was conducted, and this data point continues the observed trend at lower temperatures. It is unusual that the observed diastereomeric ratio did not increase all the way when the temperature was lowered. As shown in Graph 1a, as the temperature went lower, the diastereomeric ratio went higher at first from 2.35 to 3.1; but lowered to 2.8 from 20 °C to -10 °C. It implies either a mechanism change; or that multiple transition states govern the diastereomeric ratio.
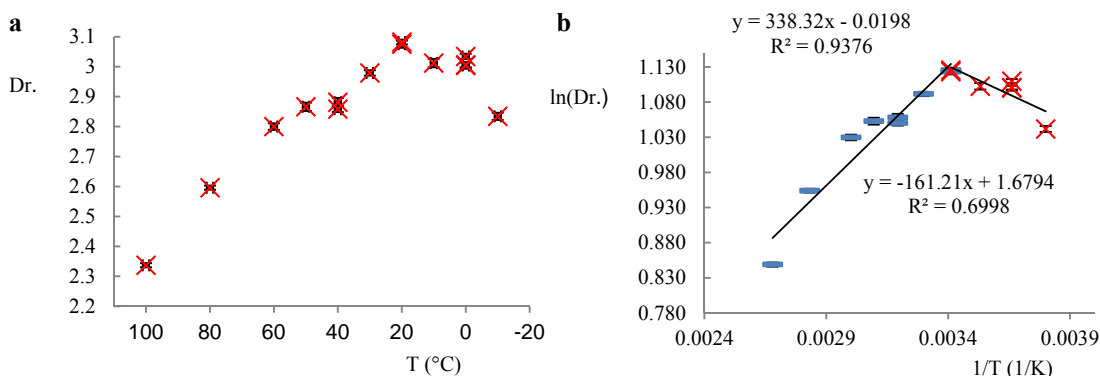
Graph 1: Diastereomeric ratio (dr.) vs. temperature for C-H insertion carried out in 1,2,3-trichloropropane with $Rh_2(OAc)_4$. a) Product ratio between 2_{HH} and 3_{HH} from 100 °C to -10 °C. The experiments at 0 °C, 20 °C and 40 °C have been carried out twice for verification. The error bars for each data point is hardly noticeable. b) Arrhenius plot: natural logarithm of the values of dr. versus 1/T over the temperature range. The blue series are from 100 °C to 20 °C and the red series are from 20 °C to -10 °C.

$$\ln\left(\frac{[\textbf{2}]}{[\textbf{3}]}\right) = \ln(e^{\frac{-\Delta\Delta G_{23}}{RT}}) = \ln\left(e^{\frac{-(\Delta\Delta H_{23} - T(\Delta\Delta S_{23}))}{RT}}\right) = -\frac{\Delta\Delta H_{23}}{R} \times \frac{1}{T} + \frac{\Delta\Delta S_{23}}{R} \cdots\cdots (7)$$

$$\Delta\Delta G_{23} = G_{\textbf{TSZ2}} - G_{\textbf{TSZ3}}$$

As we postulated that there are two interconverting zwitterions, supported by the experimentally observed decreasing (or just changing) diastereomeric ratio from 100 °C to 20 °C, the barrier between the two zwitterions is likely lower than that of the transition states leading to products. It implies the rate of interconversion between zwitterions is faster than product formation. The reaction is under Curtin-Hammett control,[62–66] thus the barrier difference between **TSZ2** and **TSZ3,** $\Delta\Delta G_{23}$ will determine product ratio according to $\exp(-\Delta\Delta G_{23}/RT)$, displayed as the red curve in Figure 4. As pointed out by Seeman in the historical review about Curtin-Hammett principle/Weisten-Holness equation,[66] it doesn't mean the barrier between **Z2** and **Z3** plays no role in determining the product ratio, the equilibrium constant K (equals to k_{23}/k_{32}) is actually proportional to the final product ratio by the relationship indicated in Equation (8). This relationship can be understood in a way that, although the net free energy that controls the product ratio is

$\Delta\Delta G_{23}$, the equilibrium constant K affects $\Delta\Delta G_{23}$ as it changes the barrier height of $\Delta G_{2,c}$ and $\Delta G_{2,c}$. As the temperature changes from high to low, the enthalpy difference, $\Delta\Delta H_{23}$ which is proportional to the slope $-\Delta\Delta H_{23}/R$ on the Arrhenius plot, is becoming smaller and finally switch sign ($\Delta\Delta H_{23}<0$). The intercept, $\Delta\Delta S_{23}/R$, also changes from negative to positive (-0.0198 to 1.6794) as displayed in Graph 1b. The structures for **TSZ2**, **TSZ3** and **TSZ** have not been optimized due to the difficulties for simulation of zwitterions. The exact nature of how the enthalpy and entropy change over temperature is not known. However, it is possible that the fast interconversion of zwitterions at a higher temperature becomes limited at a lower temperature. The barrier between zwitterion interconversion becomes comparable to that of product formation, as the blue curved shows in Figure 4, a

$$\frac{[2]}{[3]} = \frac{k_{23}}{k_{32}}\frac{k_2}{k_3} = K\frac{k_2}{k_3}\cdots\cdots (8)$$
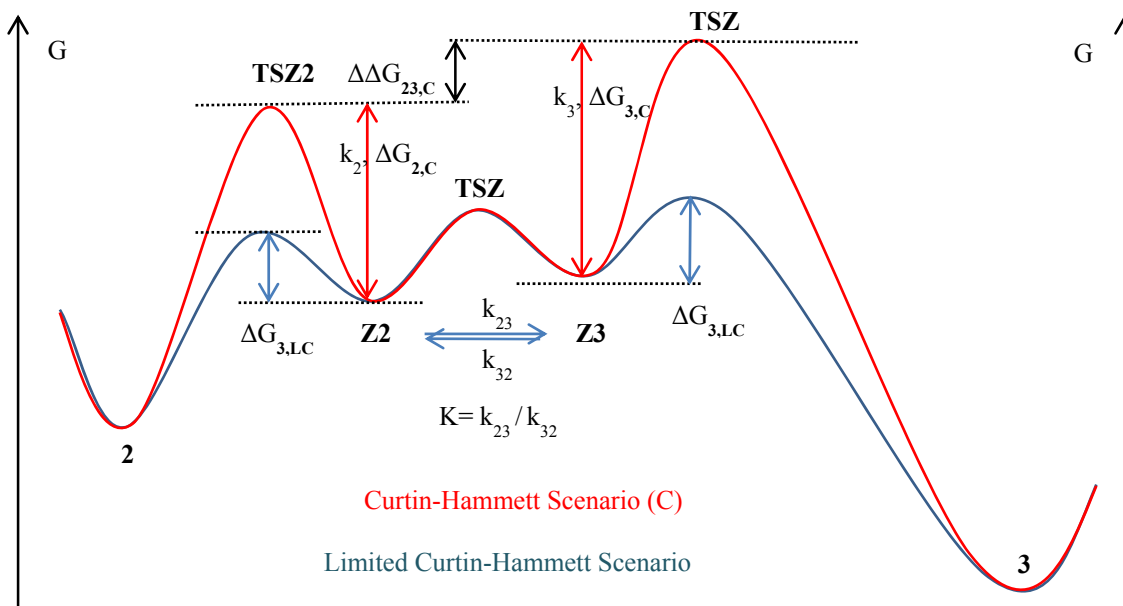

Figure 4: Energy diagram rhodium catalyzed C-H insertion-two possible Curtin-Hammett scenarios: Hydride transfer leading to the formation of two zwitterions, **Z2** and **Z3**. These two zwitterions can interconvert through transition state **TSZ**. The red curve shows the Curtin-Hammett scenario that the interconversion between zwitterions is much faster that of product formation; the blue curve shows that the barriers for the interconversion are comparable to that of product formation, which is the Limited Curtin-Hammett scenario. The barrier heights between the red curve and the blue curve are relative since all the barriers are changing dynamically with temperature. The way of drawing both curves matching with each other for the interconversion is just for a good comparison between the barrier heights for zwitterion conversion and product formation at different scenarios.

limited Curtin-Hammett Scenario (LC). It is the dynamic play between the equilibrium constant K, k_2, and k_3 in Equation (8) that controls the product ratio. A similar case could be found in Singleton's article about the mechanism of triazolinedione ene reaction.[67] The product ratio varied over a range of temperatures, and a curvature was also observed

on the Arrhenius plot. It was hypothesized that these two products resulted from two different intermediates: a biradical and a zwitterion. By adjusting the thermodynamic parameters of the activation barriers, good numerical fitting of the product ratio was achieved.

Table 3: Qualitative results for diastereomeric ratio change in chlorinated solvents with different dielectric constants for $Rh_2(OAc)_4$ catalyzed C-H insertion.

Solvents	Dielectric constants (20 °C)	Dr. Ratio (20 °C)
CCl_4	2.24	1.6
$CHCl_3$	4.81	1.8
CH_2Cl_2	9.14	2.2

Although earlier studies by Davies and co-workers[25] showed that there were no zwitterions being formed as an intermediate, the deuterium KIE study and the nonlinear Arrhenius plot demonstrated the high possibility of zwitterion's existence. Our initial qualitative results for diastereomeric ratio change in solvents, which are structurally close but different in dielectric constants, can also support the idea of zwitterion intermediates. As shown in Table 3, the higher the dielectric constants for the solvent, the higher the diastereomeric ratio. This trend suggests that the solvent can affect the stability of the two zwitterions, since it regulates the energy for the transition states and the relative barrier between the two processes.

4.4 ^{13}C KIE Investigation on $Rh_2(OAc)_4$ Catalyzed C-H Insertion

Natural abundance ^{13}C KIE method has been employed to determine the carbon that is involved during the hydride transfer and subsequent steps for this transformation. As shown in Figure 5, the compound ^{13}C KIE was measured the same way as originally described in Singleton method.[55] Position 5 was selected as the standard. The reason for this selection is partially assumed that it does not participate substantial fractionation (position 1,2,3 and 4 would be better for this reason but lack of good resolution on NMR spectrum); and partially because the two carbon peaks for different diastereomers are well separated on the NMR spectrum for accurate integration. The measured results on position 1,2,3 and 4 have proven it is a relatively good choice since the KIEs on these positions are close to unity. The sites bearing a KIE show us how much fractionation has occurred in the overall reaction. A KIE of 1.015 exists at position 7, where a hydride transfer event occurs. Position 6 also possesses a KIE of 1.005; it is a likely scenario that while the hydride transfer is happening, the positive charge developing at position 7 is demanding electron donation from the C-H bond at position 6, via hyperconjugation. Hyperconjugation itself can lower the energy of the system thus allowing the extension of the conjugation system from the benzene ring to the whole molecule, which lowers the

energy even further. This conjugation could also be the reason why position 8 and 9 bear a normal KIE of 1.010, with a π bond partially breaking between 8 and 9.
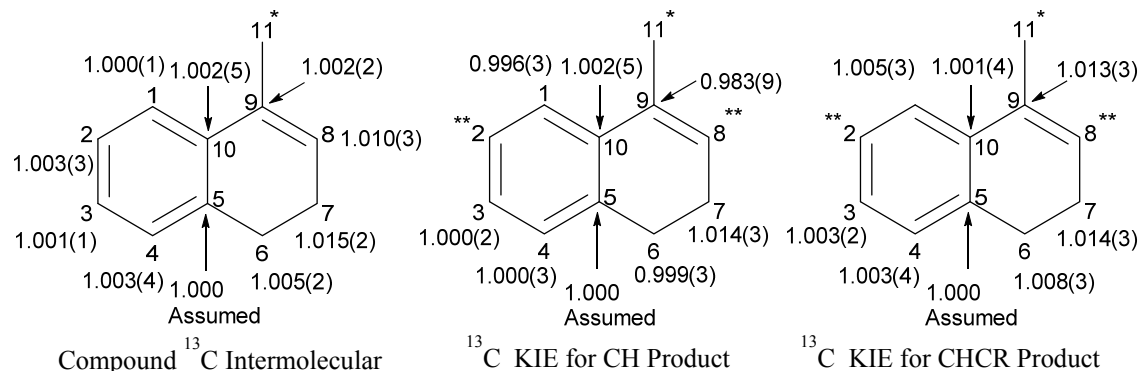

Figure 5: Experimental ^{13}C KIE for C-H insertion catalyzed by Rh$_2$(OAc)$_4$. The compound ^{13}C KIE was measured by counting the isotopic fractionation, which was determined by the percent of conversion, relative ^{13}C concentration on the starting material and reisolated starting material for each carbon, respectively. The product-specific KIE for each product requires the ^{13}C ratio between the two products at each corresponding carbon position. *: the methyl site was contaminated, and the integration was not accurate in this measurement. **: position 2 and 8 cannot be separated on NMR spectrum and accurately integrated.

Product-specific KIEs can give us more insight as to when and how these two products were formed via different pathways. It is easier to measure the ^{13}C ratio in this reaction, compared to the cobalt catalyzed reaction in Chapter 3, if we only consider the product ratio; however, it is more challenging to measure the ^{13}C ratio for products in this reaction due to two other reasons: 1) phase separation was observed in the NMR tube when higher concentration was used, even with solvent and temperature optimization; 2) significant line broadening was observed when higher concentration was used; 3) the higher molecular weight for the products, plus the product ratio of approximately 2:1 makes the concentration in mole for the minor product even lower, thus the signal to noise ratio (S/N) became even smaller. Despite the hurdles, with multiple measurements and taking the weighted average, we obtained a result that's qualitatively explainable, although caution should be taken. For example, most of the aromatic carbons, assumed not to be involved in any significant bond breaking or formation, have no KIEs observed in the range of error, when compared to the compound KIE observed for the hydride transfer site in the starting material.

The product-specific KIEs showed the same KIE 1.014 at position 7 for both CHCR and direct C-H insertion products. However, a vastly different KIE at position 9 was observed, with the direct C-H insertion process 0.983 and CHCR 1.013. An inverse ^{13}C KIE does not usually appear unless the newly formed bond is much stronger than the one being broken. One of such rare cases[68–70] has been observed in S$_{N1}$ like event that occurs on the ionization of triphenylcarbon chloride, where the broken a C-Cl or C-Br bond is

70

associated with the hyperconjugation of three benzene rings. It largely strengthens the C-C bonds between the positive charge bearing carbon and the atom on the aromatic rings connecting to it. However, a number less than one in product-specific KIE should not necessarily need to be understood in the same manner as the conventional KIE, owing to the fractionation of isotopes from the same pool of intermediates, which fully convert to products. It means, that if pathway one converts more ^{12}C to products, another pathway would inevitably end up with more ^{13}C. This is likely the case here. As shown in Figure 5, the CHCR product displayed a normal KIE 1.013 at position 9, indicating that breaking of the C-C π bond between 8 and 9, and the formation of the C-C bond between position 9 and the benzylic carbon on the carbenoid moiety. The lack of fractionation at position 7, although no explanation has been formulated at this point, is consistent with the observed almost unity secondary deuterium KIE for the retained hydrogen as shown in entry 7 and entry 9, Table 1. The fractionation at position 6 cannot be easily explained currently.

Computational results for ^{13}C KIE with tunneling correction are displayed in Figure 6. Although very similar values were afforded at position 7 for almost all conformations, only the transition state with a chair (between moiety **1** and the rhodium carbenoid) and s-trans (for the rhodium carbenoid) conformation, the second one in Figure 6, displayed a normal KIE of 1.004. It confirms the involvement benzylic C-H bond during the hydride transfer transition state through hyperconjugation. Small KIEs at position 8 and 9, 1.001 and 1.002 respectively, indicate the electron donation from the double bond to the positive center that's forming at position 7 during the hydride transfer. It is qualitatively consistent with our experimentally measured KIEs.

Up to this point, we have investigated the mechanism of the $Rh_2(OAc)_4$ catalyzed C-H insertion using experimental conventional and product-specific KIEs and computational KIEs, as well as temperature and solvent effects. The results have demonstrated that the reaction goes through a common hydride transfer to form a zwitterion (**Z3** or **Z2**) that can interconvert between itself and one of its conformational isomer (**Z2** or **Z3**), followed by the formation of the products. This mechanism is based on the comprehensive information provided by our results coupled with the following arguments: 1) The product ratio varies differently with respect to different positions where a deuterium substituting a hydrogen, at a primary or a secondary position indicates that there are two competing transition states. 2) The product specific KIEs are statistically different yet still close enough to share the same hydride transfer transition states, supported by that there's only one hydride transition state generating both ^2H and ^{13}C computed KIEs that are close to the measured the ones. 3) Temperature effects on the diastereomeric ratios also demonstrated there are two competing processes. 4) diastereomeric ratio changing with respect to solvents bearing similar size and structure, but different in dielectric constants suggests that the stability of the intermediates or the transition state is affected, most likely by affecting charge separation and distribution in a zwitterion. All those

arguments do not support the bifurcation mechanism as studied previously,[25] where a dynamic scenario governs the diastereo-selectivity, in which the diastereomeric ratio should not change significantly over temperature variation. Now we will try to apply the learned mechanism to the Rh$_2$(S-DOSP)$_4$ catalyzed C-H insertion with the same set of starting materials after a short discussion on the cyclopropanation of *3-methyl-1H-indene,* a compound structurally close to **1** with one less carbon.
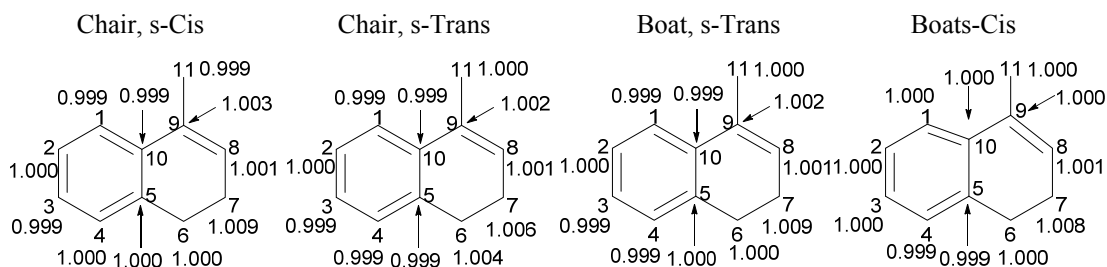

Figure 6: Computational ^{13}C KIE for four different hydride transfer transition states. The four transition states are displayed in the same order as in Figure 2. All the KIEs are with Bell tunneling corrections.

4.5 A Short Study on the Cyclopropanation of 3-Methyl-1H-indene Catalyzed by Rh$_2$(OAc)$_4$

As shown in Scheme 3, compound *3-methyl-1H-indene* (**5**) was tested with the same condition as the C-H insertion of **1.** It results in the cyclopropanation product **6** as the only product of the reaction. Since the route that leads to C-H insertion is most likely started with a hydride transfer, molecule **1** can stabilize this positive charge by conjugation with the double bond extended aromatic system and hyperconjugation from the benzylic C-H bonds, as shown in Scheme 10. However, this is not the case for molecule **5**, where eight π (4n π) electrons are connected in a head-to-tail fashion; an anti-aromatic system needs to be formed to make this hydride transfer. This situation is not likely and explains why we observed only the cyclopropanation product.
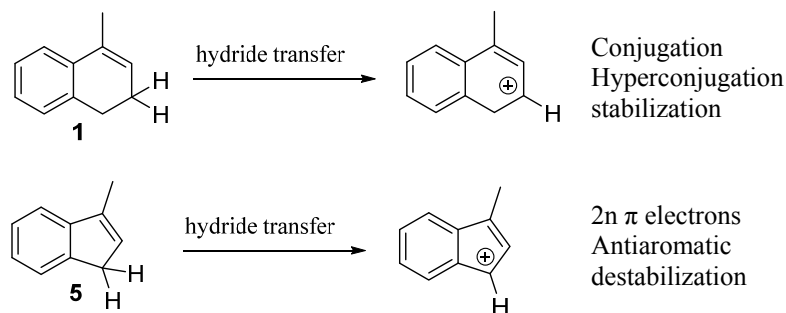
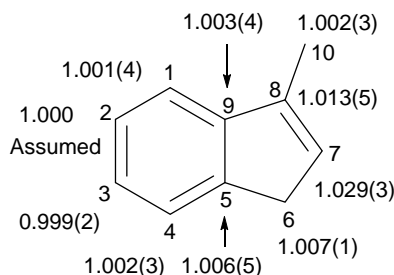Scheme 10：Hydride transfer scenarios for 4-methyl-1,2-dihydronaphthalene (**1**) and 3-methyl-1H-indene (**5**).

Figure 7: Intermolecular ^{13}C KIE experiment of 3-methyl-1H-indene (**5**)

The natural abundance ^{13}C KIE experiments were carried out, and the results are summarized in Figure 7. Position 7 and 8 display KIEs of 1.029(3) and 1.013(5), respectively. Both values are slightly larger than that of the measured ones on styrene's cyclopropanation measured by Singleton and co-workers,[19] 1.024 and 1.003 on the terminal and benzylic carbon, when reacted with ethyl diazoacetate catalyzed by either Rh_2(Octanoate)$_4$ or Rh_2(*S*-DOSP)$_4$, respectively. However, the implication on the mechanism is the same: a concerted but highly asynchronous transition state for the cyclopropanation. The reason why the KIEs are larger in the indene system is most likely due to the use of **4** (*E*)-methyl 2-diazo-4-phenylbut-3-enoate as a carbene precursor instead of ethyl diazoacetate, where the former possesses stronger electron-donating ability than the latter. This **4** induced donor-acceptor carbenoid is more selective than an acceptor only (ethyl diazoacetate as the precursor) type carbenoid. It puts a higher energy barrier for the cyclopropanation.[16] This barrier is likely to delay the transition state and causes the ^{13}C KIEs to be larger, since the vibration modes associated with the bond breaking become less starting material like.

4.6 ^{2}H and ^{13}C KIE Experiments, Results and Implication on the Mechanism of C-H Insertion Catalyzed by Rh₂(S-DOSP)₄

It is the similarity between Rh_2(OAc)$_4$ and Rh_2(*S*-DOSP)$_4$ in the formation of the CHCR product **2** that inspired us to compare these two reactions together. Both reactions generate **2'** first, and then it converts to **2** at room temperature. The previous computational mechanistic study,[25] which employed a simpler model using Rh_2(OOCH)$_4$ and cyclohexane diene in gas phase, has shown that there is no distinct transition states for the formation of CHCR and direct C-H insertion products. Since this is not the case we found for the Rh_2(OAc)$_4$ catalyzed reaction, KIE experiments for Rh_2(*S*-DOSP)$_4$ were also carried out.

73
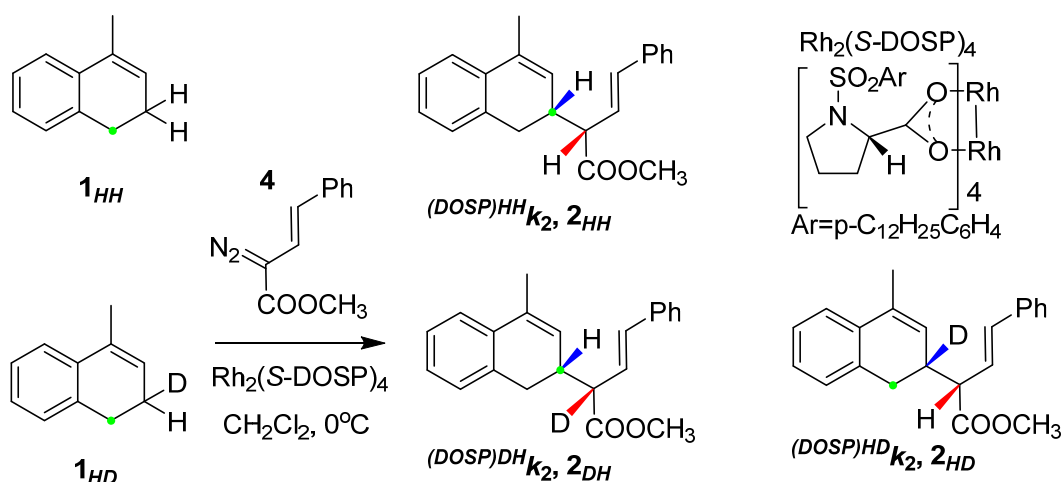
Scheme 11: Intermolecular KIE experiment between the perprotiated (1_{HH}) and mono-deuterated (1_{HD}) isotopologues catalyzed by Rh$_2$(S-DOSP)$_4$. The green-dot labeled carbons are chosen for measurement using ^{13}C spectrum.
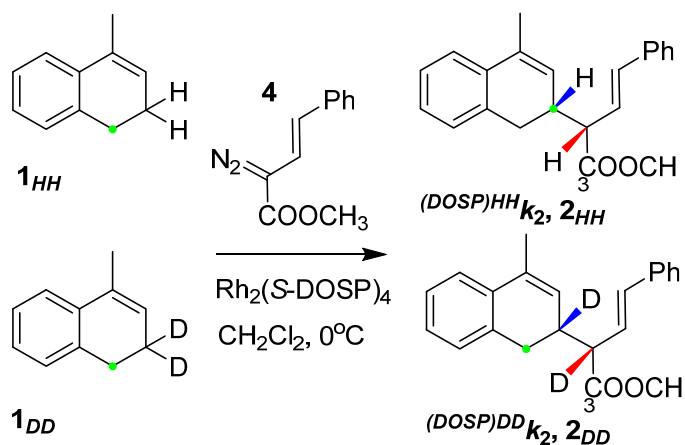
Scheme 12: Intermolecular KIE experiment between the perprotiated (1_{HH}) and mono-deuterated (1_{DD}) isotopologues catalyzed by Rh$_2$(S-DOSP)$_4$. The green-dot labeled carbons are chosen for measurement using ^{13}C spectrum.

As shown in Scheme 11, the intermolecular KIE experiment between 1_{HH} and 1_{HD} was carried out. It is important to point out that 1_{HD} is composed of equal amounts of two enantiomers. Since a chiral catalyst has been used, and we obtained only one product that is both enantiomerically and diastereomerically pure for each proton transferred; it is not an unreasonable idea to assume that the naphthalene approaches the carbene only from one side; although there is still a slight possibility for the naphthalene to approach the carbenoid from both sides and only afford one product. With this in mind, the raw data was processed in a way that each diastereomer from 1_{HD} was only generated by its corresponding enantiomer in the starting material. The intermolecular KIE experiment between 1_{HH} and 1_{DD} was also performed as shown in Scheme 12. The results of both experiments are listed in Table 4. The primary KIE of 3.96(6) between 1_{HH} and 1_{HD} is not

74

much different from that of 1_{HH} and 1_{DD}, 3.90(5), a factor of 1.02. Similar values between those two experiments are expected, since there's not much secondary KIE on the retained C-H bond at the site of insertion; and there's no fractionation after the hydride transfer since there's only one product being formed, compared to the $Rh_2(OAc)_4$ catalyzed reaction. This KIE is very close to the intermolecular KIE (3.89) when $Rh_2(OAc)_4$ was used for the reaction between 1_{HH} and 1_{DD}. Based on the deuterium KIE, it is likely that the mechanisms for these two reactions are very similar.

Table 4: KIE measured from competition experiments between 1_{HH} and 1_{HD} (entry 1 and 2), 1_{HH} and 1_{DD} (entry 3) in dichloromethane at 0°C using Rh_2(S-DOSP)$_4$ as the catalyst.

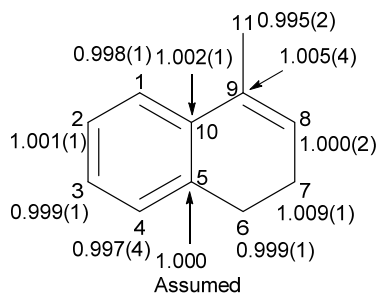| Item	Rate Ratios	Values	Products	Explanation
1	$^{(DOSP)HH}k_2/^{(DOSP)DH}k_2$	3.96(6)	$2_{HH}/2_{DH}$	H/D transfer-1_{HH}&1_{HD}-CHCR process
2	$^{(DOSP)HH}k_2/^{(DOSP)HD}k_2$	1.04(2)	$2_{HH}/2_{HD}$	H/H transfer-1_{HH}&1_{HD}-CHCR process
3	$^{(DOSP)HH}k_2/^{(DOSP)DD}k_2$	3.90(5)	$2_{HH}/2_{DD}$	H/D transfer-1_{HH}&1_{DD}-CHCR process

Figure 8: ^{13}C KIE measured for C-H insertion using Rh_2(S-DOSP)$_4$ as a catalyst. *Value was not shown due to likely contamination on the methyl carbon.

^{13}C KIE experiments were also performed for Rh_2(S-DOSP)$_4$ catalyzed C-H insertion. The ^{13}C KIE of 1.009 at site 7 is consistent with the hydride transfer transition state as discussed for $Rh_2(OAc)_4$ case. The value 1.005 at position 9 should only be compared to the intermolecular ^{13}C KIE for the $Rh_2(OAc)_4$ catalyzed reaction, not the larger magnitude product-specific KIE 1.013 for the CHCR product. The reason is that the later one does not result from the hydride transfer step; instead, it is caused by the CHCR path, which draws isotopes from a pool of zwitterion intermediates, and not directly from the starting material. According to the mechanism studied for the $Rh_2(OAc)_4$ catalyzed reaction, a concerted mechanism for the Rh_2(S-DOSP)$_4$ catalyzed reaction, if exists, could be thought as that the energy of the local minimum of the zwitterion intermediate on the potential energy surface along the reaction coordinate rises to match with the downhill slope after the hydride transfer transition state. To explain the highly enantio- and diastereo- selective nature of this S-DOSP ligated catalyst, the steric environment could make it energetically much less favorable for the zwitterion to convert to anther conformation. Solvents with different dielectric constants could also change the relative

stability of zwitterions and the height of related transition state barriers, which will affect the selectivity. It is interesting that there's no KIE observed at site 6 as was on the $Rh_2(OAc)_4$ catalyzed reaction. It could be caused by the steric constraint of the *S*-DOSP ligand, which makes the hyperconjugation of the C-H bond at position 6 to a positively charged carbon 7 less likely. However, to tell whether this difference exists, a frequency calculation with the *S*-DOSP ligand; or at least a relative similar steric environment mimic this massive ligand, would be optimal.

4.7 Summary

The mechanism of C-H insertion of compound **1** using donor-acceptor type rhodium carbenoid has been studied utilizing kinetic experiments, conventional and product-specific KIEs, DFT calculations. The exclusive information obtained from the product-specific KIE measurements lead to a hypothesized zwitterion intermediate with high confidence. Such evidence would not be easily obtained for short living intermediates in reactions with clean products. Computational methods are invaluable to the exploration of a mechanism or intermediate structures where traditional physical experiments are limited. However, over-simplified models, lack of consideration of potentially important factors and under-developed theories, makes the complete mapping of all possible intermediates and transition states on the potential energy surface unlikely. Even when extreme caution is taken, mechanistic studies that rely on computational efforts only place the investigation of a complicated reaction under great scrutiny.[46] The product-specific KIE method provides critic and previously unattainable mechanistic information regarding the existence of specific intermediates or transition states. It is capable of elucidating the isotopic fractionation events occurring at the rate-determining step and subsequent competitive product-determining step. It can be used to corroborate computational theories or methods used to determine chemical reaction mechanisms.

4.8 Experimental Section

4.8.1 Syntheses

4.8.1.1 Synthesis of 4-methyl-1,2-dihydronaphthalene[71]

A 1.0L RBF was charged with an additional funnel. The system was flame dried with vacuum and nitrogen refill cycles. After charging the RBF with 1-Tetralone (100 mmol, 13.3 ml, in 150 ml anhydrous THF) and the additional funnel with CH_3MgI solution (150 mmol, 3 M, 50 ml), the RBF was cooled down to 0 °C using an ice-water bath. The CH_3MgI solution was added to the 1-Tetralone solution dropwise in 20 min; then followed by addition of 50 ml anhydrous hexamethylphosphoramide (HMPA) into the mixture in one portion. After 9 hours of stirring at r.t., HCl solution (15%, 180 ml) was added slowly into the mixture at -78 °C. The mixture was allowed to stir about 10 hours after warming up to r.t. The resulted mixture was extracted with diethyl ether (200 ml*3).

The ether layer was dried over MgSO$_4$. The solvent was removed in *vacuo*. Flash column chromatography of the residue with pentane afforded 7.8 g colorless product. Yield: 54%. ^{1}H NMR (400 MHz, CDCl$_3$): 7.20 (m, 2H); 7.11 (m, 2H); 5.84 (m, 1H); 2.75 (t, 2H); 2.24 (m, 2H); 2.04 (q, 3H).
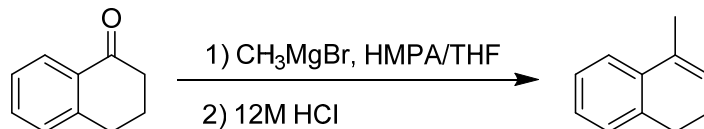
4.8.1.2 Synthesis of 3-methyl-1H-indene
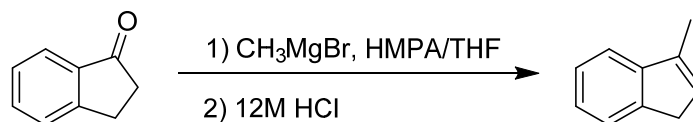
The procedure and the relative amounts of each reagent are the same as the synthesis of *4-methyl-1,2-dihydronaphthalene.* Yield: 62%. ^{1}H NMR (400 MHz, CDCl$_3$): 7.47 (d, 1H); 7.36 (d, 1H); 7.33 (dt, 1H); 7.22 (t, 1H); 6.23 (m, 1H); 3.32 (p, 2H); 2.18 (q, 3H).

4.8.1.3 Synthesis of 2-d$_1$-4-methyl-1,2-dihydronaphthalene
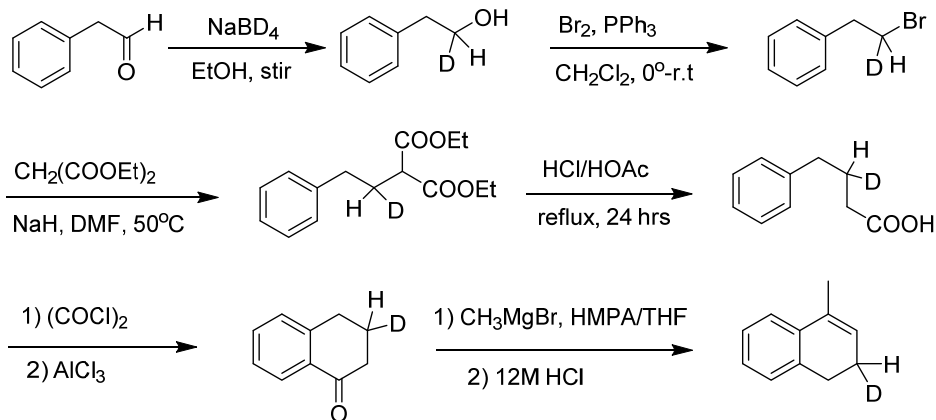
Synthesis of 1-d$_1$-2-phenylethanol

After mixing Phenylacetaldehyde (47.34 g, 394 mmol) with 600 ml dry ethanol in a 2 L-Erlenmeyer flask with stirring, Sodium borodeuteride (90%, 98% D, 6.865 g) was introduced into the mixture slowly while stirring. After one day of stirring, 900 ml DI water was added to quench the reaction, and the mixture was stirred overnight. The resulted mixture was extracted with diethyl ether (500 ml*4). The ether layer was removed under vacuum, and the resulted product was purified by flash column chromatography with hexane/ethyl ether eluent (1:1). Yield: 80%. (Alternatively, the crude product could be used directly for bromination). ^{1}H NMR (400 MHz, CDCl$_3$): 7.30 (m, 2H); 7.20 (m, 3H); 3.81 (t, 1H); 2.83 (d, 2H); 1.50 (s, 1H).
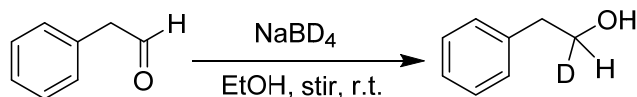
Synthesis of (2-bromo-2-d₁-ethyl) benzene
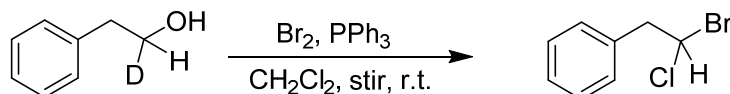
After charging a flamed dried 1 L 3-neck RBF with Triphenylphosphine (347.3 mmol, 191.07 g) and 750 ml anhydrous CH_2Cl_2, the temperature of the solution was brought down to 0 °C using an ice-water bath. Bromine (347.3 mmol, 17.9 ml) was added to the solution dropwise. 1-d1-2-phenylethanol was added after 10 min of stirring, and the resulted mixture was stirred overnight. After removing most of the solvent under vacuum, the residue was filtered and washed with pentane to remove most of the triphenylphosphine oxide. The solvent in the mixture was removed under vacuum, and flash chromatography was used to purify the residue. Yield: 40 g, 68%. ^{1}H NMR (400 MHz, CDCl₃): 7.33 (tt, 2H); 7.27 (tt, 1H); 7.22 (d, 2H);3.56 (tt, 1H); 3.16 (d, 2H).

Synthesis of 3-d₁-4-phenylbutanoic acid[72,73]
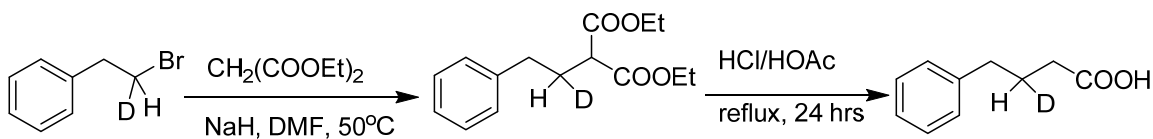

This procedure was modified from the synthesis of octanoic acid provided in the reference. Into a flame dried 1 L 3-neck RBF charged with an additional funnel, sodium hydride (8.68 g, 217 mmol) was added and followed by 170 ml anhydrous dimethyl formaldehyde (DMF) under nitrogen protection. Diethyl malonate (33.7 ml, 217 mmol) was dissolved in 50 ml DMF, and the solution was added slowly through the additional funnel in 15 min. The reaction was heated up slowly to 55 °C while constantly stirring until no more hydrogen gas evolving. The reaction mixture became clear and was cooled down to 40 °C. (2-bromo-2-d1-ethyl)Benzene (40 g, 215 mmol) was dissolved in another 50 ml DMF and was introduced through the additional funnel in 20 min. The mixture was stirred for 1 hour at 60 °C. 200 ml DI water was added to the reaction mixture after it was cool down to r.t., followed by extraction using diethyl either (200 ml*2), dried over MgSO₄, and the solvent was removed under vacuum. 57 g of crude product was afforded, which was mixed with 230 ml of acetic acid and 170 ml 6 N Hydrochloric acid, in a 1 L RBF with a condenser. After refluxing for 40 hours, all solvent was distilled at about 105 °C. 160 ml 10% NaOH was added to the residue. The mixture was washed with CH_2Cl_2, and the pH was adjusted to 1 with 6 N HCl solution. The mixture was extracted

with hexane (100 ml*2) and washed with brine (50 ml). The hexane solution was cooled down to -10 °C and the product was crystallized, filtered with a Buchner funnel and dried under vacuum at 30 °C, and was used directly for next step without further purification. Yield: 20.4 g, 74%.

Synthesis of 3-d$_1$-3,4-dihydronaphthalen-1(2H)-one
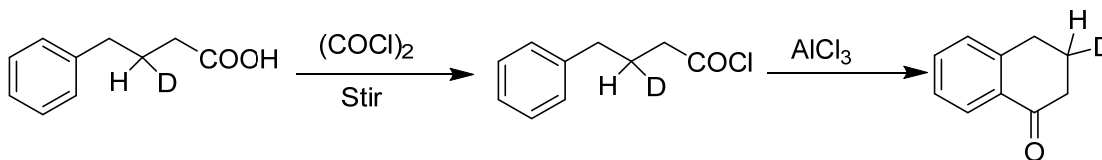
This procedure was adapted from the synthesis of α-Tetralone.[74] *3-d1-4-Phenylbutanoic acid* (20 g, 121 mmol) and thionyl chloride (SOCl$_2$) (13.2 ml, 182 mmol) were added to 500 ml dry RBF charged with a condenser on top. An acid trap (15% NaOH solution) was connected to the top of the condenser. The reaction mixture was gently heated using a heat gun until the reaction started. The heat generated by the reaction was enough for the reaction to proceed to finish. After 25-30 min, when HCl stopped evolving, the reaction was heated with a water bath for 10 min. The flask was then connected to vacuum with a cold trap in between, and the solvent was removed. Excessive SOCl$_2$ was removed by heating the flask up using a heat gun. After adding 110 ml carbon disulfide (CS$_2$), the temperature was brought down to 0 °C by an ice-water bath. Aluminum trichloride (AlCl$_3$) (21 g, 157 mmol) was added to the flask in one portion, followed by connecting the flask to a condenser with an acid trap immediately. After fast HCl evolving, the reaction mixture was heated with a water bath for 10 min, with a gentle shaking of the flask to allow the reaction to complete. After the reaction had been cooled down to 0 °C, 60 g ice was carefully added to decompose excessive AlCl$_3$, and followed by addition of 15 ml of concentrated of HCl solution. Diethyl ether (100 ml*4) was used to extract the product from the aqueous mixture. The ether layer was washed with 20 ml NaOH (15%) solution, 100 ml brine, and dried over MgSO$_4$. 17.3 g product was afforded after removing solvent under vacuum. Yield: 97%. ^{1}H NMR (400 MHz, CDCl$_3$): 7.99 (d, 1H); 7.43 (t, 1H); 7.27 (t, 1H); 7.21 (d, 1H); 2.92 (d, 2H); 2.61 (d, 2H); 2.10 (p, 1H).

4.8.1.4 Synthesis of 2-d$_1$-4-methyl-1,2-dihydronaphthalene

The procedure for the synthesis of *2-d1-4-methyl-1,2-dihydronaphthalene* is similar to the synthesis of the unlabeled *4-methyl-1,2-dihydronaphthalen.* Yield: 65%. ^{1}H NMR (400 MHz, CDCl$_3$): 7.30 (m, 2H); 7.22 (m, 2H); 5.93 (d, 1H); 2.84 (d, 2H); 2.32 (m, 1H); 2.15 (t, 3H).
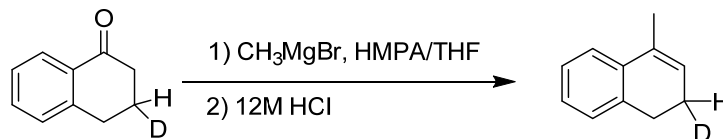
4.8.1.5 Synthesis of 2,2-d$_2$-4-methyl-1,2-dihydronaphthalene

The synthesis of the di-deuterated isotopologue of *4-methyl-1,2-dihydronaphthalene* is similar to the synthesis of the mono-deuterated isotopologue except for the first step for the synthesis of *2,2-d2-4-methyl-1,2-dihydronaphthalene,* as shown in 4.8.1.5.1.
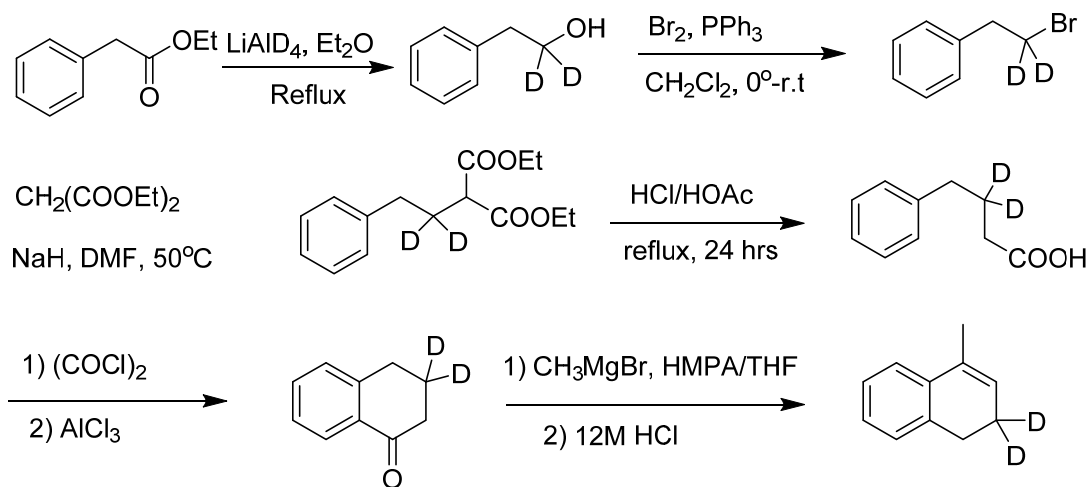
Synthesis of 1,1-d$_2$-2-phenylethanol
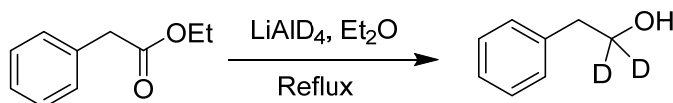
Lithium aluminum deuteride (264.9 mg, 5.679 mmol) and 10 ml anhydrous diethyl ether were added to a flame dried 50 ml RBF charged with an additional funnel. After cooling down the flask to 0 °C, ethyl 2-phenylacetate (1.066 g, 7.099 mmol) was dissolved in 15 ml of anhydrous diethyl ether and the mixture was added dropwise to the RBF through the additional funnel. After addition, the reaction mixture was heated to reflux for two hours; and followed by quenching with water (300 μl), 15% NaOH solution (300 μl) and water (900 μl) in sequence at r.t. The mixture was stirred for 10 min before the liquid was decanted and dried over MgSO$_4$. 0.762 g product was afforded. Yield: 86.4%. ^{1}H NMR (400 MHz, CDCl$_3$): 7.30 (m, 2H); 7.20 (m, 3H); 2.83 (d, 2H); 1.50 (s, 1H).

4.8.1.6 Synthesis of (E)-methyl 2-diazo-4-phenylbut-3-enoate[75,76]

Trans-styrylacetic acid (8g, 47.4 mmol), 120 ml methanol and 1.37 ml concentrated sulfuric acid were refluxed together for 24 hours. The mixture was filtered through a thin

80

pad of silica gel after cooling down to r.t. After removing the solvent under vacuum, a quick flash column chromatography with Hexane and ethyl ether (80:20) provided 8.23 g methyl ester. 2.115 g of the methyl ester (12 mmol), 3.031 g 4-acetamidobenzenesulfonyl azide and 60 ml acetonitrile were added to a dried 100 ml RBF. The mixture was cooled down to 0 °C and followed by addition of 2.010 g of 1,8-Diazabicyclo[5.4.0]undec-7-ene (DBU). After stirring for 1 hour, the reaction mixture was loaded directly onto a column and eluted with hexane and diethyl ether (80:20). The solvent was removed in *vacuo*. The resulted red powder, *(E)-methyl 2-diazo-4-phenylbut-3-enoate* was sealed and stored at - 20 °C for future use. Yield: 1.85 g, 76%.. ^{1}H NMR (400 MHz, CDCl$_3$): 7.31 (m, 4H); 7.18 (t, 1H); 6.46 (d, 1H); 6.18 (d, 1H); 1.82 (s, 3H).
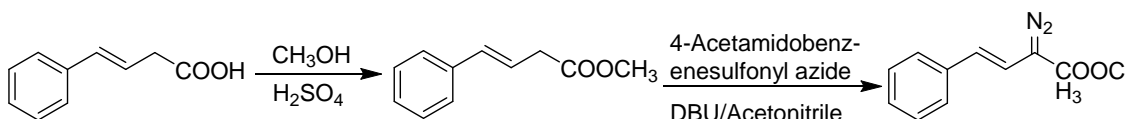
4.8.2 Structure determination and peak assignment

All the molecules were assigned using a 500 MHz Agilent NMR. The starting material **1$_{HH}$** was assigned as a pure substance products **2$_{HH}$** and **3$_{HH}$** were characterized as a mixture. All of the carbons are assigned using the combination of ^{1}H, ^{13}C, HSQC, HMBC and NOESY experiments. The following table lists the carbons from high frequency to low frequency and their corresponding position on the NMR spectrum.
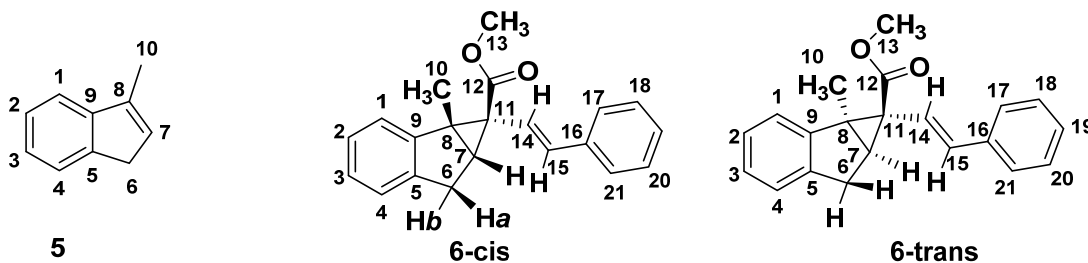
Figure 9: Carbon assignment of compound **5** and structure determination of **6**. The product **6** was determined to be with cis conformation.

Table 5: Carbon assignment of **5**

Peak	Chemical shift (ppm)	assignment
1	146.428	9
2	144.643	5
3	140.248	8
4	129.145	7
5	126.398	2
6	124.794	3
7	123.960	4
8	119.195	1
9	38.006	6
10	13.490	10
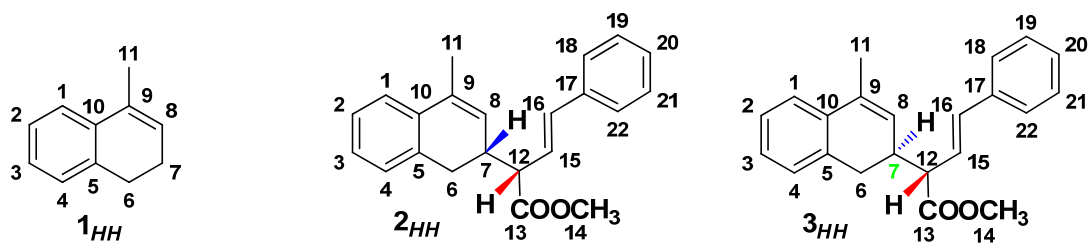
Figure 10: Structure and labeling for carbon assignment.

Table 6: Carbon assignment of **1**$_{HH}$

Peak	Chemical shift (ppm)	Assigned to carbon
1	136.617	5
2	136.203	10
3	132.568	9
4	127.709	4
5	127.048	3
6	126.721	2
7	125.700	8
8	123.131	1
9	28.760	6
10	23.626	7
11	19.650	11

Table 7: Carbon assignments of 2_{HH} and 3_{HH}. Note: For carbon 13 and 18, they show up as two separate peaks for diastereomers on 600 MHz NMR but only as one overlapped peak on 500 MHz NMR.

Peak	Chemical shift(ppm)	assignment	Peak	Chemical shift(ppm)	assignment
1	173.789	2_{HH}-13	20	126.776	2_{HH}-2 & 3_{HH}-2
2	173.785	3_{HH}-13	21	126.618	3_{HH}-18
3	136.882	2_{HH}-17 & 3_{HH}-17	22	126.606	2_{HH}-18
4	135.473	2_{HH}-10	23	126.475	2_{HH}-8
5	135.434	3_{HH}-10	24	126.245	2_{HH}-15
6	135.029	3_{HH}-5	25	126.207	3_{HH}-8
7	134.619	2_{HH}-5	26	126.140	3_{HH}-15
8	134.128	3_{HH}-16	27	123.229	2_{HH}-1
9	133.864	2_{HH}-16	28	123.118	3_{HH}-1
10	133.817	2_{HH}-9	29	53.782	3_{HH}-12
11	133.561	3_{HH}-9	30	53.364	2_{HH}-12
12	128.749	3_{HH}-19	31	52.028	3_{HH}-14
13	128.726	2_{HH}-19	32	52.003	2_{HH}-14
14	128.016	2_{HH}-4	33	36.885	3_{HH}-7
15	127.941	3_{HH}-4	34	36.370	2_{HH}-7
16	127.898	2_{HH}-20	35	33.356	3_{HH}-6
17	127.874	3_{HH}-20	36	31.918	2_{HH}-6
18	127.380	2_{HH}-3	37	19.569	2_{HH}-11
19	127.338	3_{HH}-3	38	19.539	3_{HH}-11

4.8.3 Reaction and measurement conditions for KIE and raw data

All quantitative NMR were acquired using a Bruker Avance III 600 MHz system with a TCI probe. All the quantitative NMR spectra were acquired in CDCl$_3$ at 5 °C for optimal separation of peaks, and to avoid significant line shape change due to solvent vaporization during long acquisition time. While approximately 120 µl of starting material or re-isolated starting materials were used for analysis, only 65 µl of C-H insertion product can be used with CDCl$_3$ up to the 4.0 cm mark in a 5mm NMR tube, due to line distortion and shimming problems at higher concentration. For the same reason, percent conversion samples were also limited to low concentration to avoid line shape distortion.

4.8.3.1 Competitive reaction between 1_{HH} and 1_{HD} using Rh$_2$(OAc)$_4$ as the catalyst.

In a typical experiment, a mixture of 1_{HH} and 1_{HD} (500 mg, 3.4 mmol) starting material, the catalyst Rh$_2$(OAc)$_4$ (37.5 mg, 0.085 mmol) and 1.7 ml anhydrous dichloromethane were added to a 25 ml flamed dried 2-neck RBF charged with an addition funnel under nitrogen. After cooling down the mixture with ice-water bath, (E)-methyl 2-diazo-4-phenylbut-3-enoate (687 mg, 3.40 mmol) was dissolved in 5.1 ml anhydrous dichloromethane. The solution was introduced to the starting material mixture at a rate that maintains the color of the reaction mixture green (approximately 45 min). 1 hour after the addition, the reaction was brought back to r.t. and stirred for at least 24 hours to

allow the full conversion of the CHCR intermediate to the final product, before percent conversion determination or purification for KIE measurement. 1 ml of the reaction mixture was evaporated under vacuum, and filtered through a pipette column with 1 cm silica gel, and washed with pentane (1 ml*2) to remove the catalyst. The solvent was removed under vacuum and was analyzed using ^{1}H NMR for percent conversion. The rest of the reaction mixture was evaporated under vacuum, and the residue was eluted with pentane to give the unreacted starting material, followed by pentane/diethyl ether (80:20) mixture to get product mixtures, on a 1.5-inch diameter column packed with silica gel to 8 inches. The raw data are displayed in Table 8.

Percent conversion measurement (*F*): The vinyl hydrogen in both starting materials and products are close on the spectrum and relatively clean from contaminants (dimerization product of the diazo reagent). Their peaks were used for percent conversion determination.

^{1}H NMR
Acquisition parameters: sweep width (sw): 10 ppm; center of spectrum (o1): 4.27 ppm; dummy scans (ds): 4; number of scans (ns): 16; acquisition time (aq): 1s; FID resolution: 1Hz; d1: 65 s; size of FID (TD): 12018. Processing parameters: zero filling to 32k points. Line broadening: 0; S/N ratio for smallest peak: 1000.

Starting material and re-isolated starting material ratio determination (^{13}C NMR): the benzylic carbons were used for ratio determination in a proton-decoupled ^{13}C spectrum.

Acquisition parameters: sweep width (sw): 143 ppm; center of spectrum (o1): 78.2ppm; dummy scans (ds): 4; number of scans (ns): 80; acquisition time (aq): 1.75 s; FID resolution: 1 Hz; d1: 20s; size of FID (TD): 75754. Processing parameters: zero filling to 128k points. Line broadening: 1 Hz; S/N ratio for smallest peak: 250 for **1**$_{HH}$/**1**$_{HD}$ experiment, 100 for **1**$_{HH}$/**1**$_{DD}$ experiment.

Product ratio determination (^{13}C NMR): For **1**$_{HH}$/**1**$_{HD}$ experiment, the non-deuterium bearing carbon 12 and carbon 7 in each species were used for quantification. For **1**$_{HH}$/**1**$_{DD}$ experiment, carbon 6 was used for ratio measurement for all products.

Acquisition parameters: sweep width (sw): 100 ppm; center of spectrum (o1): 45 ppm; dummy scans (ds): 4; number of scans (ns): 800; acquisition time (aq): 2.5 s; FID resolution: 0.4 Hz; d1: 20 s; Size of FID (TD): 75602. Processing parameters: zero filling to 128k points. Line broadening: 0 Hz; S/N ratio for smallest peak: 15 for **1**$_{HH}$/**1**$_{HD}$ experiment, 30 for **1**$_{HH}$/**1**$_{DD}$ experiment. Note: The reason why the smallest peak has such a low S/N ratio is a result from its small percentage presence in the product mixture and the limited sample loading. Nevertheless, the limited S/N ratio for H/D KIE analysis resulted in acceptable standard deviation.

Table 8: Raw data of the competitive reaction between 1_{HH} and 1_{HD} using $Rh_2(OAc)_4$ as the catalyst. R_0 and R stand for the ratio of isotopologues for the original starting material and the reisolated starting material, respectively. F stands for percent conversion. The values for the other four rows are relative integrations on the ^{13}C spectra. Each value in the table is an average value measured from six spectra taken for one sample from each experiment. $R_0=[1_{HD}/1_{HH}]_0=1.119 \pm 0.012$

	Expt. 1	Expt. 2	Expt. 3	Expt. 4
$R= 1_{HD}/1_{HH}$	2.418 ± 0.063	1.969 ± 0.021	1.958 ± 0.018	2.383 ± 0.034
F	0.824 ± 0.000	0.698 ± 0.000	0.69 ± 0.001	0.796 ± 0.000
3_{HH}	1.000 ± 0.000	1.000 ± 0.000	1.000 ± 0.000	1.000 ± 0.000
3_{HD}	0.728 ± 0.005	0.670± 0.005	0.692 ± 0.008	0.663 ± 0.010
3_{DH}	0.197 ± 0.005	0.191 ± 0.003	0.198 ± 0.004	0.184 ± 0.007
2_{HH}	2.207 ± 0.005	2.133 ± 0.009	2.168 ± 0.011	2.210 ± 0.013
2_{HD}	1.561 ± 0.006	1.426 ± 0.012	1.515 ± 0.010	1.456 ± 0.013
2_{DH}	0.418 ± 0.007	0.384 ± 0.007	0.409 ± 0.004	0.389 ± 0.007

4.8.3.2: Competitive reaction between 1_{HH} and 1_{DD} with $Rh_2(OAc)_4$ as the catalyst.

This experiment and the NMR measurement were carried out the same way as the competition experiment in 4.8.3.1, except using 1_{HH} and 1_{DD} isotopologue mixture as the starting material. The raw data are displayed in Table 9.

Table 9: Raw data of the competitive reaction between 1_{HH} and 1_{DD} using $Rh_2(OAc)_4$ as the catalyst. R_0 and R stand for the ratio of isotopologues for the original starting material and the reisolated starting material, respectively. F stands for percent conversion. The values in the other four rows are relative integrations on the ^{13}C spectra. Each value in the table was an average value measured from six ^{13}C spectra taken for one sample from each experiment. $R_0=[1_{DD}/1_{HH}]_0=1.126 \pm 0.010$.

	Expt.1	Expt.2	Expt.3	Expt.4	Expt.5
$R= 1_{DD}/1_{HH}$	18.5 ± 0.48	14.01 ± 0.23	13.15 ± 0.10	10.57 ± 0.13	9.68 ± 0.15
F	0.802 ± 0.000	0.781 ± 0.001	0.773 ± 0.001	0.751 ± 0.001	0.749 ± 0.000
3_{HH}	1.000 ± 0.000	1.000 ± 0.000	1.000 ± 0.000	1.000 ± 0.000	1.000 ± 0.000
3_{DD}	0.670 ± 0.004	0.644 ± 0.002	0.626 ± 0.005	0.600 ± 0.014	0.601 ± 0.005
2_{HH}	2.165 ± 0.005	2.217 ± 0.004	2.160 ± 0.016	2.177 ± 0.022	2.190± 0.017
2_{DD}	1.351 ± 0.004	1.310 ± 0.006	1.267 ± 0.014	1.211 ± 0.023	1.211 ± 0.025

4.8.3.3: Competitive reaction between 1_{HH} and 1_{HD} using $Rh_2(S\text{-}DOSP)_4$ as the catalyst.

In a typical experiment, a mixture of 1_{HH} and 1_{HD} (120 mg, 0.83 mmol) starting material, the catalyst $Rh_2(S\text{-}DOSP)_4$ (8 mg, 0.0042 mmol) was added to a 10 ml dry test tube sealed with septa and parafilm. The test tube was flushed with nitrogen and charged with 0.5 ml anhydrous dichloromethane using a syringe. After cooling down the mixture with ice-water bath, (E)-methyl 2-diazo-4-phenylbut-3-enoate (110 mg, 0.54 mmol,) was dissolved in 1.3 ml anhydrous dichloromethane and was introduced to the starting

material mixture with a syringe pump in approximately 45 min. The rest of the experiments were done analogously as 4.8.3.1. The raw data are displayed in Table 10.

^{13}C NMR

Acquisition parameters: sweep width (sw): 60.03 ppm; center of spectrum (o1): 36.76 ppm; dummy scans (ds): 4; number of scans (ns): 256 for $1_{HH}/1_{HD}$, 320 for $1_{HH}/1_{DD}$ competition experiment; acquisition time (aq): 3.61 s; FID resolution: 0.28 Hz; d1: 15 s; Size of FID (TD): 65536. Processing parameters: zero filling to 128k points. Line broadening: 0; S/N ratio for smallest peak: 40 for $1_{HH}/1_{HD}$ experiment, 25 for $1_{HH}/1_{DD}$ experiment.

Table 10: Raw data for the competitive reaction between 1_{HH} and 1_{HD} using Rh$_2$(S-DOSP)$_4$ as the catalyst. All the values are average relative integrations measured from six ^{13}C spectra taken for one sample from each experiment.

	Expt.1	Expt.2	Expt.3	Expt.4	Expt.5
2_{HH}	1.000	1.000	1.000	1.000	1.000
2_{DH}	0.202 ± 0.002	0.213 ± 0.002	0.197 ± 0.005	0.212 ± 0.002	0.212 ± 0.002
2_{HD}	0.547 ± 0.004	0.551 ± 0.003	0.544 ± 0.004	0.554 ± 0.003	0.554 ± 0.003
1_{HH}	0.452 ± 0.002	0.437 ± 0.002	0.510 ± 0.003	0.465 ± 0.002	0.465 ± 0.002
1_{HD}	0.869 ± 0.008	0.846 ± 0.006	0.938 ± 0.012	0.884 ± 0.009	0.884 ± 0.009

4.8.3.4: Competitive reaction between 1_{HH} and 1_{DD} using Rh$_2$(S-DOSP)$_4$ as the catalyst.

This experiment was carried out the same way as the one for 1_{HH} and 1_{HD}, except the amount of material used compare to $1_{HH}/1_{HD}$ with Rh$_2$(S-DOSP)$_4$. In a typical experiment, a mixture of 1_{HH} and 1_{DD} (200 mg, 1.38 mmol) starting material and the catalyst Rh$_2$(S-DOSP)$_4$ (13 mg, 0.007mmol) were added to a 10 ml dry test tube, which was sealed with septa and parafilm. The test tube was flushed with nitrogen, and 0.8 ml anhydrous dichloromethane was added. After cooling down the mixture with an ice-water bath, (E)-methyl 2-diazo-4-phenylbut-3-enoate (181 mg, 0.90 mmol,) was dissolved in 2.2 ml anhydrous dichloromethane and was introduced to the starting material mixture with a syringe pump in approximately 45 min. The rest of the experiments were done analogously as 4.8.3.1. The raw data are displayed in Table 11.

Table 11: Raw data of the competitive reaction between 1_{HH} and 1_{DD} using Rh$_2$(S-DOSP)$_4$ as the catalyst. All the values are average relative integrations measured from six ^{13}C spectra taken for one sample from each experiment.

	Expt.1	Expt.2	Expt.3	Expt.4	Expt.5
2_{HH}	1.000 ± 0	1.000 ± 0	1.000 ± 0	1.000 ± 0	1.000 ± 0
2_{DD}	0.383 ± 0.002	0.368 ± 0.005	0.386 ± 0.002	0.369 ± 0.003	0.359 ± 0.002
1_{HH}	0.206 ± 0.005	0.264 ± 0.005	0.227 ± 0.002	0.301 ± 0.002	0.311 ± 0.005
1_{DD}	0.677 ± 0.015	0.771 ± 0.021	0.730 ± 0.006	0.816 ± 0.006	0.838 ± 0.012

4.8.3.5: ^{13}C KIE experiment for 4-methyl-1,2-dihydronaphthalene (**1**) with catalyst Rh$_2$(OAc)$_4$

In a typical experiment, **1**$_{HH}$ (1.00 g, 6.94 mmol) starting material, the catalyst Rh$_2$(OAc)$_4$ (38 mg, 0.090 mmol) and 3.8 ml anhydrous dichloromethane were added to a 25 ml flamed dried 2-neck RBF charged with an addition funnel under nitrogen. After cooling down the mixture with an ice-water bath, (E)-Methyl 2-Diazo-4-phenylbut-3-enoate (1.26 g, 6.24 mmol) was dissolved in 11.6 ml anhydrous dichloromethane and was introduced to the starting material mixture at a rate that maintains the color of the reaction mixture green (approximately 45 min). The rest of the experiments were done analogously as 4.8.3.1. The raw data are displayed in Table 12 and Table 13.

^{13}C NMR for the starting materials
Acquisition parameters: sweep width (sw): 240 ppm; center of spectrum (o1): 78.06 ppm; dummy scans (ds): 4; number of scans (ns): 40; acquisition time (aq): 2.5 s; FID resolution: 0.40 Hz; d1: 80 s; size of FID (TD): 181154. Processing parameters: zero filling to 512k points. Line broadening: 0.3 Hz; S/N ratio for smallest peak: 520.

^{13}C NMR for the product
Acquisition parameters: sweep width (sw): 200 ppm; center of spectrum (o1): 96.74 ppm; dummy scans (ds): 4; number of scans (ns): 400; acquisition time (aq): 1.75 s; FID resolution: 0.57 Hz; d1: 80 s; size of FID (TD): 105842. Processing parameters: zero filling to 512k points. Line broadening: 0 Hz; S/N ratio for smallest peak: 120.

Table 12: Raw data of ^{13}C KIE experiment for 4-methyl-1,2-dihydronaphthalene (**1**) with catalyst Rh$_2$(OAc)$_4$-starting material and reisolated starting material. F stands for the percent conversion and each value at other rows stands for a KIE, which was calculated from the average integrations out of the six ^{13}C spectra taken for one sample from each experiment.

	Standard	Expt.1	Expt.2	Expt.3	Expt.4	Expt.5
F	N.A.	0.8021±0.0015	0.7910±0.0013	0.7248±0.0008	0.7497±0.0004	0.7499±0.0006
1$_{HH,C1}$	0.9805±0.0027	0.9838±0.0103	0.9839±0.0078	0.9671±0.0147	0.9840±0.0096	0.9801±0.0055
1$_{HH,C2}$	0.9833±0.0079	0.9922±0.0149	0.9907±0.0084	0.9809±0.0066	0.9897±0.0121	0.9844±0.0040
1$_{HH,C3}$	0.9844±0.0027	0.9859±0.0094	0.9887±0.0062	0.9805±0.0072	0.9862±0.0081	0.9866±0.0083
1$_{HH,C4}$	0.9797±0.0115	0.9891±0.0095	0.9856±0.0132	0.9717±0.0172	0.9901±0.0156	0.9833±0.0033
1$_{HH,C5}$	1±0	1±0	1±0	1±0	1±0	1±0
1$_{HH,C6}$	1.0683±0.0079	1.0737±0.0142	1.0761±0.0015	1.0768±0.0112	1.0824±0.0066	1.0713±0.0052
1$_{HH,C7}$	1.0637±0.0072	1.0853±0.0125	1.0854±0.0055	1.0920±0.0091	1.0945±0.0064	1.0759±0.0070
1$_{HH,C8}$	0.9868±0.0101	1.0014±0.0097	1.0011±0.0086	1.0019±0.0140	1.0120±0.0142	0.9913±0.0057
1$_{HH,C9}$	0.9969±0.0070	1.0058±0.0111	1.0054±0.0076	0.9954±0.0064	0.9981±0.0018	0.9950±0.0037
1$_{HH,C10}$	0.9994±0.0111	1.0024±0.0114	1.0073±0.0073	1.0009±0.0028	0.9968±0.0094	0.9974±0.0079
1$_{HH,C11}$	0.9563±0.0071	0.9705±0.0140	0.9719±0.0022	0.9656±0.0125	0.9819±0.0147	0.9587±0.0061

Table 13: ^{13}C KIE experiment for 4-methyl-1,2-dihydronaphthalene (**1**) with catalyst $Rh_2(OAc)_4$-Product ratio at each position. The values stand for their corresponding ratios. Each value was calculated from the average integrations out of the six ^{13}C spectra taken for one sample from each experiment.

CHCR/CH	Expt.1	Expt.2	Expt.3	Expt.4	Expt.5
$1_{HH,C1}$	2.138±0.0015	2.1386±0	2.0933±0.0126	2.1605±0	2.1098±0
$1_{HH,C2}$	N.A.	N.A.	N.A.	N.A.	N.A.
$1_{HH,C3}$	2.1442±0.0044	2.1460±0.0000	2.0945±0.0359	2.1534±0.0000	2.1865±0.0000
$1_{HH,C4}$	2.1746±0.0043	2.1764±0.0000	2.0556±0.0048	2.1881±0.0000	2.1861±0.0000
$1_{HH,C5}$	2.1530±0.0189	2.1657±0.0103	2.1588±0.0135	2.1704±0.0193	2.1466±0.0144
$1_{HH,C6}$	2.1099±0.0114	2.1553±0.0081	2.1442±0.0069	2.1391±0.0187	2.1386±0.0113
$1_{HH,C7}$	2.1330±0.0100	2.1785±0.0069	2.1763±0.0150	2.1511±0.0237	2.1455±0.0101
$1_{HH,C8}$	2.1303±0.0033	2.1316±0.0000	2.1374±0.0404	2.2436±0.0000	2.3081±0.0000
$1_{HH,C9}$	2.0933±0.0007	2.0936±0.0000	2.0708±0.0032	2.1470±0.0000	2.0855±0.0000
$1_{HH,C10}$	2.1626±0.0002	2.1625±0.0000	2.1609±0.0235	2.1732±0.0000	2.1482±0.0000
$1_{HH,C11}$	1.9975±0.0137	2.0594±0.0217	2.0741±0.0590	1.9486±0.0597	1.9665±0.0329
CH/CHCR	Expt.1	Expt.2	Expt.3	Expt.4	Expt.5
$1_{HH,C1}$	0.4677±0.0003	0.4676±0	0.4777±0.0028	0.4629±0	0.474±0
$1_{HH,C2}$	N.A.	N.A.	N.A.	N.A.	N.A.
$1_{HH,C3}$	0.4664±0.0010	0.4660±0.0000	0.4776±0.008	0.4644±0.0000	0.4573±0.0000
$1_{HH,C4}$	0.4598±0.0009	0.4595±0.0000	0.4865±0.0011	0.4570±0.0000	0.4574±0.0000
$1_{HH,C5}$	0.4645±0.0041	0.4618±0.0022	0.4632±0.0029	0.4608±0.0041	0.4659±0.0031
$1_{HH,C6}$	0.4740±0.0026	0.4640±0.0018	0.4664±0.0015	0.4675±0.0041	0.4676±0.0025
$1_{HH,C7}$	0.4688±0.0022	0.4590±0.0015	0.4595±0.0032	0.4649±0.0052	0.4661±0.0022
$1_{HH,C8}$	0.4694±0.0007	0.4691±0.0000	0.4680±0.0086	0.4457±0.0000	0.4333±0.0000
$1_{HH,C9}$	0.4777±0.0002	0.4776±0.0000	0.4829±0.0008	0.4658±0.0000	0.4795±0.0000
$1_{HH,C10}$	0.4624±0.0000	0.4624±0.0000	0.4628±0.0049	0.4602±0.0000	0.4655±0.0000
$1_{HH,C11}$	0.5007±0.0034	0.4856±0.0051	0.4825±0.0143	0.5136±0.0153	0.5086±0.0085

4.8.3.6: ^{13}C KIE experiment for 4-methyl-1,2-dihydronaphthalene (**1**) with catalyst $Rh_2(S\text{-}DOSP)_4$

This experiment was carried out with the same condition as when $Rh_2(OAc)_4$ was used as the catalyst except that the catalyst loading for $Rh_2(S\text{-}DOSP)_4$ was 33 mg, 0.017 mmol. The raw data are displayed in Table 14.

^{13}C NMR for the starting materials
Acquisition parameters: sweep width (sw): 240 ppm; center of spectrum (o1): 78.06 ppm; dummy scans (ds): 4; number of scans (ns): 40; acquisition time (aq): 2.5 s; FID resolution: 0.40 Hz; d1: 80 s; size of FID (TD): 181154. Processing parameters: zero filling to 512k points. Line broadening: 0.3 Hz; S/N ratio for smallest peak: 520.

	StartMat	Expt.1	Expt.2	Expt.3	Expt.4	Expt.5
F	N.A.	0.8199±0.000	0.7914±0.000	0.7943±0.000	0.8238±0.000	0.8017±0.000
$1_{HH,C1}$	0.9811±0.003	0.9687±0.005	0.9825±0.002	0.9778±0.002	0.9891±0.016	0.9747±0.002
$1_{HH,C2}$	0.9837±0.003	0.9745±0.004	0.9883±0.007	0.9796±0.003	1.0027±0.008	0.9831±0.008
$1_{HH,C3}$	0.9843±0.002	0.9706±0.006	0.9851±0.013	0.9853±0.009	0.9910±0.008	0.9803±0.007
$1_{HH,C4}$	0.9883±0.015	0.9763±0.006	0.9900±0.018	0.9846±0.003	0.9922±0.002	0.9781±0.008
$1_{HH,C5}$	1.0000 (std)	1.0000 (std)	1.0000 (std)	1.0000 (std)	1.0000 (std)	1.0000 (std)
$1_{HH,C6}$	1.0464±0.004	1.0300±0.011	1.0507±0.009	1.0469±0.003	1.0549±0.007	1.0395±0.007
$1_{HH,C7}$	1.0556±0.004	1.0519±0.014	1.0750±0.007	1.0722±0.004	1.0865±0.006	1.0667±0.007
$1_{HH,C8}$	1.0107±0.007	0.9906±0.013	1.0190±0.013	1.0129±0.013	1.0280±0.008	1.0048±0.006
$1_{HH,C9}$	0.9991±0.012	1.0102±0.010	0.9996±0.019	1.0075±0.010	1.0069±0.011	1.0110±0.013
$1_{HH,C10}$	0.9932±0.002	0.9948±0.010	0.9929±0.008	0.9955±0.003	1.0017±0.008	0.9946±0.002
$1_{HH,C11}$	0.9539±0.008	0.9305±0.007	0.9504±0.008	0.9503±0.005	0.9628±0.001	0.9408±0.006

4.8.3.7: ^{13}C KIE experiment for 3-methyl-1H-indene (**5**) with catalyst Rh$_2$(OAc)$_4$

	Standard	Expt.1	Expt.2	Expt.3	Expt.4	Expt.5
F	N.A.	0.8336±0.000	0.8194±0.000	0.8008±0.000	0.8442±0.000	0.8393±0.000
C_1	0.9924±0.010	0.9949±0.005	0.9975±0.008	0.9886±0.007	0.9965±0.013	1.0014±0.017
C_2	1.0000 (std)	1.0000 (std)	1.0000 (std)	1.0000 (std)	1.0000 (std)	1.0000 (std)
C_3	1.0198±0.006	1.0035±0.004	1.0272±0.010	1.0147±0.008	1.0256±0.010	1.0322±0.007
C_4	1.0000±0.008	0.9957±0.007	1.0099±0.009	1.0000±0.005	1.0065±0.014	1.0087±0.009
C_5	0.9962±0.014	1.0055±0.012	1.0102±0.007	0.9991±0.005	1.0039±0.018	1.0150±0.018
C_6	1.0177±0.001	1.0286±0.002	1.0473±0.008	1.0181±0.006	1.0327±0.019	1.0498±0.011
C_7	1.0076±0.007	1.0652±0.007	1.0567±0.009	1.0460±0.007	1.0581±0.016	1.0651±0.017
C_8	1.0124±0.014	1.0350±0.021	1.0376±0.008	1.0210±0.006	1.0352±0.009	1.0466±0.009
C_9	0.9802±0.011	0.9838±0.012	0.9931±0.007	0.9742±0.005	0.9868±0.009	0.9917±0.017
C_{10}	0.9685±0.005	0.9620±0.006	0.9815±0.011	0.9680±0.005	0.9800±0.009	0.9894±0.013

In a typical experiment, 1_{HH} (500 mg, 3.84 mmol) starting material, the catalyst Rh$_2$(OAc)$_4$ (8.5 mg, 0.019 mmol) and 1.9 ml anhydrous dichloromethane were added to a 25 ml flamed dried 2-neck RBF charged with an addition funnel under nitrogen. After cooling down the mixture with an ice-water bath, (E)-methyl 2-diazo-4-phenylbut-3-enoate (883 mg, 3.84 mmol) was dissolved in 5.8 ml anhydrous dichloromethane and was introduced to the starting material mixture at a rate that maintains the color of the

reaction mixture green (approximately 45 min). The rest of the experiments were done analogously as 4.8.3.1. The raw data are displayed in Table 15.

^{13}C NMR

Acquisition parameters: sweep width (sw): 240 ppm; center of spectrum (o1): 80.08 ppm; dummy scans (ds): 4; number of scans (ns): 24; acquisition time (aq): 2.5 s; FID resolution: 0.40 Hz; d1: 80 s; size of FID (TD): 181154. Processing parameters: zero filling to 512k points; line broadening: 0.25 Hz; S/N ratio for smallest peak: 630.

4.8.3.8: Solvent dielectric constant vs. diastereomeric ratio

In a typical experiment, $\mathbf{1}_{HH}$ (145 mg, 1.0 mmol) starting material and $Rh_2(OAc)_4$ (11 mg, 0.025 mmol) were added to a 10 ml dry test tube, which was sealed with septa and parafilm. The vial was flushed with nitrogen, and 1.0 ml anhydrous chosen solvent was introduced with a syringe. After the vial was placed into a temperature pre-equilibrated reservoir, (E)-methyl 2-diazo-4-phenylbut-3-enoate (253 mg, 1.25 mmol) was dissolved in 5 ml anhydrous solvent. The mixture was introduced into the starting material mixture with a syringe pump in approximately 45 min. All starting materials were converted. 1 hour after the addition, the reaction was brought back to r.t. and was stirred for at least 24 hours before purification. The whole reaction mixture was evaporated under vacuum, and the residue was eluted with pentane/diethyl ether (80:20) in a 1-inch diameter column, packed with silica gel to 4 inches. Approximately 65 μl was used for qualitative NMR analysis and the results were displayed in Table 3.

4.8.3.9: Temperature vs. diastereo-selectivity with catalyst $Rh_2(OAc)_4$

In a typical experiment, 1_{HH} (73 mg, 0.5 mmol) starting material and $Rh_2(OAc)_4$ (5.5 mg, 0.013 mmol) were added to a 5 ml dry vial, which was sealed with septa and parafilm. The vial was then flushed with nitrogen, and 0.5 ml anhydrous 1,2,3-trichloropropane was introduced with a syringe. After the vial was placed into a temperature pre-equilibrated reservoir (ranging from -10 °C to 100 °C), (E)-methyl 2-diazo-4-phenylbut-3-enoate (127 mg, 0.75mmol) was dissolved in 2.0 ml anhydrous 1,2,3-trichloropropane. The mixture was introduced into the starting material mixture with a syringe pump in approximately 45 min. All starting materials were converted. 1 hour after the addition, the reaction was brought back to r.t. and stirred for at least 24 hours before purification. The whole reaction mixture was evaporated under vacuum, and the resulted residue was eluted with pentane/diethyl ether (80:20) in a 1-inch diameter column packed with silica gel to 4 inches. Approximately 65 μl was used for NMR analysis. The raw data are displayed in Table 16.

^{13}C NMR

Acquisition parameters*:* sweep width (sw): 60.03 ppm; center of spectrum (o1): 38.95 ppm; dummy scans (ds): 4; number of scans (ns): 256; acquisition time (aq): 2.70 s; FID resolution: 0.37 Hz; d1: 20 s; size of FID (TD): 49000. Processing parameters*:* zero filling to 128k points; line broadening: 0 Hz; S/N ratio for smallest peak: 100.

Table 16: Diastereomeric ratios between 2_{HH}:3_{HH} in 1,2,3-trichloropropane (**5**) with catalyst $Rh_2(OAc)_4$ at different temperatures. All the values are measured at five different carbon sites as labeled in Figure 10. * indicates a second measurement with the same sample. Each value was the average out of relative integrations measured from six ^{13}C spectra taken from the single sample of one experiment. ** indicates an independent reaction and measurement was carried out the second time at a given temperature. Graph 1was plotted using the data set measured on C_{12}. The order of carbons is arranged from down field to up field on the ^{13}C spectrum.

	Average values of $2_{HH}/3_{HH}$				
Temp(^{0}C)	C_{12}	C_{14}	C_7	C_6	C_{11}
-10	2.834±0.012	2.755±0.013	2.845±0.014	2.769±0.009	2.826±0.024
0	3.004±0.011	2.956±0.010	3.036±0.014	2.969±0.013	3.054±0.024
0*	3.006±0.008	2.936±0.009	3.027±0.008	2.982±0.007	3.031±0.017
0**	3.034±0.009	2.975±0.016	3.055±0.010	2.990±0.014	3.040±0.018
10	3.012±0.014	2.922±0.007	3.03±0.020	2.964±0.013	3.010±0.019
20	3.075±0.012	3.094±0.020	3.079±0.011	3.052±0.008	3.178±0.022
20**	3.082±0.008	3.021±0.011	3.117±0.010	3.043±0.012	3.095±0.018
30	2.979±0.009	2.898±0.017	3.016±0.023	2.953±0.014	2.999±0.018
40	2.881±0.015	2.779±0.015	2.881±0.008	2.841±0.018	2.919±0.030
40*	2.858±0.010	2.734±0.019	2.881±0.020	2.816±0.015	2.865±0.035
50	2.866±0.014	2.787±0.032	2.887±0.010	2.832±0.013	2.869±0.014
60	2.800±0.011	2.713±0.008	2.798±0.010	2.756±0.021	2.893±0.030
80	2.596±0.007	2.474±0.030	2.603±0.006	2.574±0.008	2.667±0.013
100	2.337±0.007	2.204±0.012	2.357±0.019	2.293±0.010	2.391±0.011

4.9 References

(1)   Godula, K.; Sames, D. *Science* **2006**, *312*, 67–73.

(2)   Davies, H. M. L.; Manning, J. R. *J. Am. Chem. Soc.* **2006**, *128*, 1060–1061.

(3)   Davies, H. M. L. *Angew. Chem. Int. Ed.* **2006**, *4*, 6422–6425.

(4)   Davies, H. M. L.; Beckwith, R. E. J. *Chem. Rev.* **2003**, *103*, 2861–2904.

(5)   Jazzar, R.; Hitce, J.; Renaudat, A.; Sofack-Kreutzer, J.; Baudoin, O. *Chem. Eur. J.* **2010**, *16*, 2654–2672.

(6)   Díaz-Requejo, M. M.; Pérez, P. J. *Chem. Rev.* **2008**, *108*, 3379–3394.

(7)   Doyle, M. P.; Duffy, R.; Ratnikov, M.; Zhou, L. *Chem. Rev.* **2010**, 704–724.

(8)   Colby, D. A.; Tsai, A. S.; Bergman, R. G.; Ellman, J. A. *Acc. Chem. Res.* **2012**, *45* (6), 814–845.

(9)   Chen, X.; Engle, K. M.; Wang, D. H.; Jin-Quan, Y. *Angew. Chem. Int. Ed.* **2009**, *48*, 5094–5115.

(10)   Gaillard, S.; Cazin, C. S. J.; Nolan, S. P. *Acc. Chem. Res.* **2011**, *4*, 778–787.

(11)   Davies, H. M. L.; Manning, J. R. *Nature* **2008**, *451*, 417–424.

(12)   Davies, H. M. L. *Nat. Chem.* **2009**, *1*, 519–520.

(13)   Stang, E. M.; White, M. C. *Nat. Chem.* **2009**, *1*, 547–551.

(14)   Davies, H. M. L.; Jin, Q. *J. Am. Chem. Soc.* **2004**, *126*, 10862–10863.

(15)   Davies, H. M. L.; Jin, Q.; Ren, P.; Kovalevsk, A. Y. *J. Org. Chem.* **2002**, *6*, 4165–4169.

(16)   Davies, H. M. L.; Morton, D. *Chem. Soc. Rev.* **2011**, *40*, 1857–1869.

(17)   Davies, H. M. L.; Walji, A. M. *Org. Lett.* **2003**, *5*, 479–482.

(18)   Davies, H. M. L.; Hedley, S. J.; Bohall, B. R. *J. Org. Chem.* **2005**, *70*, 10737–10742.

(19)   Nowlan, D. T.; Gregg, T. M.; Davies, H. M. L.; Singleton, D. A. *J. Am. Chem. Soc.* **2003**, *125*, 15902–15911.

(20)   Nadeau, E.; Ventura, D. L.; Brekan, J. A.; Davies, H. M. L. *J. Org. Chem.* **2010**, *75*, 1927–1939.

(21)   Hansen, J.; Autschbach, J.; Davies, H. M. L. *J. Org. Chem.* **2009**, *74*, 6555–6563.

(22)   Davies, H. M. L.; Panaro, S. A. *Tetrahedron* **2000**, *56*, 4871–4880.

(23)   Chepiga, K. M.; Qin, C.; Alford, J. S.; Chennamadhavuni, S.; Gregg, T. M.; Olson, J. P.; Davies, H. M. L. *Tetrahedron* **2013**, *69*, 5765–5771.

(24)   Ventura, D. L.; Li, Z.; Coleman, M. G.; Davies, H. M. L. *Tetrahedron* **2009**, *65*, 3052–3061.

(25)   Hansen, J. H.; Gregg, T. M.; Ovalles, S. R.; Lian, Y.; Autschbach, J.; Davies, H. M. L. *J. Am. Chem. Soc.* **2011**, *133*, 5076–5085.

(26)   Wang, P.; Adams, J. *J. Am. Chem. Soc.* **1994**, *116*, 3296–3305.

(27)   Balcells, D.; Clot, E.; Eisenstein, O. *Chem. Rev.* **2010**, *110*, 749–823.

(28)   Demonceau, A.; Noels, A. F.; Costa, J.-L.; Hubert, A. J. *J. Mol. Catal.* **1990**, *732258*, 21–26.

(29)   Doyle, M. P.; Westrum, L. J.; Wolthuis, W. N. E.; See, M. M.; Boone, W. P.; Bagheri, V.; Pearson, M. M. *J. Am. Chem. Soc.* **1993**, *115*, 958–964.

(30)   Taber, D. F.; Petty, E. H.; Raman, K. *J. Am. Chem. Soc.* **1985**, *107*, 196–199.

(31)   Nakamura, E.; Yoshikai, N.; Yamanaka, M. *J. Am. Chem. Soc.* **2002**, *124*, 7181–7192.

(32)   Yoshikai, N.; Nakamura, E. *Adv. Synth. Catal.* **2003**, *345*, 1159–1171.

(33)   Davies, H. M. L.; Jin, Q. *Proc. Natl. Acad. Sci. U.S.A.* **2004**, *101*, 5472–5475.

(34)   Davies, H. M. L.; Beckwith, R. E. J. *J. Org. Chem.* **2004**, *69*, 9241–9247.

(35)   Davies, H. M. L.; Loe, Ø. *Synthesis* **2004**, No. 16, 2595–2608.

(36)   Davies, H. M. L.; Doan, B. D. *J. Org. Chem.* **1999**, *64*, 8501–8508.

(37)   Ess, D. H.; Wheeler, S. E.; Iafe, R. G.; Xu, L.; Çelebi-Ölçüm, N.; Houk, K. N. *Angew. Chem. Int. Ed.* **2008**, *47*, 7592–7601.

(38)   Hong, Y. J.; Tantillo, D. J. *Nat. Chem.* **2009**, *1*, 384–389.

(39)   Ussing, B. R.; Hang, C.; Singleton, D. A. *J. Am. Chem. Soc.* **2006**, *128*, 7594–7607.

(40)   Celebi-Olçüm, N.; Ess, D. H.; Aviyente, V.; Houk, K. N. *J. Am. Chem. Soc.* **2007**, *129*, 4528–4529.

(41)   Cheng, G.; Zhang, X.; Chung, L. W.; Xu, L.; Wu, Y. *J. Am. Chem. Soc.* **2015**, *137*, 1706–1725.

(42)   Çelebi-Ölçüm, N.; Ess, D. H.; Aviyente, V.; Houk, K. N. *J. Org. Chem.* **2008**, *73*, 7472–7480.

(43)   Carpenter, B. K. *Acc. Chem. Res.* **1992**, *25*, 520.

(44)   Carpenter, B. K. *Angew. Chem. Int. Ed.* **1998**, *37*, 3340–3350.

(45)   *Theory and Applications of Computational Chemistry: The First Forty Years*; Dykstra, C. E., Frenking, G., Kim, K. S., Scuseria, G. E., Eds.; Amsterdam-Boston-Heidelberg-London-New York-Oxford Paris-San Diego-San Francisco-Singapore-Sydney-Tokyo, 2005.

(46)   Plata, R. E.; Singleton, D. A. *J. Am. Chem. Soc.* **2015**, *137*, 3811–3826.

(47)   Glasstone, S.; Laidler, K. J.; Eyring, H. *The Theory of Rate Processes*; McGraw-Hill Book Company: New York, 1941.

(48)   Polanyi, J. C.; Zewail, A. H. *Acc. Chem. Res.* **1995**, *28*, 119–132.

(49)   Ostrom, H.; Oberg, H.; Xin, H.; LaRue, J.; Beye, M.; Dell'Angela, M.; Gladh, J.; Ng, M. L.; Sellberg, J. A.; Kaya, S.; Mercurio, G.; Nordlund, D.; Hantschmann,

M.; Hieke, F.; Kuhn, D.; Schlotter, W. F.; Dakovski, G. L.; Turner, J. J.; Minitti, M. P.; Mitra, A.; Moeller, S. P.; Fohlisch, A.; Wolf, M.; Wurth, W.; Persson, M.; Norskov, J. K.; Abild-Pedersen, F.; Ogasawara, H.; Pettersson, L. G. M.; Nilsson, A. *Science* **2015**, *347*, 978–982.

(50) Shaik, S.; Hirao, H.; Kumar, D. *Acc. Chem. Res.* **2007**, *40*, 532–542.

(51) Giagou, T.; Meyer, M. P. *Chem. Eur. J.* **2010**, *16*, 10616–10628.

(52) Meyer, M. P. *Adv. Phys. Org. Chem.* **2012**, *46*, 57−120.

(53) Simmons, E. M.; Hartwig, J. F. *Angew. Chem. Int. Ed.* **2012**, *51*, 3066–3072.

(54) Melander, L.; Saunders, Wiliam H., J. *Reaction Rates of Isotopic Molecules*; John Wiley & Sons, Inc: New York, 1980.

(55) Singleton, D. A.; Thomas, A. A. *J. Am. Chem. Soc.* **1995**, *117*, 9357–9358.

(56) Singleton, D. A.; Hang, C.; Szymanski, M. J.; Greenwald, E. E. *J. Am. Chem. Soc.* **2003**, *125*, 1176–1177.

(57) Gaussian 09, Revision B.01. M. J. Frisch, G. W. Trucks, H. B. Schlegel, G. E. S.; M. A. Robb, J. R. Cheeseman, G. Scalmani, V. Barone, B. M.; G. A. Petersson, H. Nakatsuji, M. Caricato, X. Li, H. P. H.; A. F. Izmaylov, J. Bloino, G. Zheng, J. L. Sonnenberg, M. H.; M. Ehara, K. Toyota, R. Fukuda, J. Hasegawa, M. Ishida, T. N.; Y. Honda, O. Kitao, H. Nakai, T. Vreven, J. A. Montgomery, J.; J. E. Peralta, F. Ogliaro, M. Bearpark, J. J. Heyd, E. B.; K. N. Kudin, V. N. Staroverov, T. Keith, R. Kobayashi, J. N.; K. Raghavachari, A. Rendell, J. C. Burant, S. S. Iyengar, J. T.; M. Cossi, N. Rega, J. M. Millam, M. Klene, J. E. Knox, J. B. C.; V. Bakken, C. Adamo, J. Jaramillo, R. Gomperts, R. E. S.; O. Yazyev, A. J. Austin, R. Cammi, C. Pomelli, J. W. O.; R. L. Martin, K. Morokuma, V. G. Zakrzewski, G. A. V.; P. Salvador, J. J. Dannenberg, S. Dapprich, A. D. D.; O. Farkas, J. B. Foresman, J. V. Ortiz, J. C.; Fox, and D. J. Gaussian, Inc.: Wallingford CT, 2010.

(58) Bigeleisen, J. *J. Chem. Phys.* **1955**, *23*, 2264–2267.

(59) West, J. D.; Stafford, S. E.; Meyer, M. P. *J. Am. Chem. Soc.* **2008**, *130*, 7816–7817.

(60) Amin, M.; Price, R. C.; Saunders, William H., J. *J. Am. Chem. Soc.* **1988**, *110*, 4085–4086.

(61) Gold, V. *Advances in Physical Organic Chemistry*; Gold, V., Ed.; Academic Press: London and New York, 1969; Vol. 7.

(62) Barton, D. H. R. *J. Chem. Soc* **1953**, 1027–1040.

(63) Pollak, P. I.; Curtin, D. V. *J. Am. Chem. Soc.* **1950**, *72*, 961–965.

(64) Curtin, D.; Crew, M. *J. Am. Chem. Soc.* **1955**, *1848*, 354–357.

(65) Eliel, E. L.; Lukach, A. *J. Am. Chem. Soc.* **1957**, *79*, 5986--5992.

(66) Seeman, J. I. *Chem. Rev.* **1983**, *83*, 83–134.

(67) Singleton, D. A.; Hang, C. *J. Am. Chem. Soc.* **1999**, *121*, 11885–11893.

(68) Kresge, A. J.; Lichtin, N. N.; K. N. Rao. *J. Am. Chem. Soc.* **1963**, *85*, 1210–1211.

(69) Kresge, A. J.; Lichtin, N. N.; Rao, K. N.; Weston, R. E. *J. Am. Chem. Soc.* **1965**, *87*, 437–445.

(70) Bron, J.; Stothers, J. B. *Can. J. Chem.* **1969**, *47*, 2506–2509.

(71) Adamczyk, M.; Watt, D. S. *J. Org. Chem* **1984**, *49*, 4226–4237.

(72) Kasumov, T.; Brunengraber, H. *J. Label. Compd. Radiopharm.* **2006**, *49*, 171–176.

(73) Jobdevairakkam, C. N. Process For Preparation of Liquid Dosage Form Containing Sodium 4-Phenylbutyrate. WO2007005633 A2, July 10, 2008

(74) E.L.Martin; Fieser, L. F. *Org. Synth.* **1935**, *15*, 77.

(75) Donohoe, T. J.; O'Riordan, T. J. C.; Peifer, M.; Jones, C. R.; Miles, T. J. *Org. Lett.* **2012**, *14*, 5460–5463.

(76) Davies, H. M. L.; Clark, T. J.; Smith, H. D. *J. Org. Chem.* **1991**, *56*, 3817–3824.